NIST-GCR-92-607

Flow Through Horizontal Vents as Related to Compartment Fire Environments

Qing Tan and Yogesh Jaluria

United States Department of Commerce
Technology Administration
National Institute **of** Standards and Technology

NIST-GCR-92-607

Flow Through Horizontal Vents as Related to Compartment Fire Environments

Qing Tan and Yogesh Jaluria
Rutgers University
New Brunswick, NJ 08903

June 1992

Sponsored by:
U.S. Department of Commerce
Barbara Hackman Franklin, ***Secretary***
Technology Administration
Robert **M.** White, ***Undersecretary*** of ***Technology***
National Institute of Standards and Technology
John **W.** Lyons, ***Director***
Building and Fire Research Laboratory
Gaithersburg, MD 20899

Notice

This report was prepared for the Building and Fire Research Laboratory of the National Institute of Standards and Technology under grant number 60NANB7D0743. The statements and conclusions contained in this report are those of the authors and do not necessarily reflect the views of the National Institute of Standards and Technology or the Building and Fire Research Laboratory.

FLOW THROUGH HORIZONTAL VENTS AS RELATED TO COMPARTMENT FIRE ENVIRONMENTS

QING TAN

AND

YOGESH JALURIA

ABSTRACT

A detailed investigation has been carried out on the flow exchange through a horizontal vent in a compartment containing a fire. A plexiglass tank with a vented horizontal partition in the middle was constructed to simulate the warmer interior environment due to a fire and the cooler ambient environment by filling the upper and lower compartment with brine and pure water, respectively. Experiments have been carried out on the combined natural and forced convection flow by imposing a pressure difference across the vent. The flow rates through the vent were determined over wide ranges of the governing variables, such as the pressure difference A P across the opening, density difference $\Delta\rho$ across the opening and the opening length to diameter ratio L/D. The basic characteristics of the flow, particularly whether it is unidirectional or bidirectional, was also studied. Volume flow rates were obtained as functions of the governing parameters in terms of correlating equations, from which quantitative information of the effect of AP, $\Delta\rho$ and L/D on the flow exchange through the vent can be determined. These results can thus be applied to the modeling of fire growth in vented rooms.

Table of Contents

List of Tables

List of Figures

List of Abbreviations

A	aspect ratio of the vent opening
A_V	vent area in standard vent flow model
B	buoyancy parameter
C_D	flow coefficient in standard vent flow model
C_{SHAPE}	shape function
d	diameter of the light source used in the shadowgraph
D	opening diameter
fl	focal length of the lens in the projector
Fr	dimensionless Froude number
Fr_{FLOOD}	dimensionless purging or flooding Froude number
$\overline{Fr_{FLOOD}}$	averaged dimensionless purging or flooding Froude number
g	magnitude of gravitational acceleration
H_1	height of the water column in manometer3
H_2	height of the air column in manometer3
AH	thickness of the opening support plate
l	distance between the photograph screen and the center of the test section
L	opening length
L/D	vent opening length to diameter ratio
L/S	vent opening length to side of square opening ratio
$\dot{m}_a$	mass air flow rate in room fires with a vertical opening
$\dot{m}_j$	mass gas flow rate in room fires with a vertical opening
$\dot{m}_e$	mass gas flow rate from the lower layer in room fires with a vertical opening
	mass gas flow rate from the upper layer in room fires with a vertical opening
Nu	Nusselt number
Gr	Grashof number

AP	pressure difference across the vent
ΔP_{FLOOD}	purging or flooding pressure difference across the vent
P_{BOT}	pressure above the vented horizontal partition
P_H	pressure at the elevation of the top surface of the opening support plate
P_L	pressure at the elevation of the bottom surface of the opening support plate
P_{tap3}	pressure measured at the manometer tap3
P_{TOP}	pressure above the vented horizontal partition
q	volume purging flow rate of Epstein and Kenton's study
Q	volume exchange flow rate with $AP = 0$
QBF	buoyancy-driven component of the combined convection
$QBOT$	volume flow rate through the vent from the bottom space to the top space of Cooper's study
$Q_{BOT,ST}$	volume flow rate through the vent from the bottom space to the top space of standard vent flow model
Q_{CC}	purely buoyancy-driven exchange flow rate with $AP = 0.0$
QD	volume flow rate of the brine from the upper compartment to the lower compartment
QEX	volume exchange flow rate through the vent
$Q_{EX,MAX}$	maximum volume exchange flow rate through the vent at $AP = 0$
$QFLOOD$	volume purging or flooding flow rate
Q_I	volume flow rate of the fresh water from the storage tank
$QMEAS$	volume flow rate from the outlet of the top tank of Mercer and Thompson's experiment
QN	net upward volume flow rate across the vent opening
QO	volume overflow rate of the brine at the overflow notch in the upper compartment
Q_{TOP}	volume flow rate through the vent from the top space to the bottom space
$Q_{TOP,ST}$	volume flow rate through the vent from the top space to the bottom space of standard vent flow model
Q_U	volume flow rate of the fluid from the lower compartment to the upper compartment
V_C	characteristic velocity for nondimensionalization of Q

V_H	volume of the heavier liquid (brine) in the upper compartment
V_L	volume of the less dense liquid (water) in the lower compartment
W	length of the flow wedge flowing back into the pipe in Mercer and Thompson's experiment
W/D	wedge length to pipe diameter ratio
ρ	density
$\Delta\rho$	density difference across the vent opening
$\bar{\rho}$	average density across the vent opening
$\rho/\bar{\rho}$	density difference ratio across the vent opening
ρ_{AIR}	air density
ρ_{BOT}	fluid density below the vented horizontal partition
ρ_H	density of fluid in the upper compartment at time *t*
$\rho_{H,0}$	density of fluid in the upper compartment at time zero
ρ_L	density of fluid in the lower compartment at time *t*
$\rho_{L,0}$	density of fluid in the lower compartment at time zero
θ	the pipe inclination in Mercer and Thompson's experiment
ρ_{TOP}	fluid density above the vented horizontal partition
ρ_{water}	density of fresh water

Chapter 1
Introduction

1.1 The Problem

The study of the flow of the combustion products out of a room with a fire and the mass flow rate of oxygen being added to the room by the flows at the openings and the vents of the room is of considerable importance in the mathematical modeling of the fire and of the changing environment in the room[24]. It also has a number of applications in many other analogous situations. One application involves the flow that arises during the venting procedure employed by firefighters while combating room or building fires. Another application concerns fluid motion through apertures connecting various rooms in buildings. Street drains, partially filled with water that is warmer than the ambient air, represent yet another application. This is especially important if a highly volatile toxic liquid or gas that is lighter than air finds its way into the drainage system [17]. Similarly, many environmental and geothermal flow processes, flows in nuclear reactor vessel systems and flows in passive solar heating energy systems give rise to vent flows that are often of crucial importance in such systems.

Among various vent flows, the exchange flow through a small vent opening in a horizontal partition is of particularly importance and needs to be studied in detail. The rate of movement of radiological or toxic gases in tall industrial or commercial buildings under emergency conditions is mainly a function of the leakage between the floors rather than that through the walls. Also, from a fundamental point of view, there is a big difference between horizontal and vertical opening or passage with respect to the relative motion of the two fluids. The flow pattern in a vertical passage through a horizontal partition, such as ceiling or floor vent, is often disturbed and chaotic and

may not be amenable to analysis. However, the two fluid regions in a horizontal passage through a vertical partition have been observed to be stably stratified and easily analyzed by Bernoulli's equation [19,22].

Basically, the flow exchange through a horizontal vent involves a combination of a buoyancy-driven exchange flow and a forced flow . The density difference $\Delta\rho$ across the opening between the cold (heavier) ambient fluid and the warm (lighter) enclosure fluid arises partly from the difference in composition and partly from the difference in temperature due to the heating up of the gases in the enclosure containing the fire. The density difference gives rise to a buoyancy-driven downflow of the heavier fluid fiom the ambient environment into the enclosure. However, if the compartment is sealed and has no other openings, mass conservation dictates an equal volume upflow of the lighter gas. The pressure difference **AP** across the opening arises from a momentum force balance in the flow, with the pressure in the enclosure higher than outside. The pressure difference generates a forced upflow of the lighter gas against the buoyancy-driven downflow of the heavier ambient fluid. The resulting flow rate through the vent, as a function of **Ap, AP** and the thickness to diameter ratio **L/D** of the vent, is of direct relevance to fire research. Here $\mathbf{AP} = P_{BOT} - P_{TOP}$, and $\mathrm{Ap} = \rho_{TOP} - \rho_{BOT}$, the subscripts "TOP" and "BOT" refer to the regions above and below the vent, respectively (Fig.1.1). Thus, positive values of **AP** and Ap are of particular interest in typical enclosure fires.

Some work has been done on buoyancy-driven vent flows for the special case of AP = 0.0. Work has also been done on flows due to an applied pressure difference, with no buoyancy effects present. But very little information is available for nonzero pressure differences combined with buoyancy effects, this circumstance is of particular interest in vented room fires. The flow exchange needs to be quantified over wider ranges of **Ap, ΔP** and **L/D** ratio in order to provide the necessary inputs for fire modeling studies.

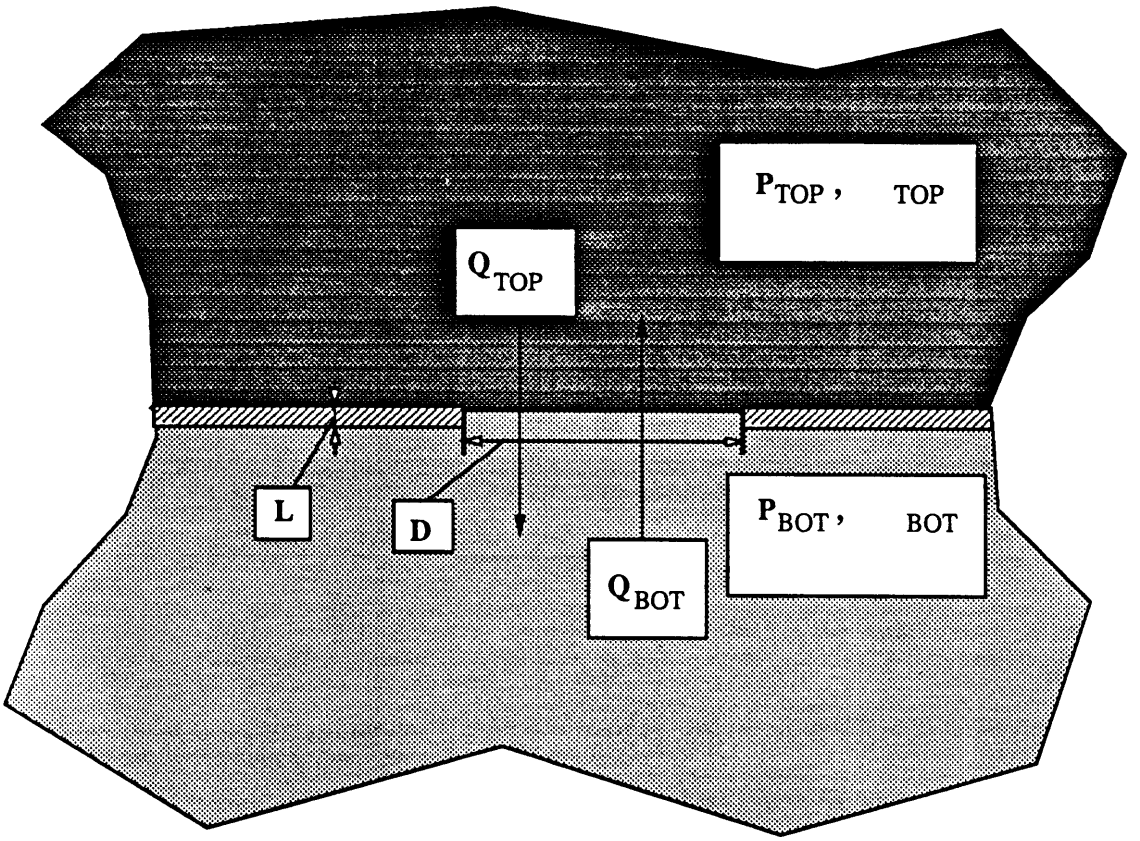

Figure 1.1: The basic horizontal **vent** configuration.

1.2 Literature Survey

Buoyancy-driven flows in enclosures have received a tremendous amount of attention[1,2]. However, not much work has been done on the flow through openings, such as those between connecting rooms in buildings. Vertical openings have received some attention because of their importance in several practical problems, such as electronic and energy systems and room fies. Fig.l.2 shows a sketch of the frequently considered circumstance of fire in a compartment with a single vertical opening (a door or a window). In this model, the hot gases rising above the fie, toward the ceiling, from a distinct layer of the hot gases. Air flows into the room at a rate $\dot{m}_a$, shears or entrains some gas from the hot upper layer at a rate $\dot{m}_j$, and mixes with it in the lower layer. The fie plume entrains gas fiom the lower layer and "pumps" it to the upper layer at a rate $\dot{m}_e$. Under steady conditions the mass flow rate through the opening from the upper layer ($\dot{m}_g$)equals the fuel flow rate plus $\dot{m}_a$[8].

Experiments on the exchange flow through openings (windows or doors) of smallL/S ratio, which is the ratio of opening length to the side of square opening, were reported by Brown and Solvason [3] and Shaw [4]. Shaw also studied combined buoyancy-driven and forced air flow across a door in a vertical partition. Buoyancy-driven flow through a horizontal duct or tube, in a vertical partition, between two compartments was studied experimentally by Leach and Thompson[5] and Bejan and Rossie[6]. Experimental and theoretical studies of steady state, fire-induced flow through vertical openings were also conducted by Prahl and Emmons [7], Steckler et. al. [8], [9] and Emmons[10]. In the later paper by Steckler et. al. [9], the brine-water technique was used to model the buoyancy driven flow of combustion products within a multicompartment structure. Several numerical studies have been carried out on this problem, such as those by Chan and Tien [11] and Abib and Jaluria [12]. As mentioned before, the flow across a vertical opening is stably stratified and can be obtained by using Bernoulli's equation and a jet contraction coefficient to estimate the velocity distribution at the vent.

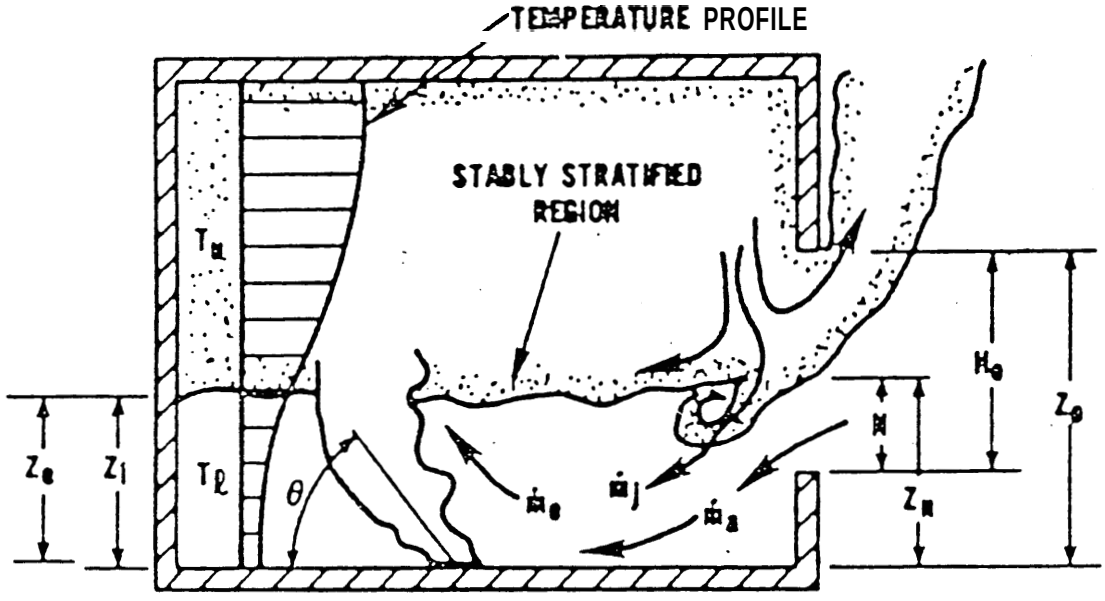

Figure 1.2: Fire in a compartment with a single vertical opening

The work done on the flow through horizontal vents, such as the one shown in Fig.1.3, is very limited. From a survey of the literature, it appears that the only prior papers dealing with vertical buoyancy-driven exchange flow across a horizontal partition between two compartments connected by a single opening are those of Brown[13] and Mercer and Thompson [14]. In Brown's experiments, air was used as the fluid and the countercurrent flow through a square aperture was investigated by imposing a temperature difference between the two compartments. His test covered ratio L/D, of the opening length(or partition thickness) to the side of the square opening, in the range of 0.0825 to 0.66. Brown interpreted the countercurrent flow as a heat transfer phenomenon and expressed his results in terms of a correlation for the Nusselt number Nu, versus Grashof number Gr. By introducing the definitions for Nu and Gr, and canceling viscosity and thermal conductivity, his correlation can be re-expressed, for practical purposes, in the form of a single functional relationship between the exchange flow rate and $\Delta\rho/\bar{\rho}$ and L/S. Here, $\Delta\rho$ is the density difference across the aperture and $\bar{\rho}$ is the mean density between two compartments. A major result of Brown's investigation is that the exchange flow rate increases with increasing L/S.

Mercer and Thompson's [14] experiments investigated the buoyancy-driven flow through inclined short tubes by using brine and water as the working fluids to accomplish the density difference between two compartments. Their experiments with vertical tubes, which are of interest here, covered a tube length-to-diameter ratio(L/D) range of 3.5 to 18.0. Interestingly enough, the exchange flow rates were observed to decrease with increasing L/D which is opposite to that observed by Brown. They suggested that, for a single opening, a maximum exchange flow rate exists at L/D or L/S between 0.66 and 3.5.

Several other investigations have been carried out on the buoyancy-driven flow through a horizontal vent. These include papers by Thomas et al. [15], Hinkley[16], Myrum[17], Cooper[18], Epstein[19], and Mercer and Thompson [20]. All of these studies mainly concentrated on the special circumstance of $\Delta P = 0.0$. Air was used as the

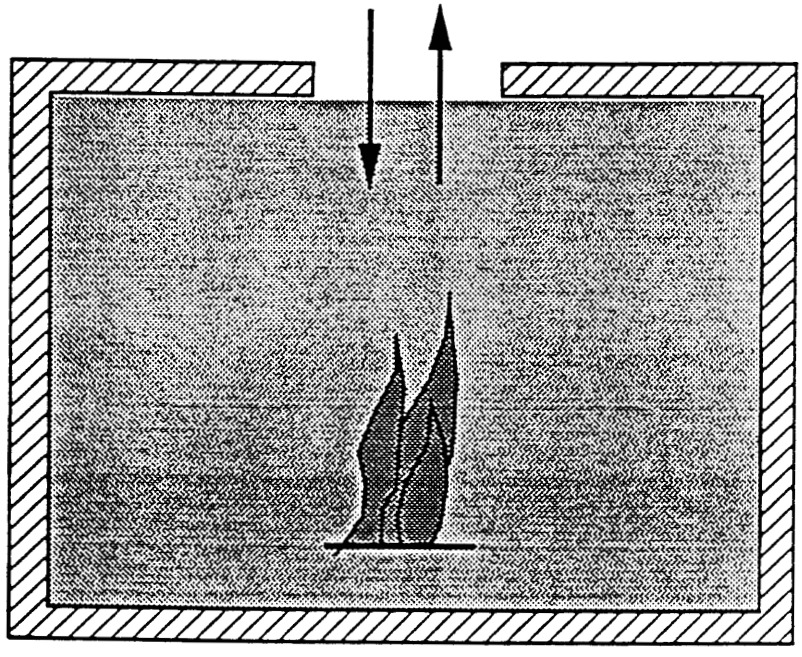

Figure 1.3: Fire in a compartment with a single horizontal opening

working fluid in some of the references while water/brine for the rest.

Employing water/brine as the working fluid, Epstein [19] experimentally considered the effect of varying the L/D ratio on the exchange flow rate and identified four different flow regimes. Fig.1.4 gives a sketch of the experimental arrangement used and the major results obtained. An empirical correlating equation for the dimensionless exchange flow rate, in terms of a Froude number Fr, versus L/D ratio is expressed as below:

$$Fr = \frac{Q}{(g\Delta\rho D^5/\bar{\rho})^{1/2}} = \frac{0.055[1+400(L/D)^3]^{1/6}}{[1+0.00527(1+400(L/D)^3)^{1/2}((L/D)^6+117(L/D)^2)^{3/4}]^{1/3}} \quad (1.1)$$

The parameter ranges covered are :

$$0.01 < L/D < 20.0 \text{ and } 0.025 < \Delta\rho/\bar{\rho} < 0.17$$

where Q is the volume exchange flow rate, g the magnitude of gravitational acceleration, $\Delta\rho$ the density difference across the vent and $\bar{\rho}$ the mean density.

It may be mentioned here that the characteristic velocity V_C in a buoyancy-induced flow is given by[1,2] as:

$$V_C = \sqrt{g\Delta\rho D/\bar{\rho}} \quad (1.2)$$

since the area of a circular vent is $\pi D^2/4$, the flow rate varies as $V_c\pi D^2/4$. Thus, this quantity is used to nondimensionalize Q, yielding the F'roude number.

The various flow regimes were termed by Epstein as Oscillatory Exchange Flow, Bernoulli Flow, Combined Turbulent Diffusion and Bernoulli Flow, and Turbulent Diffusion Flow. The results of Epstein's experiments suggested that there exists an influence of the density ratio on the Froude number $Q/(g\Delta\rho D^5/\bar{\rho})^{1/2}$, especially at low L/D where an increase fiom $\Delta\rho/\bar{\rho} = 0.04$ to 0.09 was observed to give rise to modest

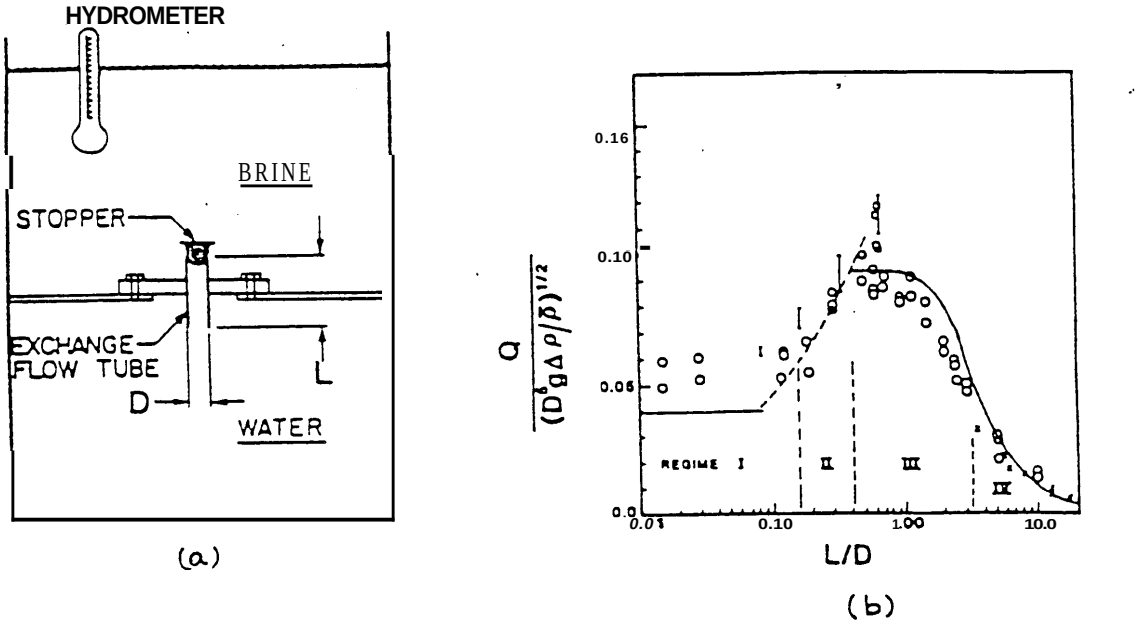

Figure 1.4: Sketch of Epstein's experimental arrangement and his major results

reductions in the Froude number ($\sim$ 20 percent). A further increase in $\Delta\rho/\bar{\rho}$ above 0.09 or, for that matter, decrease below 0.04, were found not to lead to significant changes in the Froude number. Thus, it was concluded that no additional density parameter is needed to characterize the results. The flow rate attains a maximum value at an L/D of about 0.6. At lower L/D the flow rate decrease with decreasing L/D and appears to be tending toward a constant value as L/D $\rightarrow$0. At the higher L/D the opposite behavior is noted, with the flow rate decreasing with increasing L/D. This might explain the conflict between the results of Brown [13] and Mercer and Thompson [14].

The conditions of steady, purging flow between space connected by a relatively long, straight, inclined, circular pipe of diameter D have been determined experimentally by Mercer and Thompson [20]. The configuration for their experiments is sketched in Fig.l.5, The bottom and top tanks contained fresh water and a relatively-dense salt-water solution, respectively . Each experimental run involved a steady uni-directional flow of salt-water, from the outlet of the top tank, at a measured volume-flow-rate, Q_{MEAS}. For small enough Q_{MEAS} and at the entrance to the lower tank, a wedge of the lower-tank fresh water was observed flowing back into the pipe. The length of the flow wedge W increased with decreasing Q_{MEAS} and W/D was taken as a measure of the purging effectiveness associated with the dimensionless flow rate, $Q_{MEAS}/(g\Delta\rho D^5/\rho_{TOP})^{1/2}$. A total purging implies a unidirectional flow through the vent from one space to the other, depending on the sign of AP, where $AP = P_{BOT} - P_{TOP}$. A minimum totally purging value of Q_{MEAS} is defined here as a flow rate which would lead to W = 0 exactly. The "purging" terminology in the above discussion is taken from the technology for nuclear reactor safety, where it is important to be able to predict conditions where totally purging flows will give way to flows involving nonzero exchange flows between reactor vessels and outside fluid sources. As seen in Fig.l.6, the W/D vs. $Q_{MEAS}/(g\Delta\rho D^5/\rho_{TOP})^{1/2}$ data are a strong function of pipe inclination, 8, where 8 = 90 (vertical pipe in a horizontal partition) is of special interest in the present study. It is impossible to observe the wedge length for values of W/D less than about two because of oscillations. The critical purging flow rate is therefore

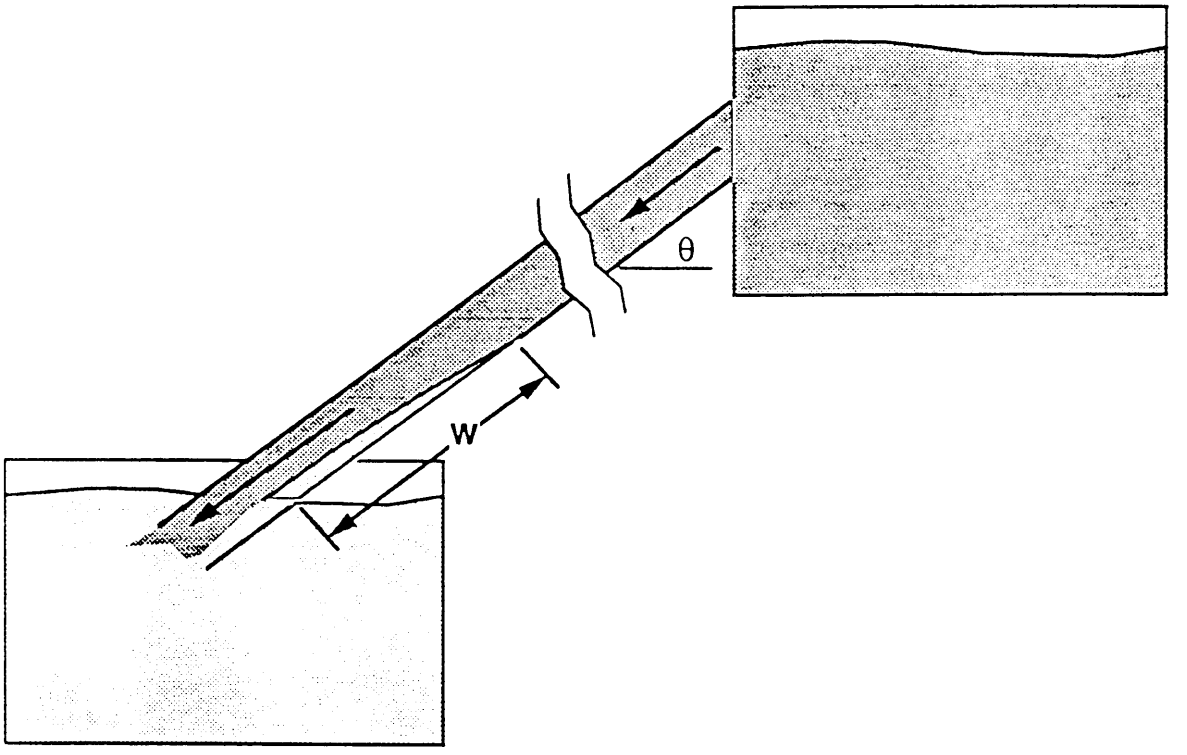

Figure 1.5: Configuration of Mercer and Thompson's experimental set up

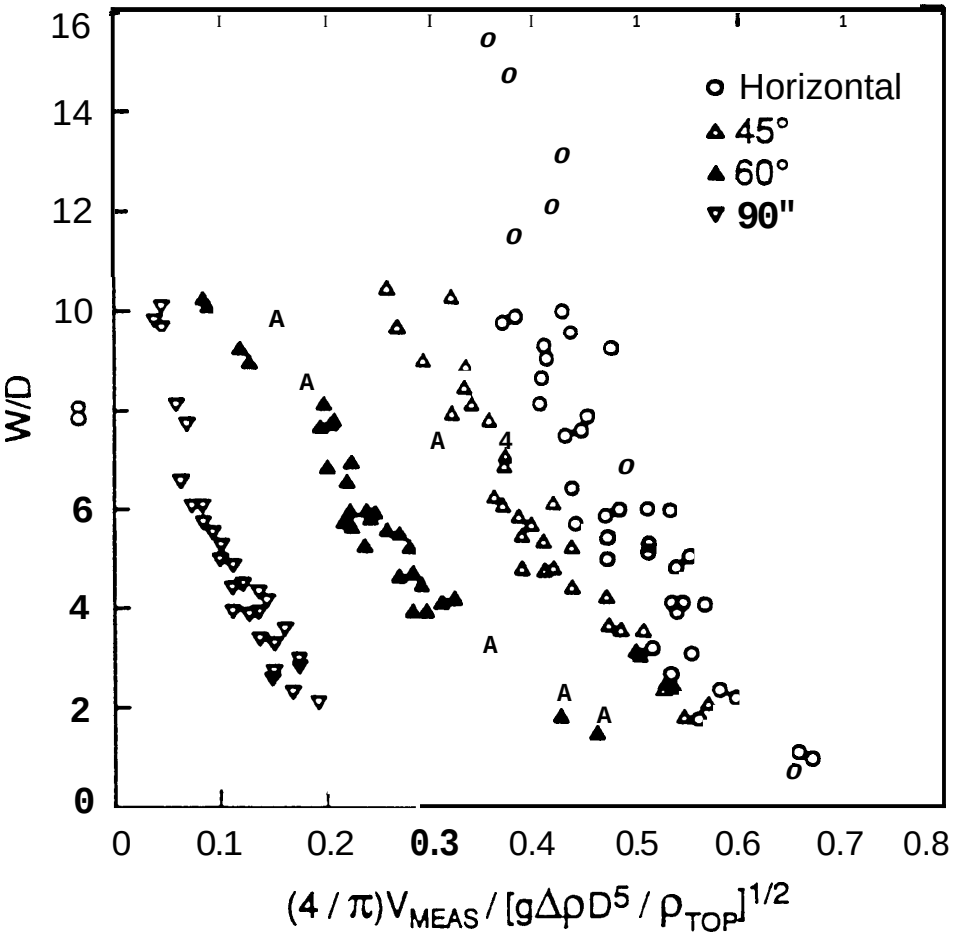

Figure 1.6: Experimental results of Mercer and Thompson's: Non-dimensional wedge length as a function of the non-dimensional velocity: results for 0", 45°, 60°, and 90" inclinations.

taken as that corresponding to a wedge length-to-diameter ratio of two. Fig.l.7 shows the purging flow rates required to give a minor W/D ratio **(W/D = 2)** as a function of $\Delta\rho/\bar{\rho}$ and inclination θ.

Few studies have considered the combined natural and forced convection through horizontal vents. Cooper[21] calculated the flow through a horizontal vent located in **a** ceiling or floor of a multi-room compartment. he took the cross-vent pressure difference **AP** into consideration in addition to the density difference. He assumed that in each space (bottom or top), near the vent elevation, but away from the vent flow itself, the environment is relatively quiescent with the pressure well-approximated by the **uniform** pressure field **which** would be derived from hydrostatic momentum considerations, that is to say **AP** = P_{BOT}-P_{TOP}, where P_{BOT} and P_{TOP} are the hydrostatic pressures at the vent elevation. By employing the experimental results of Epstein [19] and Mercer and Thompson [20] and the Standard Vent Flow Model[10], Cooper developed an algorithm for flow through horizontal vents.

The Standard Vent Flow Model, based **on** Bernoullis's equation, assumes unidirectional flow and breaks down if a bidirectional flow exchange occurs under the effects of buoyancy and the applied pressure difference. According to the Standard Vent Flow Model, for different **AP** and with $\rho_{TOP} > \rho_{BOT}$, the volume flow rate $Q_{BOT,ST}/Q_{TOP,ST}$ through the vent, **as** illustrated in Fig.l.8, is given by:

For arbitrary $\Delta\rho = \rho_{TOP} - \rho_{BOT}$:

$$Q_{BOT,ST} = C_D A_V |2\Delta P/\rho_{BOT}|^{1/2}, \quad Q_{TOP,ST} = 0 \quad \text{if } \Delta P > 0 \tag{1.3}$$

$$Q_{BOT,ST} = 0, \qquad Q_{TOP,ST} = 0, \qquad \text{if } \Delta P = 0 \tag{1.4}$$

$$Q_{BOT,ST} = 0, \quad Q_{TOP,ST} = C_D A_V |2\Delta P/\rho_{TOP}|^{1/2}, \quad \text{if } \Delta P < 0 \tag{1.5}$$

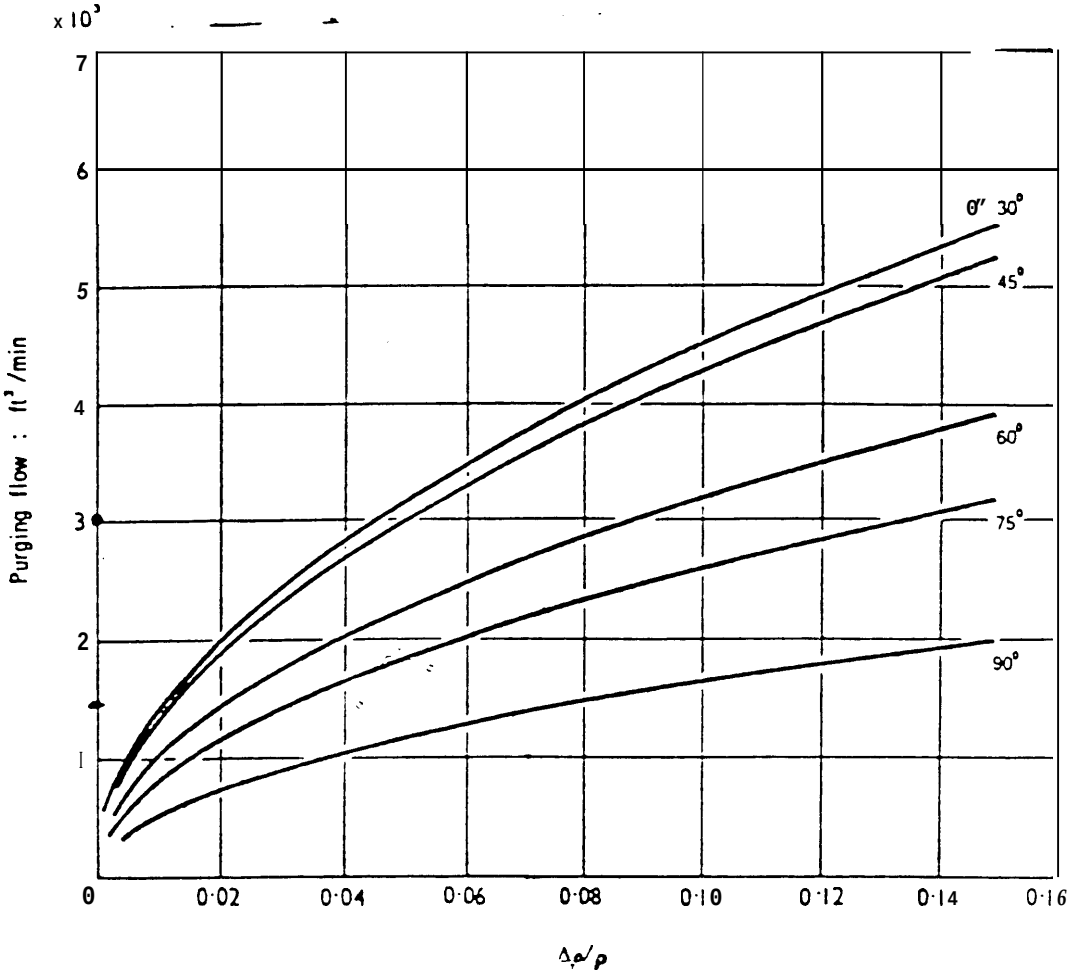

Figure **1.7:** Experimental results of Mercer **and** Thompson's: Full-scale purging **flow** requirements **for a** wedge length of twice the diameter($D = 1.8$ m)

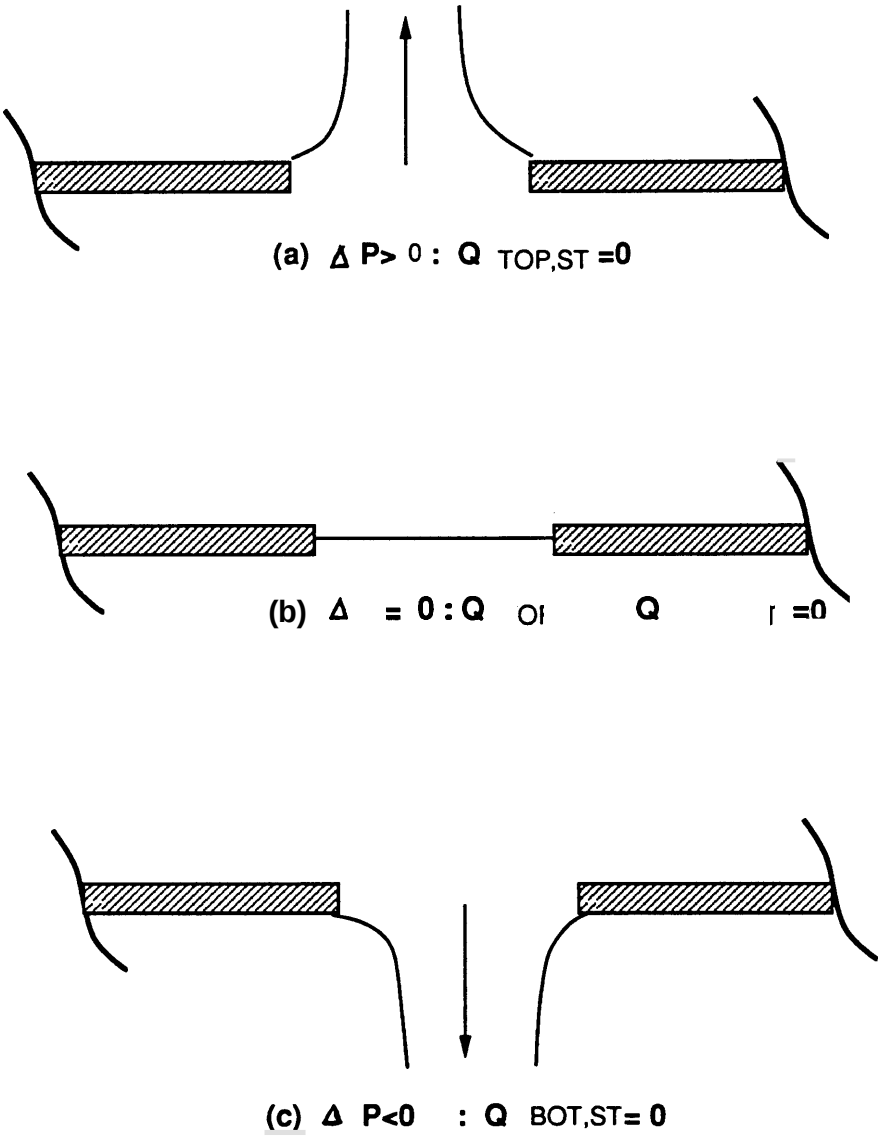

Figure 1.8: The standard vent-flow model for horizontal vents.

where $Q_{BOT,ST}$ and $Q_{TOP,ST}$ are the volume-flow-rates through the vent from the bottom space to the top space and from the top space to the bottom space, respectively, subscript "ST" stands for the Standard Vent Flow Model, A_V is the vent area, and C_D is the flow coefficient. So, the Standard Vent Flow Model predicts a zero flow rate when $\mathbf{AP} = 0$, which is obviously wrong when a heavier fluid overlies a lighter fluid, because of the resulting instability, it is evident that a two-directional **or** an exchange flow, develops where the top and bottom spaces exchange fluid across the opening.

By assuming the correct vent flow, Q_{TOP} and Q_{BOT}, can be predicted by a sum of the standard model flow components of **Eqs.**[3] - [5] and an exchange-flow component, Q_{EX}, which is to be determined. Cooper[21] assumed that:

$$QTOP = Q_{TOP,ST} + Q_{EX} \tag{1.6}$$

$$QBOT = Q_{BOT,ST} + Q_{EX} \tag{1.7}$$

where he further assumed that Q_{EX} is a linear function of $\Delta \mathrm{P}/|\Delta P_{\mathrm{FLOOD}}|$, as shown in Fig.l.9. Then from Epstein's experimental results without pressure difference:

$$Q_{EX} = Q_{EX,MAX} = 0.055[g\Delta\rho D^5/\bar{\rho}]^{1/2} \qquad \text{at } \Delta P = 0 \tag{1.8}$$

The pressure at which $Q_{EX} = 0$ is the flooding pressure $\Delta P_{\mathrm{FLOOD}}$, which is the critical point leading to the totally purging flow from one side of the vent to the other, depending on the sign of **AP.** Again, by assuming that the exchange flow through the vent is irrelevant to vent inclination when it is very close to the totally purging flow, Cooper deduced the value of $\Delta P_{\mathrm{FLOOD}}$ based on Mercer and Thompson's experimental results as below:

$$|\Delta P_{\mathrm{FLOOD}}| = C^2_{\mathrm{SHAPE}} g\Delta\rho D^5/(2A_V^2) \tag{1.9}$$

where C_{SHAPE} is the shape function. So, when $|\Delta P| = 0$, there is the maximum countercurrent exchange flow due to the buoyancy force. As $|\Delta P|$ increases from zero, but

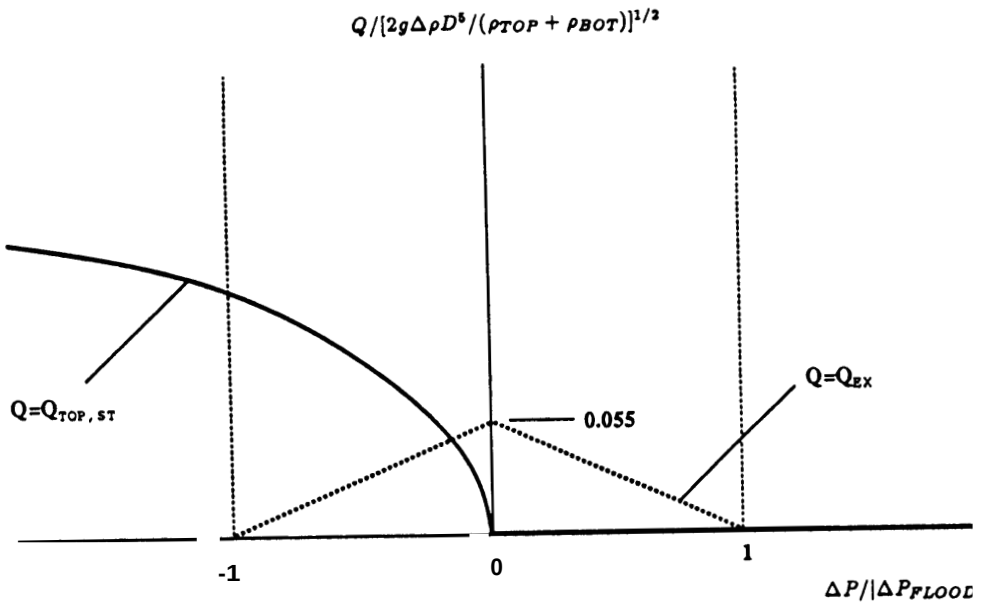

Figure 1.9: The volume-flow rate components $Q_{TOP,ST}$ and Q_{EX} for unstable Fig.1.8 configuration, $Ap > 0$, **plotted as a** function **of** AP.

is less than $|\Delta P_{FLOOD}|$, there is some flow exchanges, i.e., non-zero V_{EX}, between the environments of the two spaces. If $|\Delta P|$ keeps increasing and exceeds $|\Delta P_{FLOOD}|$, there is no exchange flow and the flow through the vent is uni-directional. Following the Standard Vent Flow Model, this leads to a total purging flow from one space to the other determined by the sign of AP. The VENTCL algorithm developed by Cooper is suitable for general use in zone-type compartment fire models.

Epstein and Kenton[22] investigated the combined natural convention and forced flow through small openings in a horizontal partition based on the former research of Epstein[19]. Two different experimental apparatus had been employed by them. One was with the draining technique and the other with the water injection technique. These are shown in Fig.1.10 and Fig.1.11, respectively. Separate experiments, with these two methods, were performed on forced flow through the vent opening to obtain a definitive relation between the flooding flow rate q, above which the buoyancy-driven exchange flow is prevented, and the opening length-to-diameter ratio L/D. An empirical relation for the flooding (purging) flow rate in terms of the Froude number versus L/D was found as depicted in Fig.1.12 and the following correlation was given with a relative error of less than about 20 percent:

$$\frac{q}{(g\Delta\rho D^5/\bar{\rho})^{1/2}} = \frac{0.19[1 + 4 \times 10^3(L/D)^3]^{1/9}}{(1 + 5.091 \times 10^{-2}(L/D)^{16/7}[1 + 4 \times 10^3(L/D)^3]^{4/9})^{1/4}} \qquad (1.10)$$

Here q is the purging volume flow rate. Interestingly enough, the shape of the curve is similar to the exchange flow rate versus L/D trend reported in Epstein's previous paper, which was without the presence of an external pressure. The main intention of their later study was to determine the effects of forced-fluid motion on natural convection for horizontal venting flow. A correlation for this flow was obtained and is shown in Fig.1.13. Here Q_{BF} is the buoyancy-driven component of the combined convection, Q_{CC} the purely buoyancy-driven exchange flow rate with AP = 0.0, Q_U the net supplying flow rate and q the purging flow rate. It can be seen fiom the Fig.13 that the

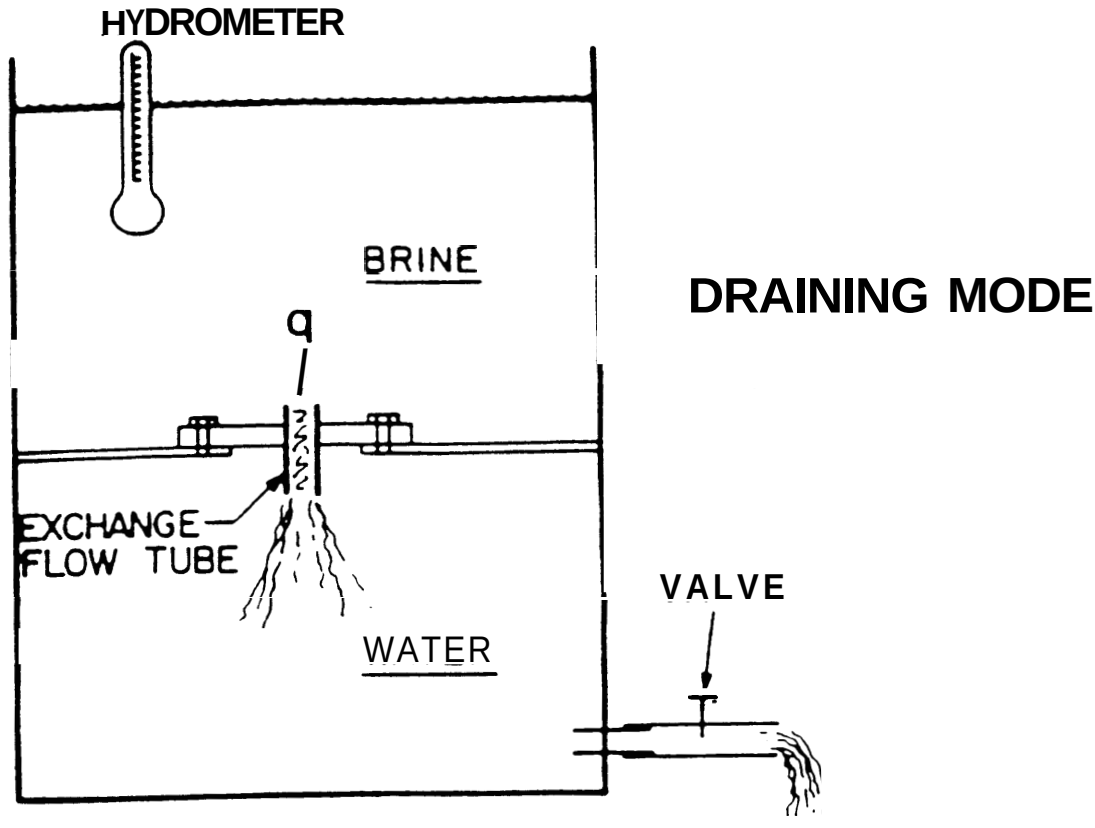

Figure 1.10: Schematic diagram of the Epstein and Kenton's apparatus for the determination of the flooding flow rate via a quasi-steady draining technique.

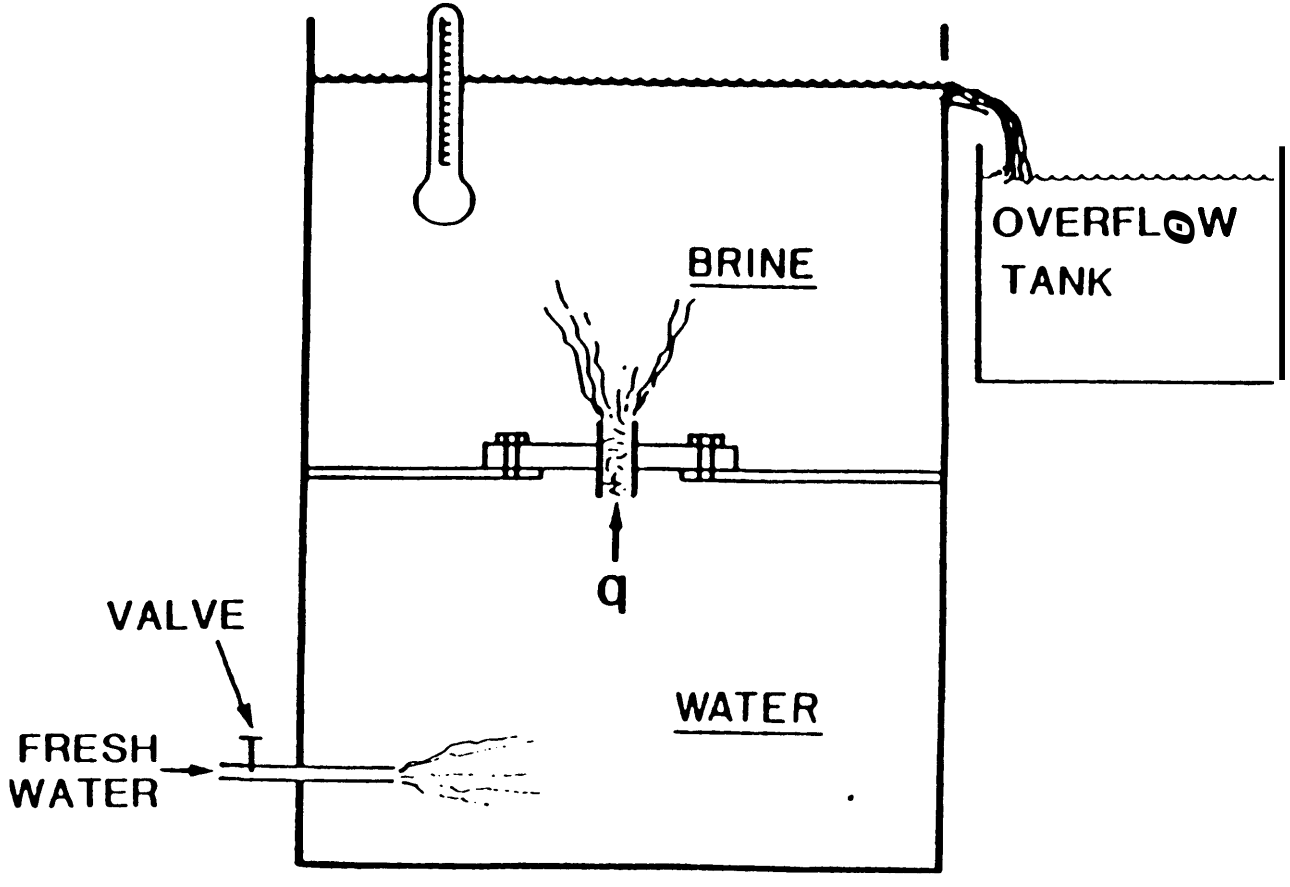

Figure 1.11: Schematic diagram of the Epstein and Kenton's apparatus for the determination of the flooding flow rate at steady state by water injection

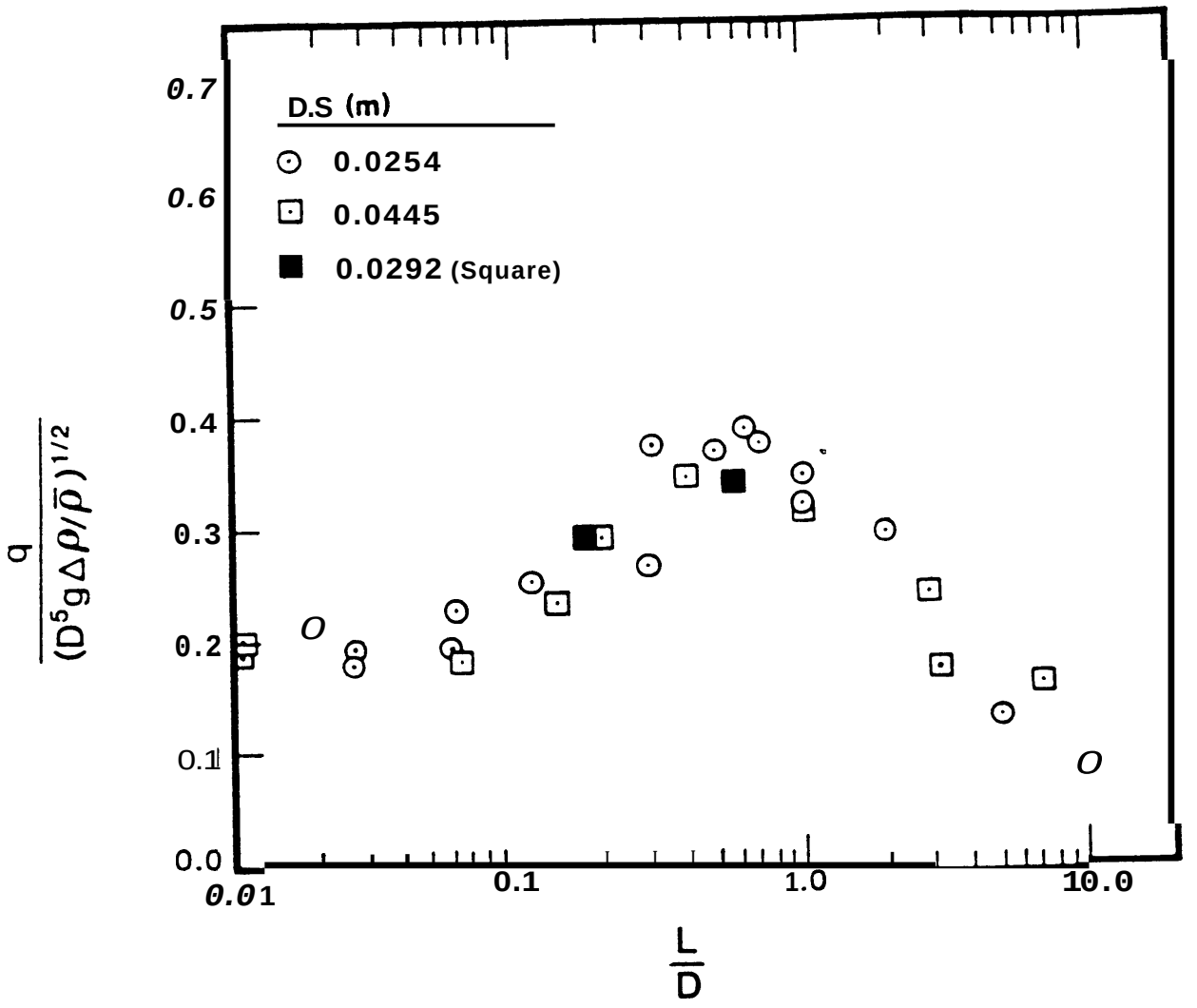

Figure 1.12: Epstein and Kenton's experimental results for the critical purging (or flooding) **flow rate into a single opening in a horizontal partition**

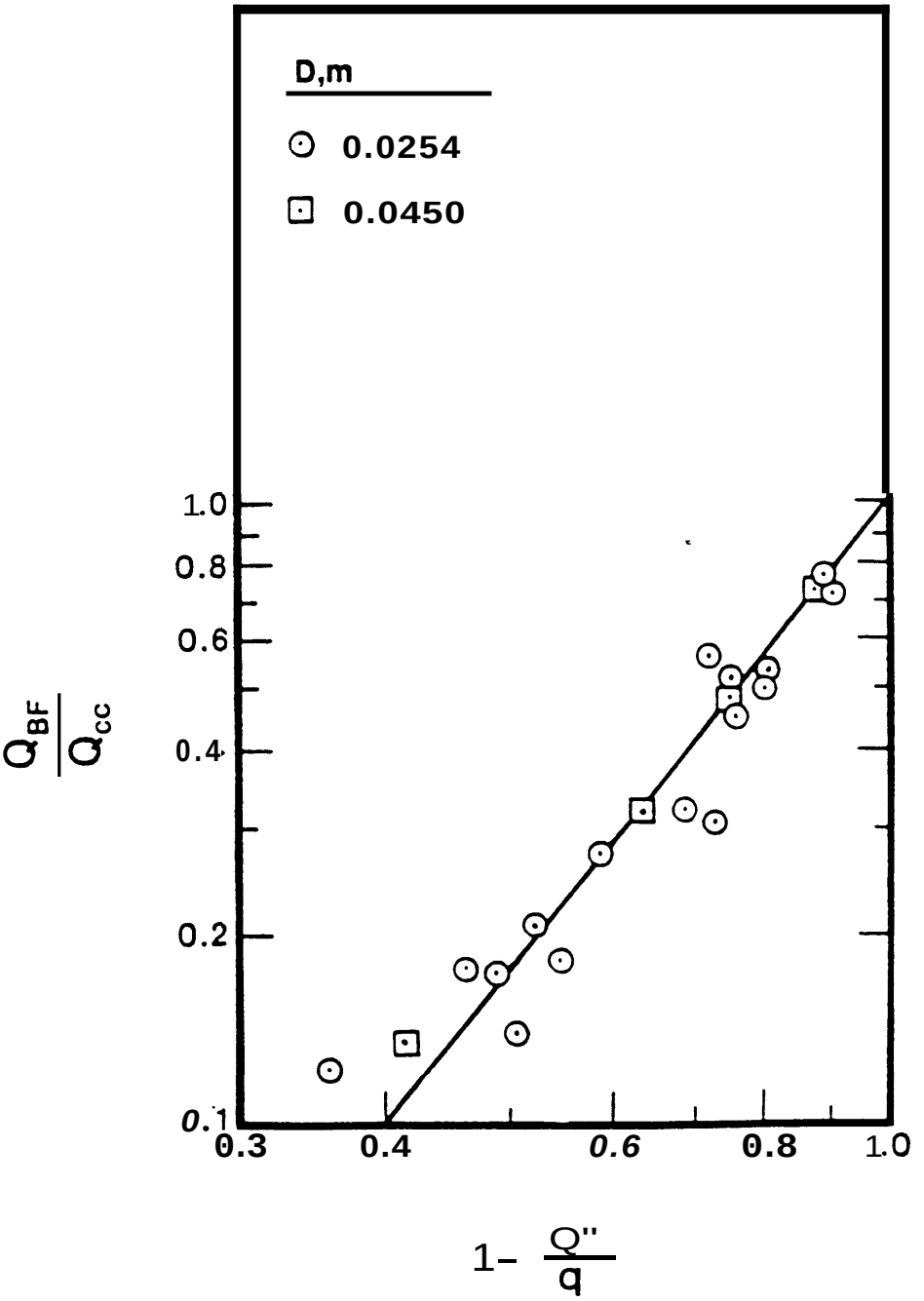

Figure 1.13: Epstein and Kenton's experimental results: The natural convection component Q_{BF} of combined natural convection and forced flow across circular openings in a horizontal partition; correlation of data in terms of Q_{CC}, Q_U, and q.

externally supplied flow rate Q_U need only exceed a value equivalent to about 60 percent of the flooding rate **q** to essentially "wipe away" the natural convection component Q_{BF}. An expression for the solid, correlating line in the Fig.13, which gives Q_{BF} to an accuracy of **25** percent, is:

$$Q_{BF} = Q_{CC}(1 - Q_U/q)^{2.3} \tag{1.11}$$

this equation compares well with the theoretical prediction. However, only the volume flow rate value was determined and **no** pressure information was given.

1.3 Objectives

As reviewed in the preceding sections, the flow through horizontal vents, such as those in the ceiling or the floor of **a** multi-room compartment, is important in the modeling of fire in a vented enclosure. Such flows are driven by buoyancy effects, due to the difference in density of the fluids **on** either side of the vent , as well **as** by any pressure difference that exists across the vent. Some work has been done **on** the flow through horizontal vents due to the density difference for a zero pressure difference. Similarly, the Standard Vent Flow Model works well for unidirectional flow and for circumstances where the density difference is small or the distribution is stable. Some experimental work has **also** been done to study the combined effect of AP and Ap and to quantify the purging effectiveness of the flow. Clearly, the flow through horizontal vents is an important consideration in the modeling of compartment fires for several circumstances of practical interest. Due to the lack of detailed, quantitative information **on** the flow exchange **as** a function of arbitrary values of the governing variables AP, $\Delta\rho$ and L/D, the main objective of this work is to carry out a detailed investigation **on** this combined natural and forced convection phenomena. The flow rate through the horizontal vent was determined over wide range of the governing variables. The basic characteristics of the flow, particularly whether it is unidirectional or not, was **also** studied. The main thrust of the study **was** to obtain the flow exchange rate through a horizontal vent as a

function of AP, $\Delta\rho$ and L/D and to present the results obtained in terms of correlating equations which may by readily applied to modeling of fire in vented rooms.

The experiment made use of the fact that saline water is denser than fresh water. This attractively simple choice of fluids to represent buoyancy-driven gas movement between rooms is valid so long as molecular viscosity and thermal diffusivity are not important parameters. The brine-water technique has some advantages over performing a heat transfer experiment with gas as the working fluid. There is no need to cover the test section with insulation as the flow exchange process is isothermal, and there is no significant waiting time requirement for the steady state to be reached. The maximum compartment-to-compartment density difference ratio $\Delta\rho/\bar{\rho}$ that can be achieved with the brine-water system is approximately 0.2. This corresponds to a gas exchange rate driven by a temperature difference of 100K between two rooms when the average temperature is 500K. The nondimensionalization will allow the use of the results obtained for modeling of air and gases, which are obviously of greater interest in fires. Since the water is incompressible, the application of the pressure difference AP in water is also relatively easy. Comparison of the small-scale experimental results with previously conducted fire tests in a full-scale facility has demonstrated the utility of the brine-water technique in predicting full-scale results with hot gases.

For the buoyancy-driven flow across a horizontal vent of small height L, such as the one shown in Fig.l.3, the velocity level may be estimated to be of order $(g\Delta\rho D/\bar{\rho})^{1/2}$ by using Bernoullis' equation. Therefore, for a circular opening, the flow rate Q varies as $(g\Delta\rho D^5/\bar{\rho})^{1/2}$, which may be taken as the characteristic volume flow rate for nondimensionalizing Q, as done by Epstein[19]. For a vent of significant height L, the parameter L/D arises as an additional variable. Considering now the forced flow due to a pressure difference AP, Bernoulli's equation gives an estimate for the velocity across the vent $(2\Delta P/\bar{\rho})^{1/2}$. Therefore, a buoyancy parameter B and the dimensionless flow rate Fr as Froude number may be defined as:

$$B = \left(\frac{g\Delta\rho D}{2\hat{A}\hat{P}}\right)^{1/2} \qquad Fr = \frac{Q}{(g\Delta\rho D^5/\bar{\rho})^{1/2}} \tag{1.12}$$

As $B \to 0$, the forced flow circumstance, with negligible buoyancy effects, is obtained, and as $B \to \infty$, the pure buoyancy-driven flow, with no externally imposed pressure difference AP, is achieved. Thus, the flow rate Q is to be determined at different dues of B, particularly for the mixed convective circumstance where both transport mechanisms are significant.

In summary, the experimental study quantitatively determined the volume flow rate through horizontal vents over a range of the governing physical parameters AP, Ap and L/D. Employing the fresh-water/salt-water system, the flow exchange was studied both by visualization and by measurement of the transport across the vent. The flow rate Q was obtained as a function of these variables and the results were presented as correlating equations which can be easily applied to modeling of flows in rooms with horizontal vents.

Chapter 2

Experimental System

2.1 Experimental Arrangement

Fig.2.1 and Fig.2.2 show a sketch and a photograph of the experimental arrangement. A rectangular tank has been fabricated with the interior region 0.373m long, 0.432m wide and 0.622m high. The tank is made of plexiglass so as to allow flow visualization, for which a shadowgraph is used. A horizontal plexiglass partition plate located 0.311m above the bottom of the tank divides the tank into an upper compartment and a lower compartment. The lower compartment is filled with pure water and the upper one with brine. The partition plate is bolted with a gasket onto a shelf constructed along the wall. The gasket can effectively prevent leaks between two compartments. At the center of the partition there is an aperture whose cross-sectional area is large compared with the vent openings used in the experiments. A steel frame, which is made of angle iron, is constructed around and underneath the plexiglass tank to support and prevent bulging of the tank.

Two types of openings were employed in the experiments. In one case, the brine-water flow was directed through a simple orifice, which was constructed by cutting a circular hole in a plexiglass or metal plate. In the other, the brine-water flow passed through a plexiglass tube that was bounded by a plexiglass support plate. The plexiglass orifice plate, or the tube support plate, was mounted on the partition. As illustrated in Fig.2.1, the centerline of the orifice or the tube was aligned with the centerline of the aperture cut in the partition. The support plate and the partition were pressed together by six bolts and a rubber gasket. Again, the rubber gasket was to prevent leaks between the compartments. Twelve round openings of different diameters and

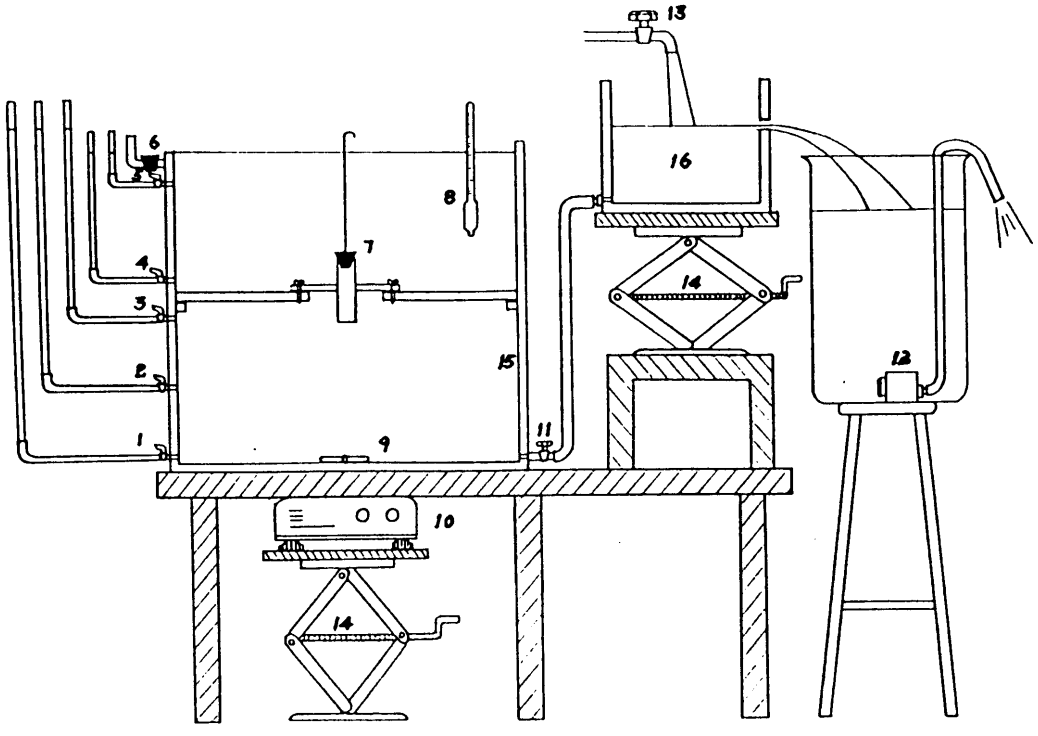

1 ~ 5: Manometers 1 ~ 5.
6: Stopper for overflow notch.
7: Stopper for vent openning.
8: Hydrometer.
9: Magnetic stirring bar
10: Magnetic Mixer.
11: Control valve
12: Suction Pump.
13: Faucet.
14: Lifting jack.
15: Plexiglass tank.
16: Storage tank.

Figure 2.1: Sketch of the experimental set up

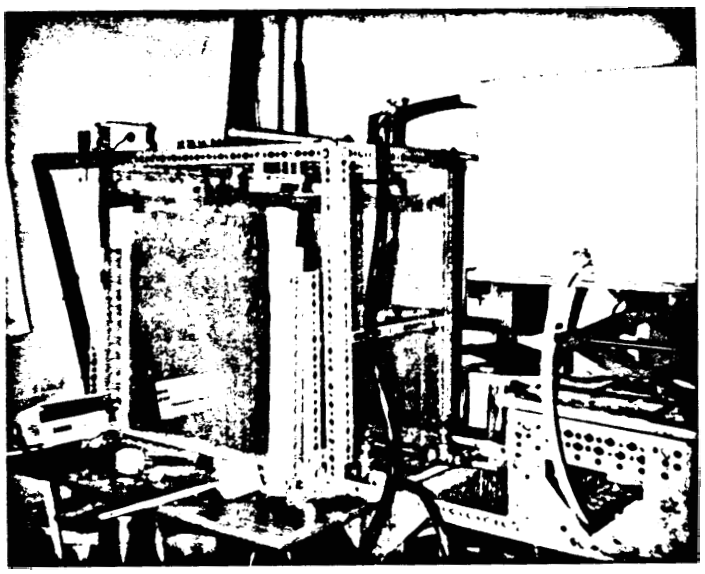

(a) Front view.

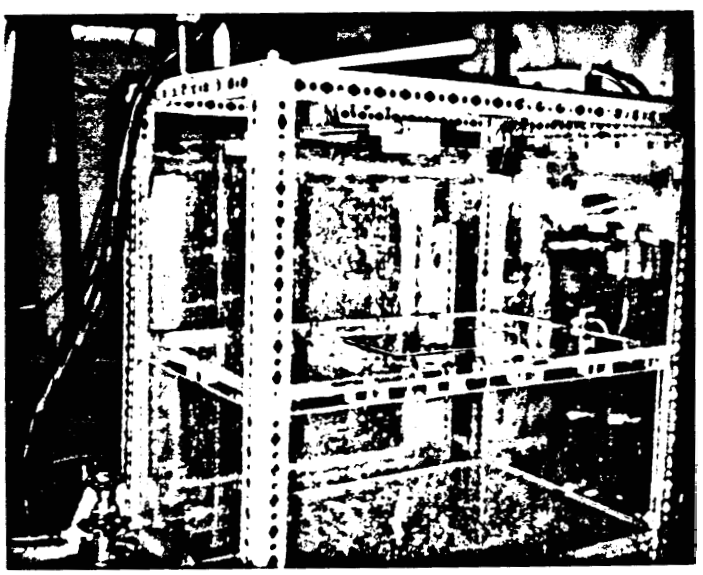

(b) Back view.

Figure 2.2: Views of the experimental set up

lengths were fabricated from tubes or holes cut in the support plate. The diameters of the openings varied from 0.009525 to 0.03175 m, and the length of the openings varied from 0.00127 to 0.076 m. This combination of orifices and tubes resulted in the L/D ratio varying from 0.05 up to 6.008. $L/D < 0.25$ were orifices and L for this configuration actually corresponds to the thickness of the orifices plate. The $L/D > 0.25$ cases were achieved with tubes or ducts, and L for this geometry is simply the tube or duct length. Tests were carried out with average brine densities over the duration of a run in the range of 1025-1180 kg/m^3. The corresponding average density difference ratio range was $\Delta\rho/\bar{\rho} = 0.024$ to 0.17.

A notch is located on the left hand side wall of the tank with its base line 0.572 m above the bottom of the tank. This was designed to maintain the salt water level in the upper compartment at a constant height. The upper compartment is opened to the atmosphere and, therefore, the pressure is simply the hydrostatic distribution in the salt water. A small plexiglass container with a duct at bottom, which is designed to collect the overflow salt water, is attached to the notch (Fig.2.1). It works like a guide tubing for the notch to prevent disturbances to the overflow, and it can be closed at the bottom with a rubber stopper during the miring of the salt water. Thus, it serves as an overflow collecting box.

The pressure difference AP between two compartments was imposed by a translucent plastic storage tank of fresh water. The storage tank was set on a movable platform with a lifting jack underneath it. The bottom of the storage tank was connected to the bottom of the lower compartment's right hand side wall via a tygon tubing with a control valve at the lower compartment end(Fig.2.1). The storage tank also has a notch on the side wall, so it can maintain a constant water level when fresh water enters the tank from a faucet. By vertically moving the storage tank up and down with the lifting jack to a fixed position, and with the control valve being opened, the lower compartment was then pressurized according to the height of the water level in the storage tank. The pressure in the upper compartment is the atmospheric pressure plus the

hydrostatic distribution in the salt water, and the pressure in the lower compartment is the atmospheric pressure plus the water head of the storage tank. Thus, different values of ΔP between two compartments could be obtained. In the experiments, the pressure in the lower compartment was generally kept higher than that in the upper compartment.

Five manometer taps are located on the same side wall of the plexiglass tank with the notch opening. They are all on the vertical center line of the side wall and are 0.0127, 0.1524, 0.2731, 0.3334 and 0.4731 m above the bottom of the tank, respectively (Fig.2.1). Three of them are in the lower compartment while two are in the upper one. These are used to measure the tank pressure at different height locations, and, therefore, the pressure difference ΔP between two compartments can be deduced. By connecting the tap to the manometer through the tygon tubing, the pressure is obtained. The pressure readings were obtained directly from the manometer and also from the differential pressure transducer (Omegabrand, Model PX154-001DI). The pressure transducer was placed at the top of the steel frame and was on the side the closest to the manometer taps. The output of the transducer was connected to a multimeter (Hewlett Packard Brand, Model 3466A) and a chartrecorder (Omegabrand, Model 585) which were placed at lower front comer of the plexiglass tank.

The shadowgraph technique was applied here for visualization purposes. The arrangement used in the shadow method, which is usually attributed to Dvorak(1880), is the simplest of all optical visualizing procedures[25]. As illustrated in Fig.2.3 and Fig.2.4, a projector was placed at the back of the tank while a smoke glass screen was placed in the front. The almost parallel light beam generated by the projector passes through the section around the vent opening. Because of the different deflection of light for different density fluid, a shadow of the density variation is projected onto the screen. One could readily observe the phenomenon or take a photograph of the shadow on the screen. The sharpness of the image obtained on this screen depends on the size of the light source. By tracing the most-separated rays emerging from an extended light

source, one finds that the lack of image sharpness is approximately given by ld/f_1[25], where d is the source diameter, I the distance between the smoke glass screen and the center of the test section, and f_1 the focal length of the lens in the projector. It follows that the light source should be small-not smaller, however, than a certain limit where the lack of sharpness due to diffraction effects becomes appreciable. The projector was placed 1.0m away from the tank and the screen 0.05m in order to get the clearest shadows on the screen.

In order to mix the fluid in the lower compartment after running the experiment, a magnetic stirring mixer(Fisherbrand model 11-500-12SH) was employed. Unlike the upper compartment, the lower compartment of the tank is hard to reach when the opening is closed. Lying at the bottom of the tank, the stirring bar (Magnet) was driven by the magnetic field generated by the mixer underneath the plexiglass tank and fulfilled the task very well without drilling a hole in the lower compartment(Fig.2.1). The mixing is much easier in the upper compartment, since it can be done manually by stirring the brine with a handy mixer.

A drainage hole is located at the bottom comer of the right hand side wall of the plexiglass tank and is connected to a hose via a control valve. This was made to discharge the contents after the experiment.

2.2 Experimental Procedure

2.2.1 General Description

To carry out the experiment, the lower compartment and the storage tank were filled with pure water. The opening(orifice or tube) across the partition was then closed with a rubber stopper and brine was introduced into the upper compartment. The pure water was filled up to the overflow notch of the storage tank and the brine up to that in the upper compartment. The storage tank was brought to a certain height with

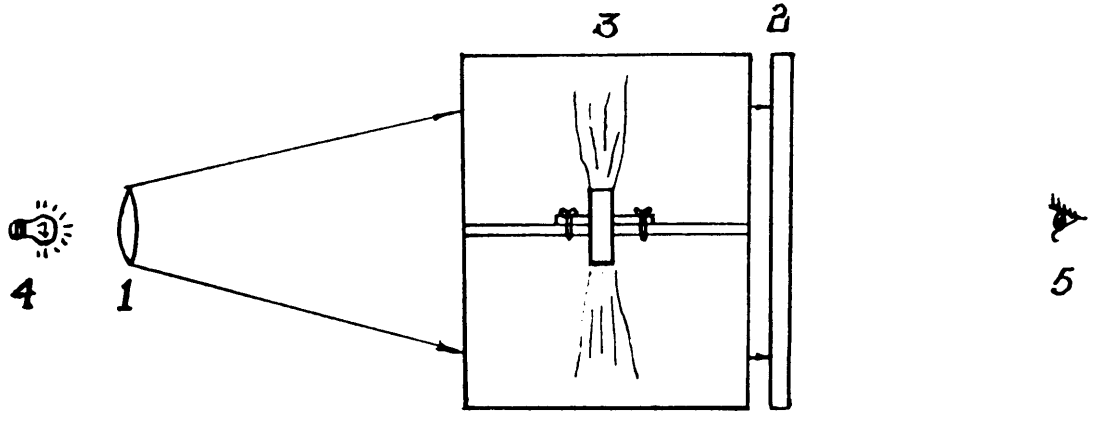

1. Lens in projector.
4. Light source in projector.
2. Smoke glass screen.
5. Camera
3. Test section.

Figure 2.3: Sketch of the shadowgraph arrangement

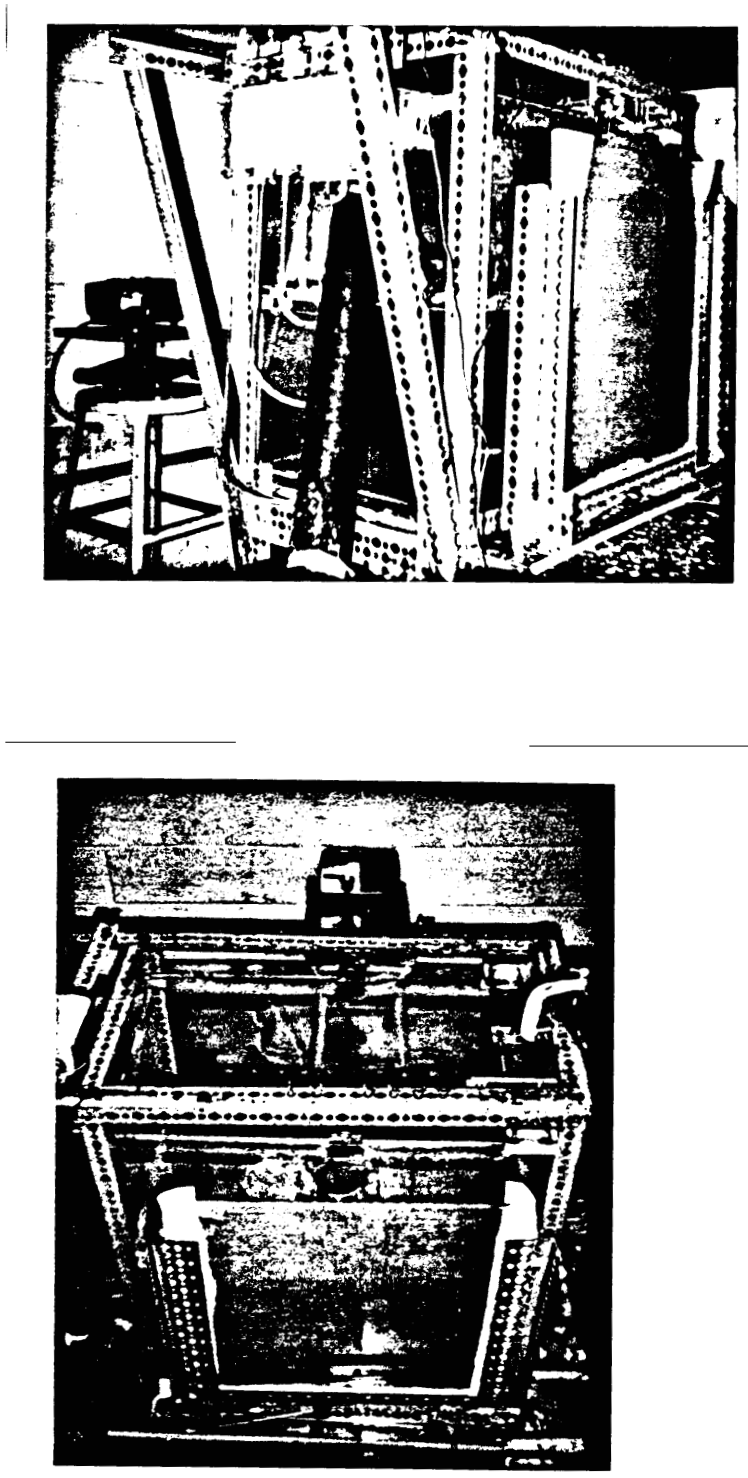

Figure 2.4: Photographs of the shadowgraph arrangement

its water head being maintained at a desired value. The control valve connecting the storage tank and the lower compartment was kept open, so was the opening of the duct in the overflow collecting box.

A run was initiated by removing the rubber stopper. A countercurrent exchange flow or a unidirectional flow of brine or water was observed close to the opening by means of the shadowgraph. The pressures in the upper and lower compartments were measured. The opening was then closed, the brine density in the upper region and the volume overflow rate were measured. All of these were accomplished over regular time intervals. Further details on these measurements are given below.

2.2.2 Density measurement

Hydrometers(Fisher brand Precision Specific Gravity Hydrometers) have been employed in the experiment to determine the brine density. Hydrometers of five different ranges, with the lowest one being from $1.000 kg/dm^3$ to $1.070 kg/dm^3$ and the highest one from $1.240 kg/dm^3$ to $1.310 kg/dm^3$, were used to ensure high accuracy in the density reading. The resolution of the lowest range hydrometer is as small as $0.1 kg/m^3$. This can readily accommodate a $10 kg/m^3$ change of the density during a run.

Each density reading of the brine in the upper compartment was acquired by closing the vent opening after it was opened for a certain amount of time. The overflow salt water collected from the notch was measured and poured back into the upper compartment. The brine solution was mechanically stirred and then the density was carefully measured by the submergence of the hydrometer. The stratification in the upper compartment was corrected by stirring while the lower region was made uniform by the magnetic stirring mixer. It was assumed that they were both fully mixed, so the density in the lower compartment could be determined from the density in the upper one by employing mass conservation.

2.2.3 Pressure Measurement

Since the pressure difference ΔP between the two compartments is very small and since salt water is incompatible with most pressure measurement instruments on the market, a considerable effort was made to obtain a suitable pressure measurement device. An Omega brand (Model PX154-001DI) low differential pressure transducer was employed in the experiment for the sake of its reasonable cost and high accuracy. The resolution of the transducer is as low as 0.1% of the full scale which is one volt for zero pressure difference and five volts for a one inch water high pressure difference. Since it is only compatible with air, it could not be directly connect to salt water, this could damage the diaphragm of the transducer. As shown in Fig.2.5 and Fig.2.6, the high pressure end of the transducer was connected to tap3, which is the one in the lower compartment and is the one nearest to the partition plate, that is, the closest to the opening where the flow exchange occurs. Instead of directly connecting the water to the transducer, an air column was left at the top of the water column.

Since in the experiment, the brine level in the upper compartment is constant due to the overflow at the notch, the pressure in the upper compartment is constant except for the hydrostatic difference. This was verified later by the manometer readings in the upper compartment, which indicate that only hydrostatic pressure variation exists in the upper region with liquid columns in the manometers being the same as the brine level in the upper compartment. So for simplicity, only the high pressure end of the transducer was connected to tap3 and the lower pressure end of the transducer was left open to the atmosphere. Thus, the pressure value obtained from the transducer was the lower compartment's relative pressure to the atmosphere at location tap3. The pressure in the other locations of the lower compartment can be deduced from this value by employing hydrostatics.

Because of the air column and position of the transducer being higher than that of tap3, the reading obtained directly fiom the transducer is not the real pressure value

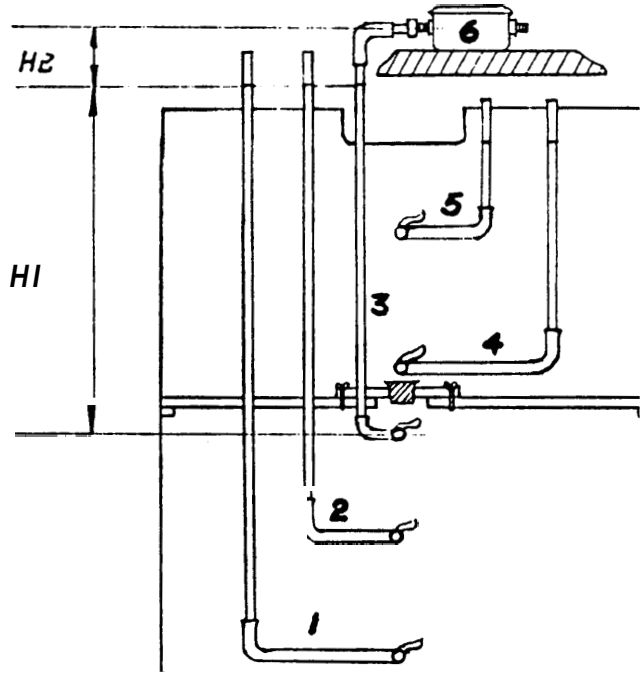

1 - 5: Manometers 1- 5.

6: Pressure transducer.

Figure 2.5: Sketch of the pressure measurement arrangement

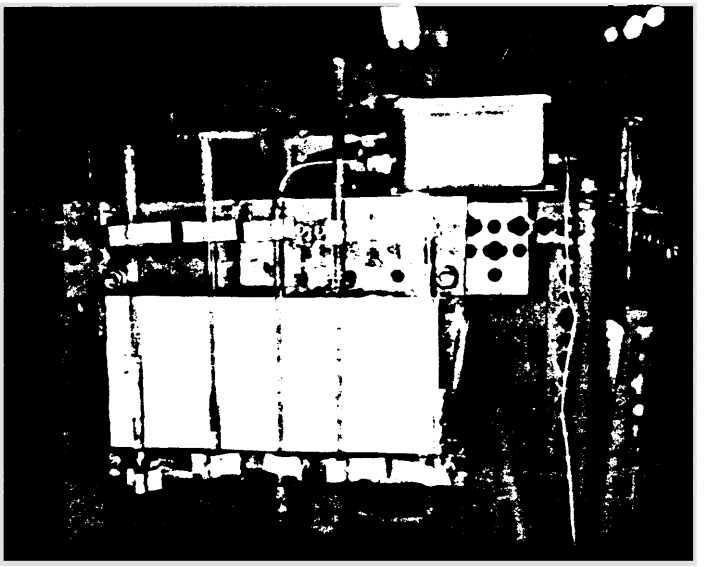

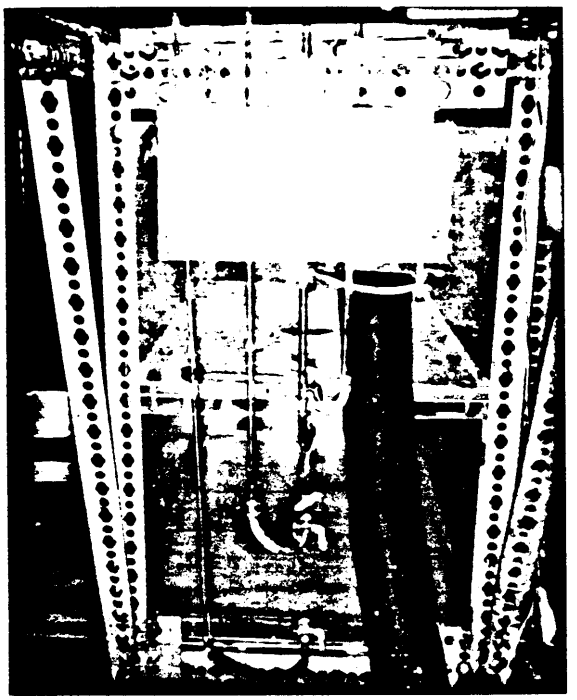

Figure **2.6:** Photographs of the pressure measurement arrangement

at tap3(Fig.2.3), actually it is $P_{tap3} - \rho_{BOT} g H_1 - \rho_{AIR} g H_2$. Since ρ_{AIR} is much less than ρ_{BOT}, the last term can be neglect. Anyway, the transducer can measure the pressure change due to the depression and expansion of the air column, which is caused by the changing of the water column, once it was calibrated. The temperature was essentially constant and the thermal expansion effect of air column is negligible. Therefore, the exact water column change can be obtained and used to figure out the real pressure value by using the static pressure formula. The manometer readings from tap1 and tap2 helped us to check if the transducer reading was within the right range.

To calibrate the transducer, the lower compartment manometer readings were set at the same value as the upper one by moving the storage tank. This implied that all the five manometers readings were aligned with the brine level in the upper compartment. At this time, both ends of the transducer were left open to the atmosphere. The output was one volt representing zero pressure difference. Next, the tube of the manometer3 was connected to the high pressure end of the transducer by a quick connection fitting while the other end of transducer was still left open to the atmosphere. Because of the sudden sealing, there was either vacuum or extra pressure inside tube connection which changed the output of the transducer away from one volt. The reading was brought back to one volt by turning the zero adjustment button of transducer with a screwdriver. Then the storage tank was raised to set the lower compartment manometer readings 0.0254m (1 inch) higher than the upper one. This can be accomplished by observing the other two manometer readings in the lower compartment rather than manometer3, because of the inaccuracy caused by the air column. The full span adjustment button of the transducer was adjusted with the screwdriver to bring the reading back to five volts, if it is not, which represents a one inch water pressure difference (248.92 N/m^2). This procedure was repeated several times to make sure that the reading of the transducer is one volt with cero pressure difference and five volts with one inch water pressure difference while the storage tank was moved up and down.

While doing the experiment, the lower compartment manometer level was brought

to the desired value according to the transducer reading. As the stopper was removed, the water columns of the lower compartment manometers dropped because of the pressure loss in the connection between the storage tank and the lower compartment. This variation was measured precisely from the chartrecorder and the multimeter which were connected to the transducer. Thus the pressure difference over the duration of a run was obtained accordingly. Results from experiments performed for the same conditions indicated that the repeatability of the pressure measurement was within ±1.0 percent.

2.2.4 Fluid Overflow Measurement

The volumetric overflow measurement is relatively easier. This was done by using a beaker, which was placed underneath the overflow collecting box, to collect the brine that overflows the notch in the upper compartment during each experimental run. After the running time was over and the vent opening was closed, usually there was still some continuous brine overflows because of the surface tension at the notch. The duct of the overflow collecting box was closed with a rubber stopper when it was confirmed that there was no more brine overflow. The total overflow rate was obtained by measuring the amount of brine in the beaker with a measuring cup. This overflow salt water was then poured back into the upper compartment before stirring the brine. Once the density measurement was carried out, the extra amount of brine was drained out through the duct at the bottom of the overflow collecting box by removing the stopper.

Chapter 3

Results and Discussion

3.1 Preliminary Experiments

Before discussing the results, the definition of the governing parameters is given below with reference to Fig.3.1, for combined natural and forced convection flow through a horizontal vent. Q_U is the volume flow rate of the fluid from the lower compartment to the upper compartment, Q_D is the volume flow rate of the brine from the upper compartment to the lower compartment, Q_I is the volume flow rate of the fresh water from the storage tank, whose vertical positioning is used for the pressurization of the lower compartment, and Q_O is the volume overflow rate of the brine at the overflow notch in the upper compartment. Therefore,

$$Q_O = Q_I \tag{3.1}$$

Q_N is the net upward volume flow rate across the vent opening and,

$$Q_N = Q_U - Q_D = Q_O = Q_I \tag{3.2}$$

P_H is the static pressure at the elevation of the top surface(upper compartment side) of the support plate, P_L is the static pressure at the elevation of the bottom surface(lower compartment side) of the support plate, both pressure were measured after the vent was opened, and $\Delta P = P_L - P_H$. Also, ρ_H is the density of the fluid in the upper Compartment and ρ_L is the density of the fluid in the lower compartment. The fluids in the two regions are well mixed before opening the vent as well as after the vent is closed following an experiment.

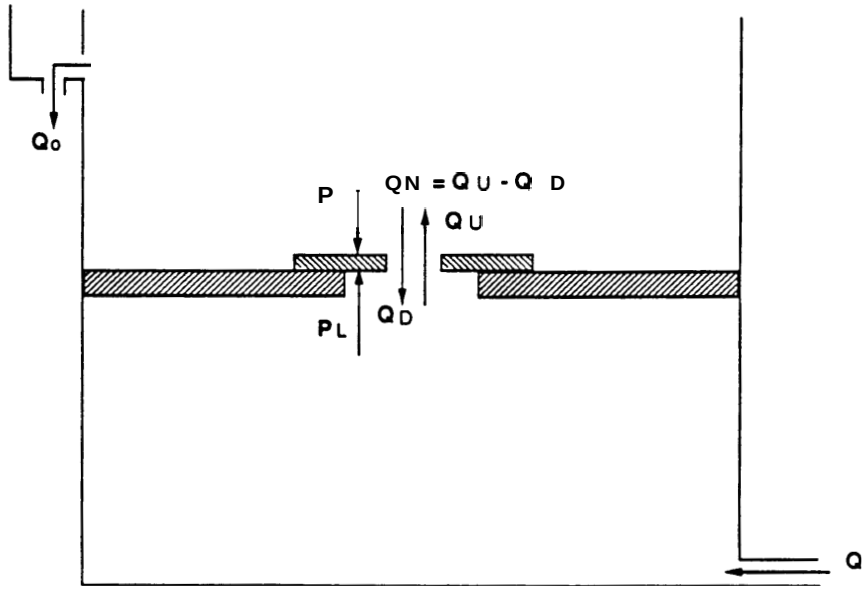

Figure **3.1:** Combined natural and forced convection **flow** through a horizontal vent.

3.1.1 Experiments for $\Delta P = 0$.

Some preliminary experiments have been carried out for the circumstance of zero pressure difference across the vent. The upper compartment was filled with brine and the lower compartment with pure water. The control valve which connects the storage tank and the lower compartment together being kept closed. Thus, no external pressure is applied to the lower compartment. The length to diameter ratio L/D of the vent was varied, as was the initial brine density in the upper compartment. The exchange volume flow rate Q, which is the volume flow rate at zero ΔP, was thus measured for a range of L/D and $\Delta\rho$. Obviously, there is a hydrostatic pressure difference across the opening support plate due to the plate thickness and the density difference across the plate. Here, A P = 0 means that the external imposed pressure difference is equal to zero. Since there is no overflow Q_O,

$$Q_O = Q_I = Q_N = 0 \tag{3.3}$$

Thus,

$$Q = Q_U = Q_D \tag{3.4}$$

according to Eqn.(3.2).

Photographs of the flow exchange phenomenon obtained from the shadowgraph are shown in Figures 3.2(a) and 3.2(b) for two different vent openings. A vigorous flow exchange was observed to occur in a cylindrical region with its axis coinciding with the axis of the vent opening. The brine enters the lower compartment, seen as a plume flow region in the lower half portion of the picture, due to the buoyancy force. Fresh water enters the upper compartment, seen as a plum flow region in the upper half portion of the picture, due to the mass conservation. The flow exchange looks similar to a jet injection circumstance, but the speed is much lower, since it is due to natural convection arising fiom the density difference between the two compartments.

The volume exchange flow rate (in $m^3 s^{-1}$) fiom the upper compartment to the lower compartment, or vice versa, in terms of the rate of dilution of the brine can be shown

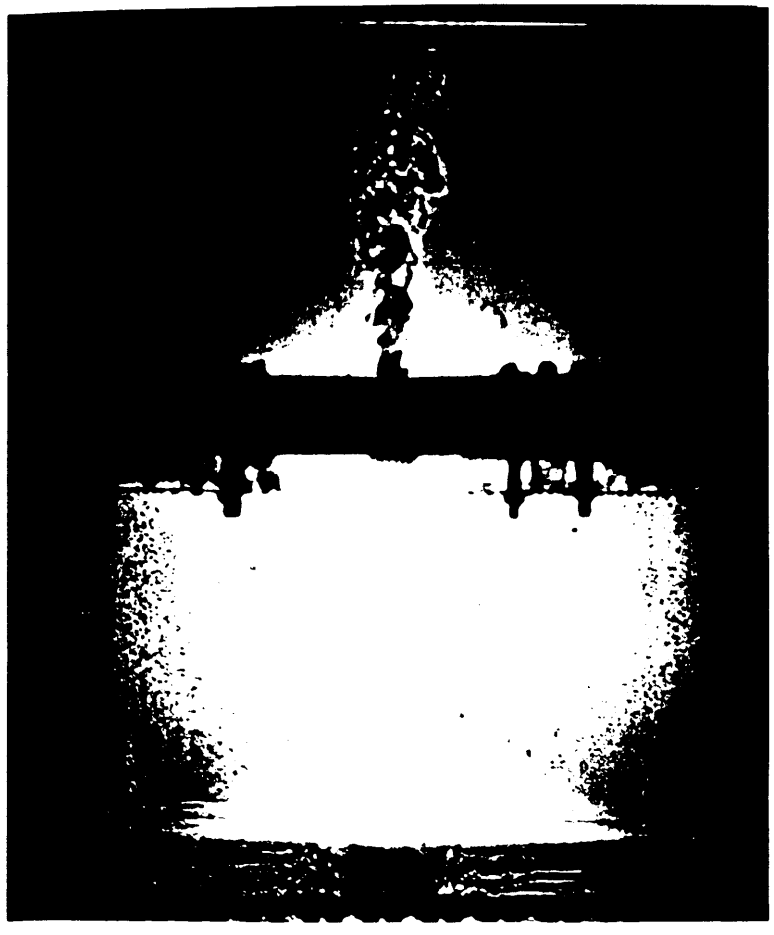

(a) $\rho_{H,O} = 1049.2\ (kg/m^3)$, $\rho_{L,O} = 1009.6\ (kg/m^3)$,

D = 0.0445 (m), L/D = 1.0

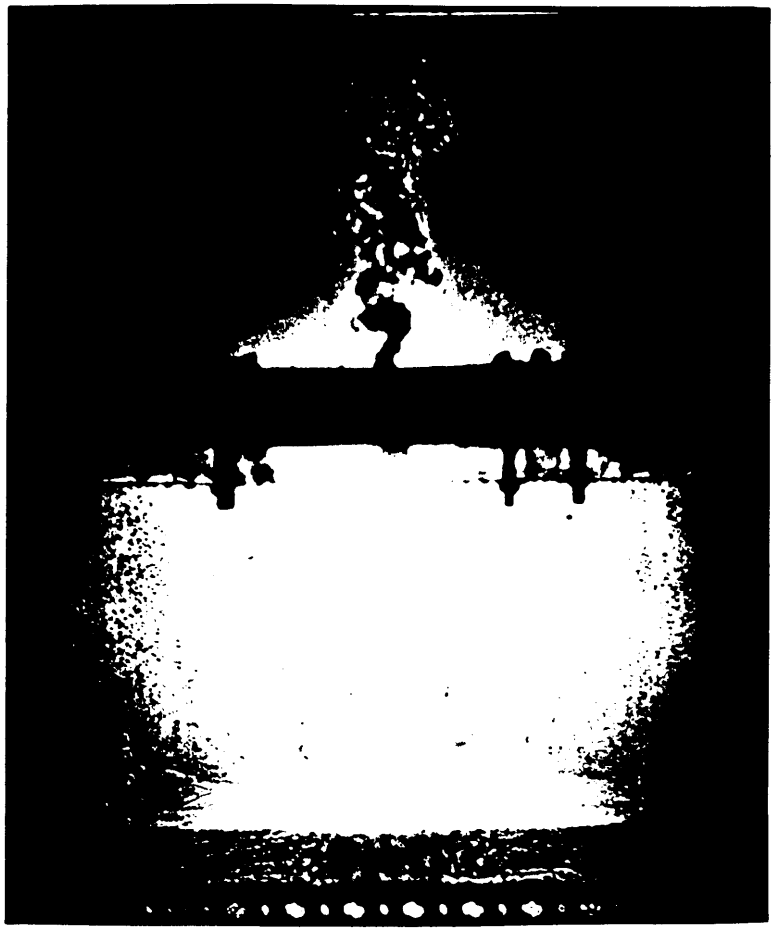

(b) $\rho_{H,O} = 1091.5\ (kg/m^3)$, $\rho_{L,O} = 1007.3\ (kg/m^3)$,

D = 0.0254 (m), L/D = 1.0

Figure 3.2: Shadowgraph photographs for the experiments with $\Delta P = 0$.

to be given by(see appendix A):

$$Q = \frac{-V_H(d\rho_H/dt)}{(\rho_H - \rho_{L,0}) - \frac{V_H}{V_L}(\rho_{H,0} - \rho_H)} \tag{3.5}$$

where V_H and V_L are the volume of the heavier liquid (brine) in the upper compartment and the volume of the less dense liquid (water) in the lower compartment, respectively, ρ_H is the density of the brine solution at time t, and $\rho_{L,0}$ and $\rho_{H,0}$ are the densities of the contents of the water- and brine-Wed compartments at zero time. Thus, to obtain Q, ρ_H was plotted against time t and derivative obtained.

Two typical plots of the brine density variation with time, with density measured by the hydrometers, as mentioned earlier, are shown in Fig.3.3 and 3.4, respectively. In each figure, two experiments were carried out with the same L/D ratio but different initial brine density $\rho_{H,0}$. The total duration of the experiment (or the total number of individual density measurements) was selected to obtain the brine density variation as a linear function of time. Best-fit curves were obtained for these linear segments of the density-time plots, and the volume rate of exchange flow were thus calculated from Equ. (3.5). Note that each density measurement represents opening the vent for a specified time interval, mixing the fluid region after closing the vent and measuring the resulting density.

As can be seen fiom the figures, for the same L/D ratio, the increase of the initial brine density $\rho_{H,0}$ in the upper compartment gives rise to an increase in the absolute value of the slope $d\rho_H/dt$. This is reasonable, because higher the $\rho_{H,0}$, the stronger is the buoyancy force. Thus, the dilution of the brine in the upper compartment, which is determined by the exchange flow rate Q and is reflected in the rate of decrease in ρ_H, is also faster at larger initial density difference. According to Eqn.(3.5), the exchange volume flow rate Q is larger if the rate of decrease in ρ_H concentration is greater.

In Figures 3.5 and Fig.3.6, the volume exchange flow rate Q is plotted in the form

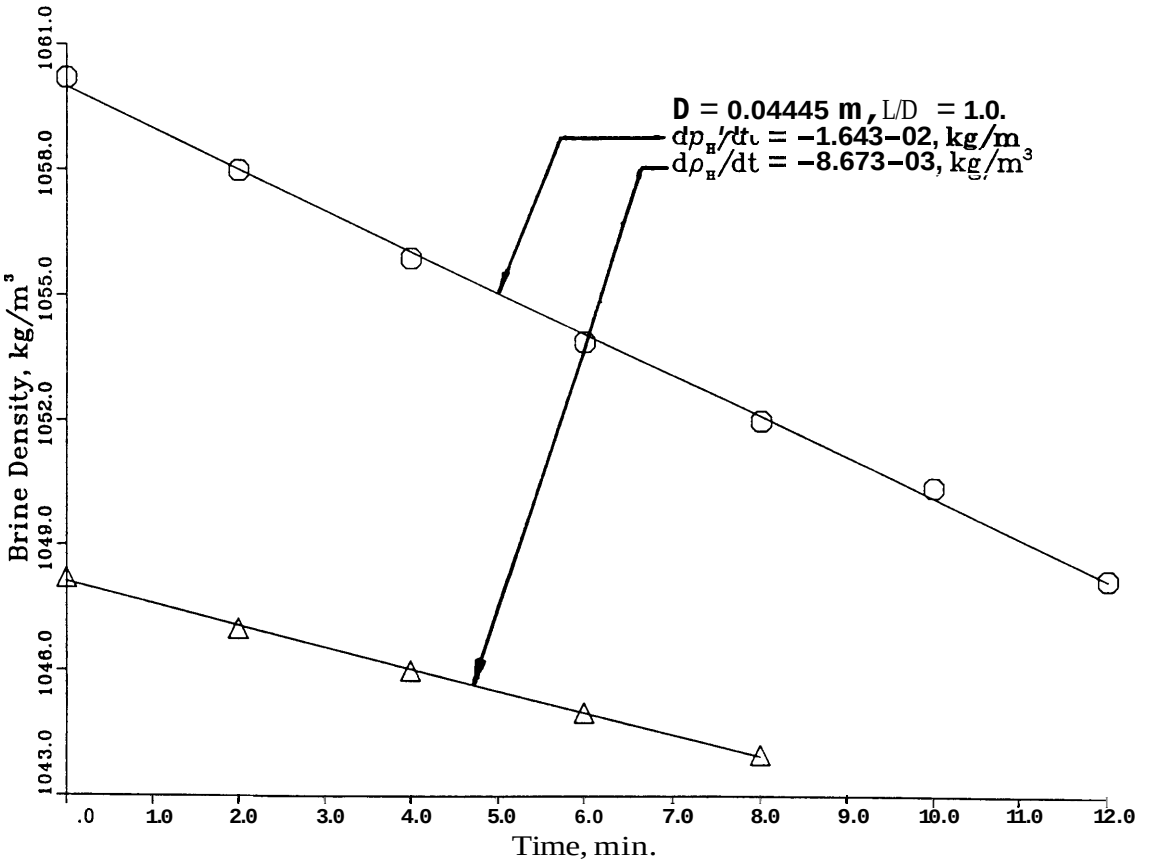

Figure 3.3: Brine density versus time for $\Delta P = 0$ and $L/D = 1.0$.

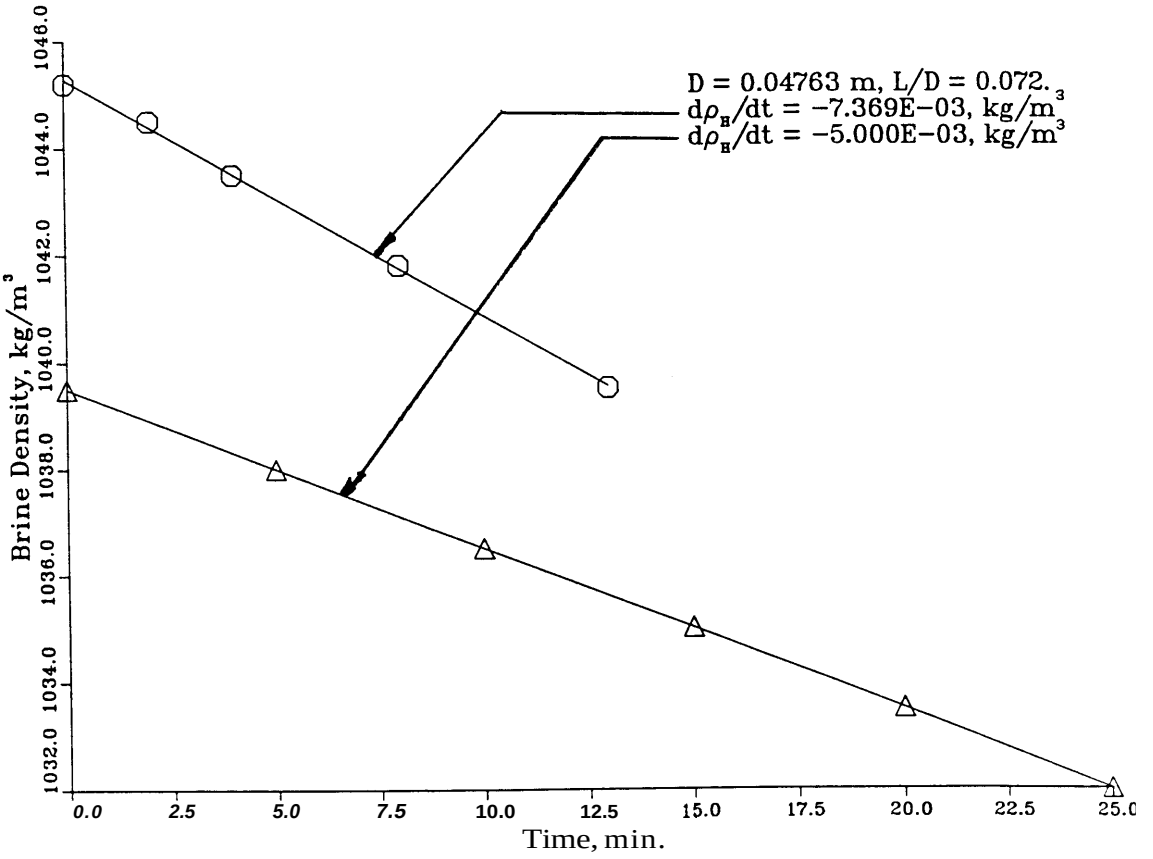

Figure 3.4: Brine density versus time for $\Delta P = 0$ and $L/D = 0.072$.

of a dimensionless Froude number, $Fr = Q/(g\Delta\rho D^5/\bar{\rho})^{1/2}$, as a function of the length-to-diameter ratio of the opening **L/D** for two different sets of experiments. For the first set of experiments, the opening diameter ranged from 0.032m to 0.048m and the density difference ratio from 0.03 to 0.09. While for the second set of experiments, the opening diameter chosen was 0.0127m and the density difference ratio was fiom 0.05 to 0.08. Actually, with increasing time t, the brine is diluted because of the flow of the water from the lower compartment, and the density in the lower compartment gets higher because of the flow of the brine from the upper compartment. Thus, the density difference $\Delta p = \rho_H - \rho_L$ across the vent decreases with increasing time t. So, in the calculation of the Froude number Δp is taken as the averaged value over the duration of the entire experiment. Also plotted in Fig.3.5 and Fig.3.6 are the flow exchange data obtained by Epstein[19] with brine/water as the working fluid. The range of the opening diameter and density difference ratio of his experiment was 0.025m to 0.048m and 0.03 to 0.17, respectively. The experimental conditions and the measured exchange flow rates Q are given in Table 3.1.

For the first set of experiments, the range of the opening diameter D and the average density difference ratio $\Delta\rho/\bar{\rho}$ are within the corresponding range of earlier studies. As shown in Fig.3.5., a comparison with the earlier work on this circumstance indicates fairly good agreement. The dependence of Q on L/D follows the trend predicted by analysis in the earlier study, lending support to these measurements. The experimental results were found to be repeatable to within $\pm$ 1.0 percent, indicating accurate measurement of the flow rate Q by the chosen procedure.

For the second set of experiments, the opening diameter employed was much smaller than those used in the earlier work. Interestingly enough, in Fig.3.6, it is seen that much higher Froude numbers arise for smaller diameter vents than those obtained in the earlier work with larger diameters. However, the trend of the dependence of Q on L/D is similar to the one obtained in the earlier study. This difference for small diameters may be due to the way the dimensionless exchange flow rate, $Fr = Q/(g\Delta\rho D^5/\bar{\rho})^{1/2}$,

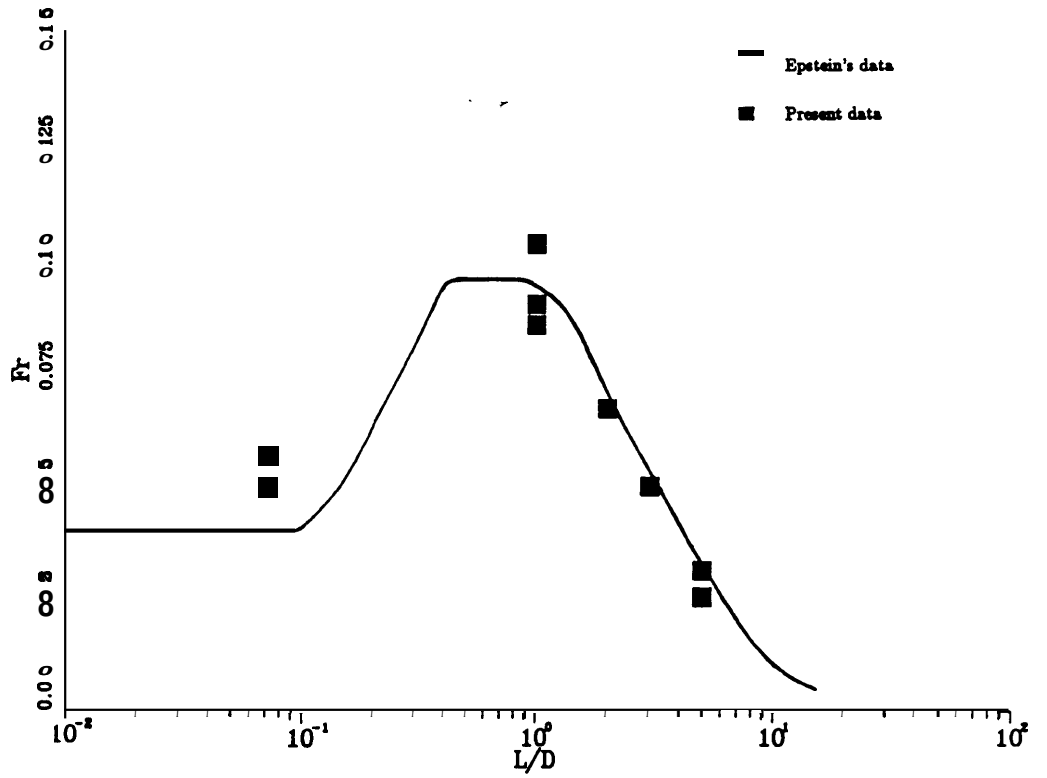

Figure 3.5: Experimental results for countercurrent exchange flow through a horizontal vent for $\Delta P = 0$ (data set I).

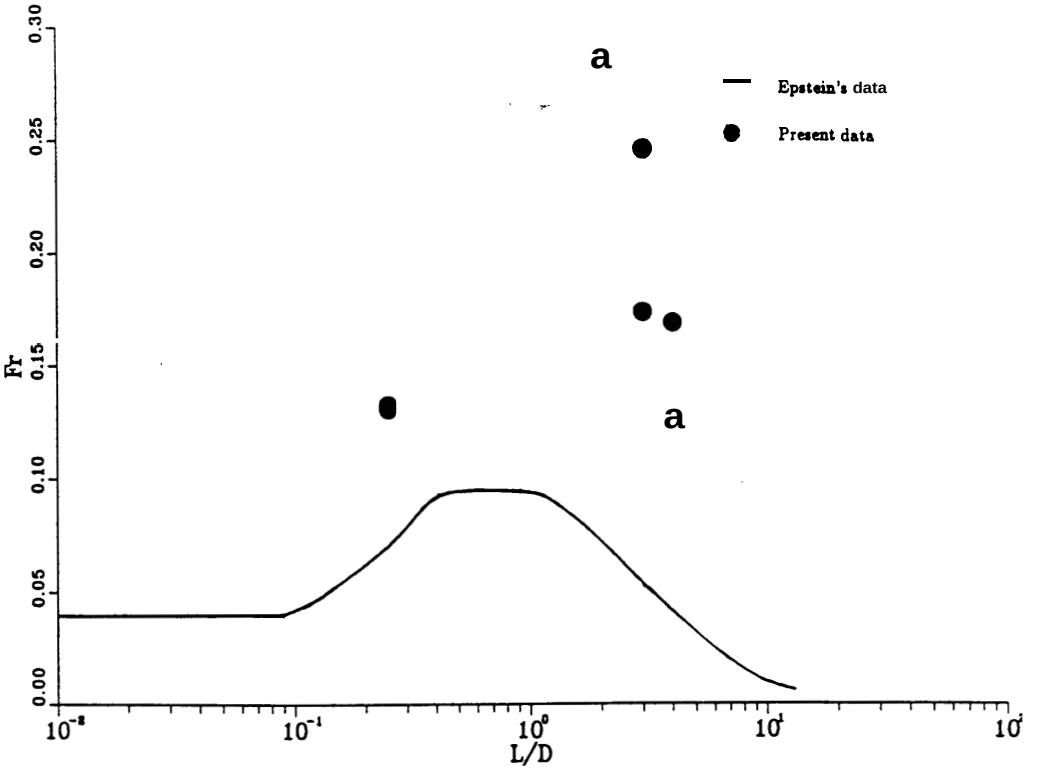

Figure 3.6: Experimental results for **countercurrent exchange flow through a horizontal vent** for $\Delta P = 0$ **and very small vent diameter,** $D = 0.0127$ m **(data set II).**

Table 3.1: **Measured Buoyancy-Driven Exchange Flow Through a Horizontal Vent** $(\Delta P = 0)$

Opening	D(m)	L(m)	$\rho_H(kgm^{-3})$	$\rho_L(kgm^{-3})$	$Q(m^3s^{-1})$ x 10^{-6}
Orifice	0.0476	3.43×10^{-3}	1045.2	1000.2	15.07
Orifice	0.0476	3.43×10^{-3}	1039.5	1004.8	14.43
Orifice	0.0127	3.18×10^{-3}	1051.5	1000.0	1.66
Orifice	0.0127	3.18×10^{-3}	1099.0	1000.5	2.28
Tube	0.0445	0.0445	1060.2	1000.0	28.42
Tube	0.0445	0.0445	1048.2	1009.6	20.29
Tube	0.0445	0.0889	1049.5	1000.0	17.65
Tube	0.0445	0.1333	1049.5	1000.0	13.32
Tube	0.0318	0.0159	1033.5	1002.8	2.91
Tube	0.0318	0.0159	1032.8	1003.4	2.36
Tube	0.0254	0.0254	1091.5	1007.3	8.06
Tube	0.0127	0.0254	1051.4	1000.0	3.54
Tube	0.0127	0.0350	1048.5	1000.0	2.10
Tube	0.0127	0.0350	1099.5	1000.0	3.48
Tube	0.0127	0.0508	1110.0	1000.0	3.06
Tube	0.0127	0.0508	1052.5	1000.0	0.78

is calculated. Though the numerator Q decreases because of the smaller diameter, the $D^{5/2}$ in the denominator decreases even faster leading to higher Froude numbers. This implies that the nondimensionalization for very small diameter vents may have to be done differently. Also surface tension effects may become significant at these diameters.

Since the current work is largely directed at the flow exchange with nonzero external pressure difference **AP** across the vent, only limited data with $\Delta P = 0$ were obtained. The range of the **L/D** ratio and the density difference **Ap** investigated here may not appear to be wide enough to establish the generality of Figure **3.6.** However, results fiom experiments performed for the same conditions indicated that Fr was reproducible to within ±1.0 percent leading support to the accuracy of the data obtained.

3.1.2 Experiments for Unstratified Situation, $\Delta\rho = 0$

Some preliminary experiments have been carried out for the unstratified circumstance, $\Delta\rho = 0$. The upper and lower compartment were both filled with pure water, and the pressure was applied to the lower compartment by raising the storage tank. There is no buoyancy exchange flow but an upward forced flow Q_U arises due to the pressure. Also, Q_D is equal to zero in this case. Therefore,

$$Q_N = Q_I = Q_O = Q_U \tag{3.6}$$

The volume overflow rate Q_O was measured for different values of the pressure difference **AP** across the vent opening. Here **AP** is the pressure head maintained by the storage tank. The dependence of Q_O on **AP** is shown in **Fig.3.7(a).** It is obvious that an increase in **AP** gives rise to an increase in Q_O, as expected. This variation of Q_O with **AP** can be used to develop a correlating equation which will allow an exhibition of velocity across the vent at large pressure difference. This is the standard vent flow model which was discussed earlier and which is based on Bernoulli's equation. For forced flow through the vent opening due to a pressure difference, Bernoulli's equation gives an estimate for the velocity across the vent as: $[2(\Delta P - g\rho_{water}\Delta H)/\rho_{water}]^{1/2}$.

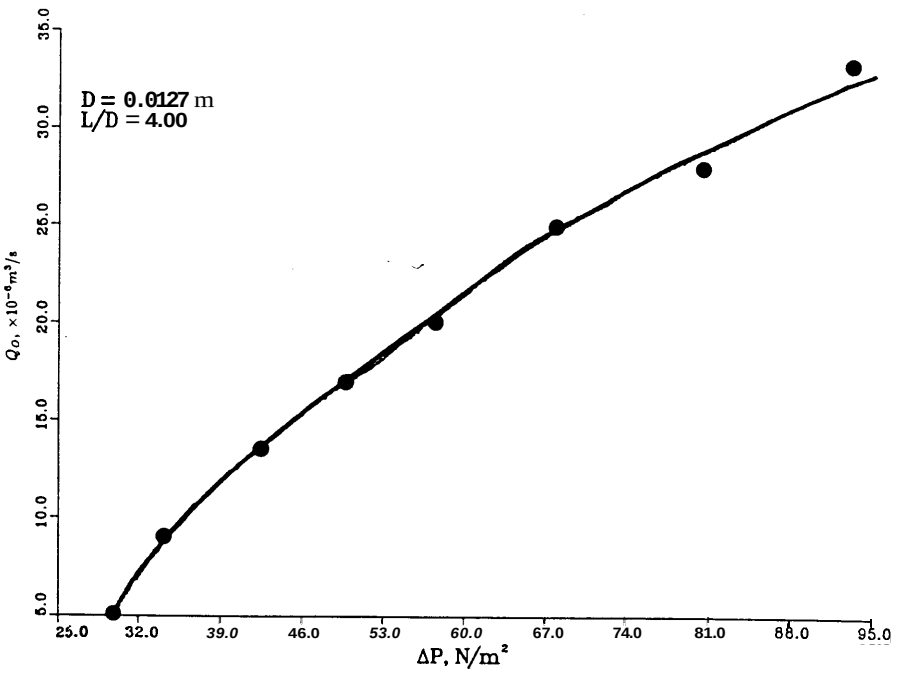

Figure 3.7(a): Experimental results for the unstratified situation, $\Delta\rho = 0$: Volume flow rate Q_O versus ΔP.

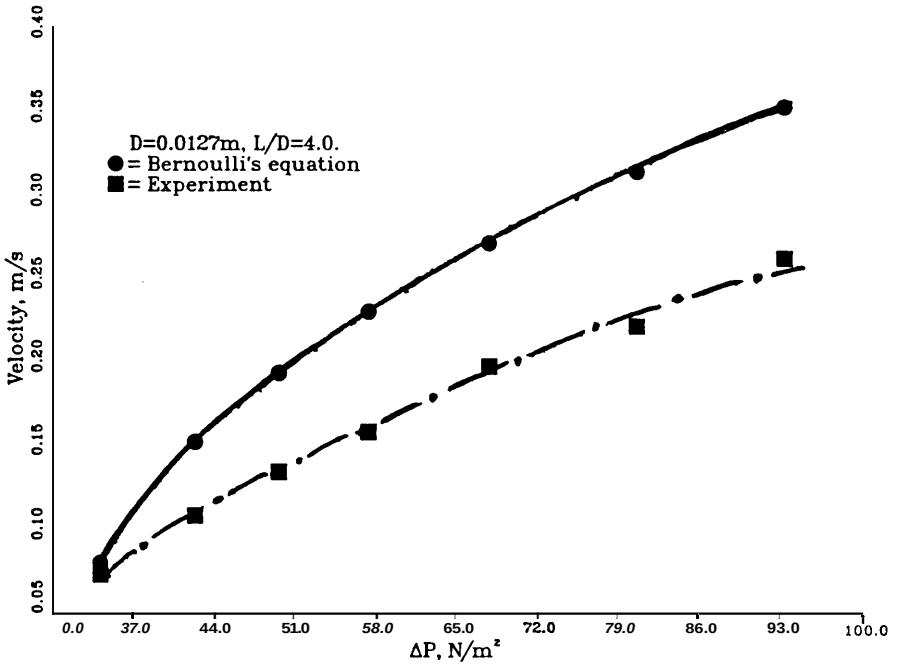

Figure 3.7(b): Experimental results for the unstratified situation, $\Delta\rho = 0$: Velocities obtained by two different methods versus ΔP.

Where ρ_{water} is the density of the pure water, AH the thickness of the opening support plate. Also, from the volume overflow rate Q_O obtained, average velocity across the vent opening is calculated as: Q_O/A_V, where A_V is the vent area. Velocities calculated from the Bernoulli's equation and from the volume overflow rate Q_O are plotted in Fig.3.7(b). As shown in the figure, the former one are substantially higher than the later one, since Bernoulli's equation is an ideal equation, it doesn't count the pressure loss and any other loss caused by the disturbance of the flow. In fact, a flow coefficient C_D should be taken into consideration, as described by the standard vent flow model [Eqns.(1.3)~(1.5)].

3.2 Purging Flow Experiments

Conditions for unidirectional flow between the spaces connected by a horizontal vent opening had been determined by purging flow experiments. The upper and lower compartment contain brine solution and fresh water, respectively. Each experimental run involved a unidirectional upward flow of fresh water, from the lower compartment, at measured pressure difference A P across the opening and volume overflow rate Q_O at the notch of the upper compartment. Here A P = $P_L - P_H$ is the static pressure Merence across the support plate for the vent opening. Therefore it includes the hydrostatic pressure difference and the pressure difference due to the imposed external force.

In each experiment, fresh water flows into the lower Compartment through the control valve at the bottom of the lower compartment due to the pressure head maintained by the storage tank(see Fig.2.1). An equivalent volumetric flow of the brine overflows from the upper compartment across the overflow notch. At small A P, a limited amount of brine solution Q_D was observed to flow downward through the opening against the upward fresh water flow. In this case, the A P was not strong enough to completely overcome the buoyancy force due to the density difference $\Delta\rho$ across the opening. At higher A P, the brine solution was prevented from flowing across the opening. This situation was evident by the absence of any sign of brine solution below the opening,

either as a plume or in the form of individual packets(drops) of fluid. The shadowgraph technique was applied here for the observation of these transient pressure. The flooding or purging condition was determined as a ΔP value that represented a transition from countercurrent, or bidirectional flow to a unidirectional flow.

For openings of small L/D, the purging condition was detected by adjusting the pressure head of the storage tank so that the downward flow rate of the brine solution was reduced to a very slow rate of release of brine fluid packets into the lower compartment, ultimately reducing to zero downward flow. With the tube opening (high L/D) it was possible to adjust the A P so that the brine - water mixing zone filled the tube without any net downflow of brine solution.

The pressure difference A P that produced this condition of zero downward buoyancy driven flow was defined and recorded as the purging (or flooding) pressure ΔP_{FLOOD}, and the unidirectional upflow rate of the fresh water Q_U was therefore the flooding flow rate. Thus, since $Q_D = 0$, we have:

$$Q_{FLOOD} = Q_U = Q_I = Q_O \tag{3.7}$$

In Fig.3.8, shadowgraph pictures taken from the purging flow experiments show the transition from a bi-directional flow to a uni-directional flow. As ΔP approaches the value of ΔP_{FLOOD}, but with the pressure difference lower than the purging value, tiny down flow of the brine solution was observed as a plume in the lower compartment(Fig.3.8a). As ΔP was maintained at ΔP_{FLOOD} or little higher, a uni-directional upflow of the fresh water was found to arise with no observable downflow. (Fig.3.8b).

The measured flooding pressure ΔP_{FLOOD}, flooding flow rate Q_{FLOOD} and the experimental variables are presented in Table 3.2. The dependence of ΔP_{FLOOD} on the buoyancy force $gApD$ for two different vent opening diameters and various L/D ratios

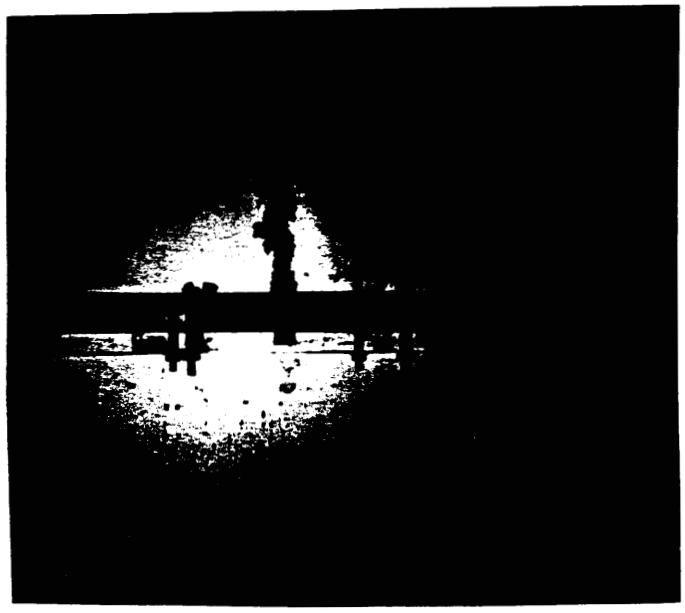

(a) D = 0.0127, L/D = 2.75, $\rho_{H,O} = 1062.5(kg/m^3)$, AP = $45.92(\mathrm{N}/m^2)$

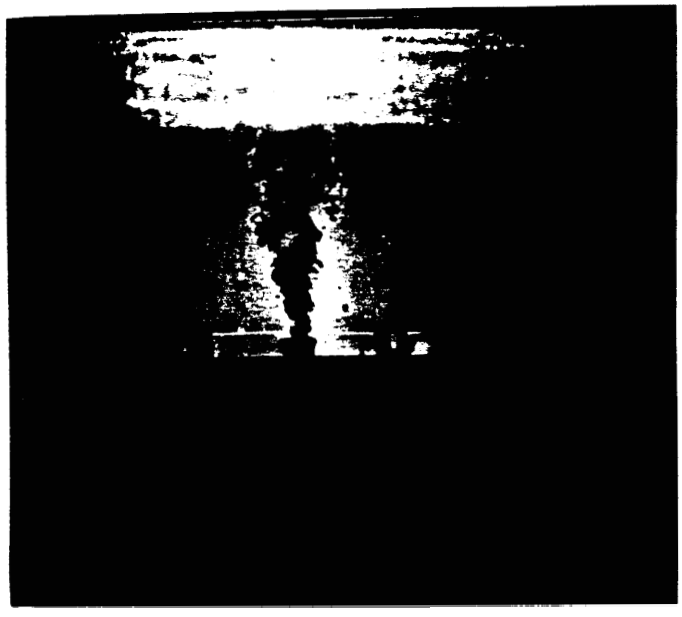

(b) D = 0.0127, L/D = 2.75, $\rho_{H,O} = 1062.5(kg/m^3)$, $\Delta P = \Delta P_{FLOOD} = 53.70(\mathrm{N}/m^2)$

Figure 3.8: Shadowgraph pictures of purging flow experiments: Uni-directional up flow.

Table 3.2: **Measured Uni-directional Purging Flow Through a Vent Opening, while** $\rho_L = 1000.0 kg/m^3$.

Opening	D(m)	L(m)	$\rho_H(kgm^{-3})$	$\Delta P_{FLOOD}(Nm^{-2})$	$Q_{FLOOD}(m^3s^{-1}) \times 10^{-6}$
Orifice	0.0159	1.27×10^{-3}	1048.0	49.01	6.08
Orifice	0.0159	1.27×10^{-3}	1068.0	50.49	12.46
Orifice	0.0159	1.27×10^{-3}	1094.0	56.86	11.50
Orifice	0.0159	1.27×10^{-3}	1128.6	63.57	15.92
Orifice	0.0159	1.27×10^{-3}	1168.0	69.01	16.92
Tube	0.0159	0.0159	1040.5	43.88	11.21
Tube	0.0159	0.0159	1054.0	58.13	15.80
Tube	0.0159	0.0159	1098.4	72.83	23.83
Tube	0.0159	0.0159	1147.0	80.73	20.00
Tube	0.0159	0.0159	1183.5	82.88	26.17
Tube	0.0127	0.0762	1059.5	32.79	1.19
Tube	0.0127	0.0762	1063.5	33.61	5.26
Tube	0.0127	0.0762	1067.5	35.71	9.56
Tube	0.0127	0.0762	1094.5	37.23	4.48
Tube	0.0127	0.0762	1180.5	38.06	7.08
Tube	0.0127	0.0508	1047.5	45.31	7.73
Tube	0.0127	0.0508	1068.0	48.35	6.25
Tube	0.0127	0.0508	1095.9	50.16	6.15
Tube	0.0127	0.0508	1112.0	51.13	7.40
Tube	0.0127	0.0508	1126.0	50.62	12.83
Tube	0.0127	0.0508	1151.0	51.84	5.22
Tube	0.0127	0.0350	1031.6	57.42	8.92
Tube	0.0127	0.0350	1050.5	59.62	6.61
Tube	0.0127	0.0350	1088.6	62.59	15.25
Tube	0.0127	0.0350	1112.6	63.34	14.83
Tube	0.0127	0.0350	1147.0	65.86	9.12
Tube	0.0127	0.0127	1029.6	46.63	10.25
Tube	0.0127	0.0127	1062.5	53.70	12.75
Tube	0.0127	0.0127	1088.0	58.79	13.50
Tube	0.0127	0.0127	1111.5	64.84	19.33
Tube	0.0127	0.0127	1146.5	73.41	18.50
Orifice	0.0127	3.18×10^{-3}	1035.7	44.93	5.67
Orifice	0.0127	3.18×10^{-3}	1061.6	49.97	10.50
Orifice	0.0127	3.18×10^{-3}	1087.0	55.60	10.58
Orifice	0.0127	3.18×10^{-3}	1116.3	56.27	11.64
Orifice	0.0127	3.18×10^{-3}	1145.0	57.03	8.87

are shown in Fig.3.9(a) and Fig.3.9(b), respectively. As seen in Fig.3.9, the purging pressure ΔP_{FLOOD} increases with an increase in $g\Delta\rho D$, which represents the buoyancy force due to a density difference $\Delta\rho$ across the opening whose diameter D is taken as the characteristic dimension. This is reasonable, since higher the buoyancy force across the opening, higher the purging pressure needed to'overcome this force to give rise to a uni-directional upflow. It is found that the dependence of ΔP_{FLOOD} on $gApD$ follows a square root curve behavior.

The opening length to diameter ratio L/D does have an effect on the purging pressure ΔP_{FLOOD}. As seen fiom Fig.3.9(a), an L/D value of around 1.0 is the turning point. As L/D decreases below this value to L/D = 0.25, the purging pressure *difference* ΔP_{FLOOD} also decreases. As L/D increases from this value to L/D = 6.0, an opposite behavior is noted, with the purging pressure ΔP_{FLOOD} decreasing with increasing L/D. There is an intersection of the two pressure curves for L/D = 1.0 and L/D = 2.754. At smaller density difference $\Delta\rho$, ΔP_{FLOOD} increases with increasing L/D. At larger Ap, ΔP_{FLOOD} is found to decrease with increasing L/D. At extremely high L/D ratio, which is a tube opening, the purging pressure ΔP_{FLOOD} needed to generate the uni-directional upflow is much smaller than that at moderate L/D values. As L/D goes to the other extreme, the orifice, which has a very low L/D ratio, the purging pressure ΔP_{FLOOD} needed to generate the uni-directional upflow drops down to a lower value again. Clearly, L/D is an important parameter and affects the flow patterns and regimes that arise, as discussed by Epstein[19]. A more detailed effort on the flow field is therefore needed to fully understand these effects.

The opening diameter D also has effect on the purging pressure difference ΔP_{FLOOD}. As tabulated in Table 3.3 and depicted in Fig. 3.10, when D increases from D = 0.0127 m to D = 0.0159 m, ΔP_{FLOOD} becomes higher for the same L/D ratio and density difference Ap range. So, for a larger opening diameter, the purging pressure difference ΔP_{FLOOD} must be maintained at a higher value to prevent any downflow of brine solution from entering the lower compartment. A higher opening diameter D leads to

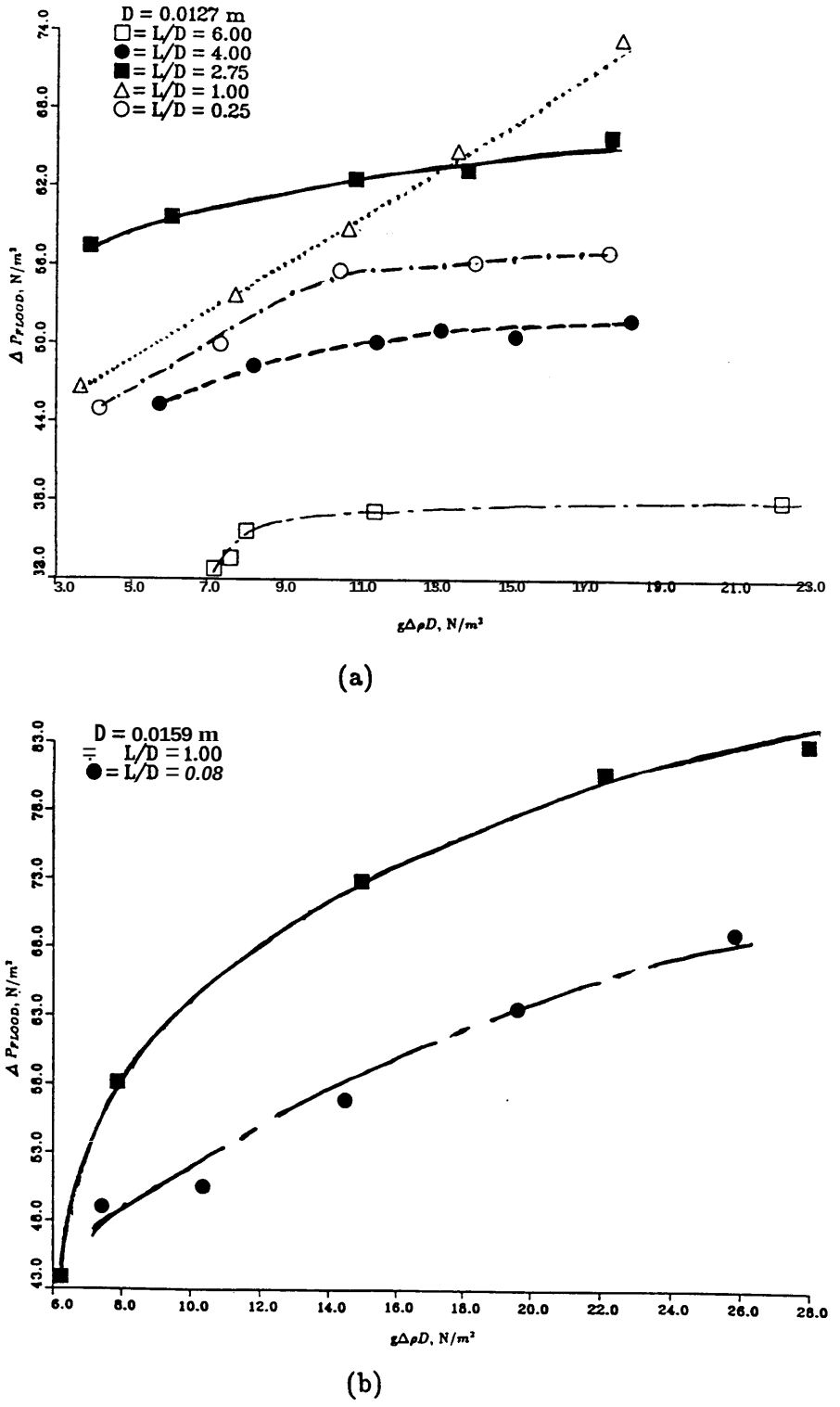

Figure 3.9: **Purging flow** experiments: **The** dependence of ΔP_{FLOOD} on $g\Delta\rho D$

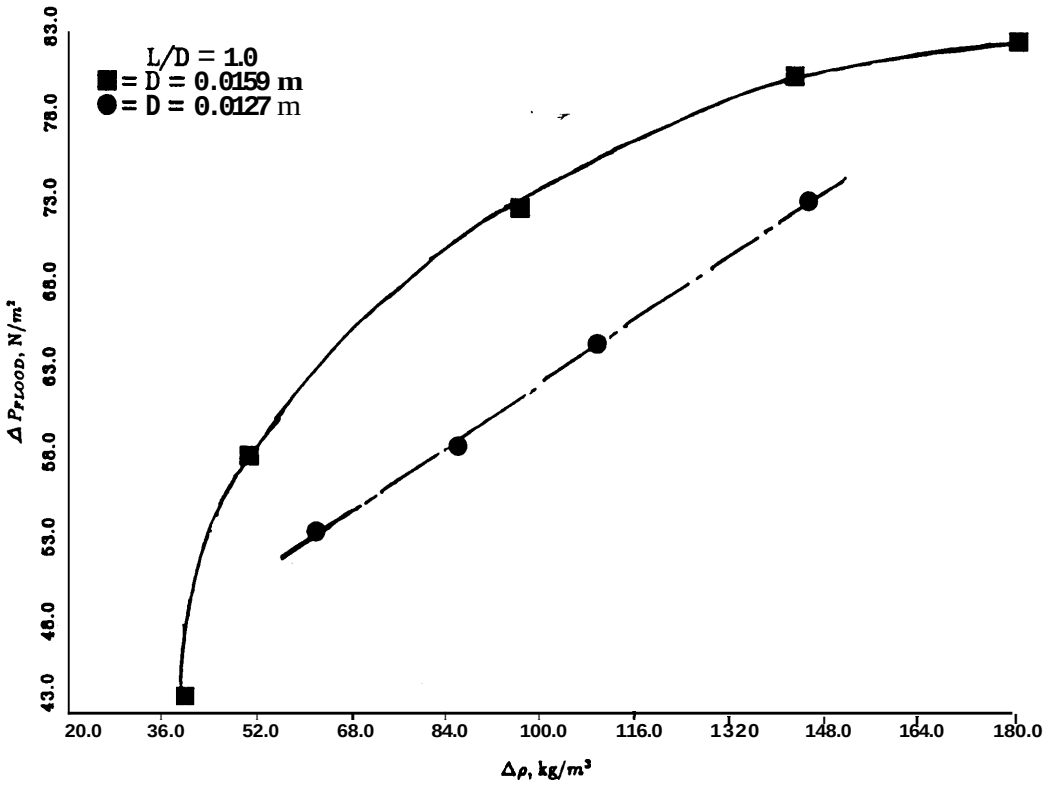

Figure 3.10: **Purging flow** experiments: The **effect** of the opening diameter D on purging pressure.

a stronger buoyancy force $gApD$. Thus, the purging pressure needed is also higher. Therefore, the purging pressure depends on the diameter D through the buoyancy force and an L/D which represents the geometry of the vent and which affects the flow pattern.

Considering now the flooding flow rate Q_{FLOOD}, it is found that the dimensionless Froude number, $Fr_{FLOOD} = \frac{Q_{FLOOD}}{(g\Delta\rho D^5/\bar{\rho})^{1/2}}$, does depend on the density difference Ap, along with its dependence on the L/D ratio. Actually, as tabulated in Table 3.2, Q_{FLOOD} is relatively scattered for a given L/D ratio but different Ap, since Q_{FLOOD} is determined by the two other parameters: ΔP_{FLOOD} and the density difference Ap across the opening. When ΔP_{FLOOD} is maintained at a very high value, the density difference Ap, which reflects the buoyancy force to be overcome by the purging pressure ΔP_{FLOOD}, is also very high. Thus, the resulting Q_{FLOOD} is found to be lower. However, Fr_{FLOOD} is averaged over different Ap for a given L/D ratio and plotted in Fig.3.11, from which the dependence of $\overline{Fr_{FLOOD}}$ on L/D is shown to be similar to the one obtained by Epstein and Kenton[22](see Fig.1.22). The magnitude of the Froude number obtained here is relatively higher. The reason is the same as the one in section 3.1.1, because the opening diameters employed are much smaller than those in the early work. In fact, Epstein's conclusion of the independence of Fr_{FLOOD} on $\Delta\rho$ was based on his former experiment with purely buoyancy force, only the density difference Ap determine the exchange flow rate for a given opening size, and the dimensionless flow rate, $Fr = Q/(g\Delta\rho D^5/\bar{\rho})^{1/2}$, eliminates the effectiveness of the Ap. But for the forced upward flow with buoyancy force, as mentioned before, pressure difference AP also plays a role in Q_{FLOOD}, and it is not reflected in dimensionless F'roude number. Thus, more scatter data was obtained.

The dependence of the dimensionless Froude number Fr_{FLOOD} on the dimensionless parameter $\Delta P/g\Delta\rho D$, for different $\Delta\rho$ across the vent opening is shown in Fig.3.12. The data fall well within a band, indicating that the increase $\Delta P/g\Delta\rho D$ gives rise to an increase in Fr_{FLOOD}. Here, $\Delta P/g\Delta\rho D$ is a buoyancy parameter which reflects the

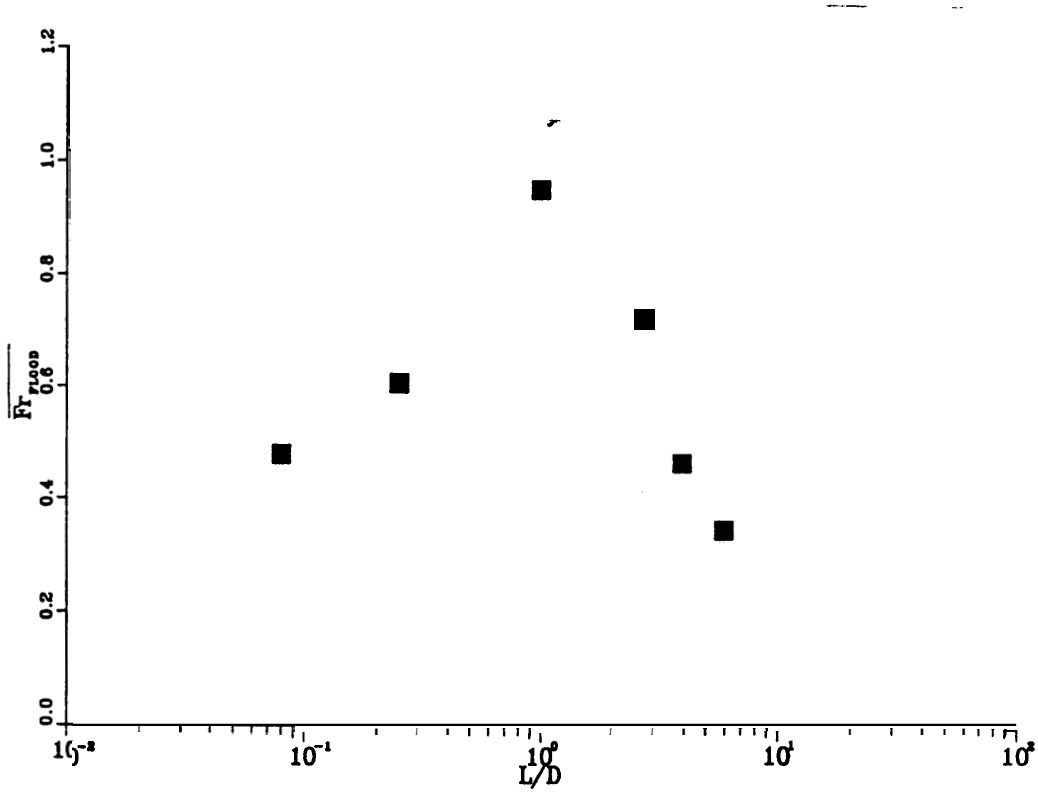

Figure 3.11: **Purging flow** experiments: Dimensionless purging **flow** rate versus opening aspect ratio L/D.

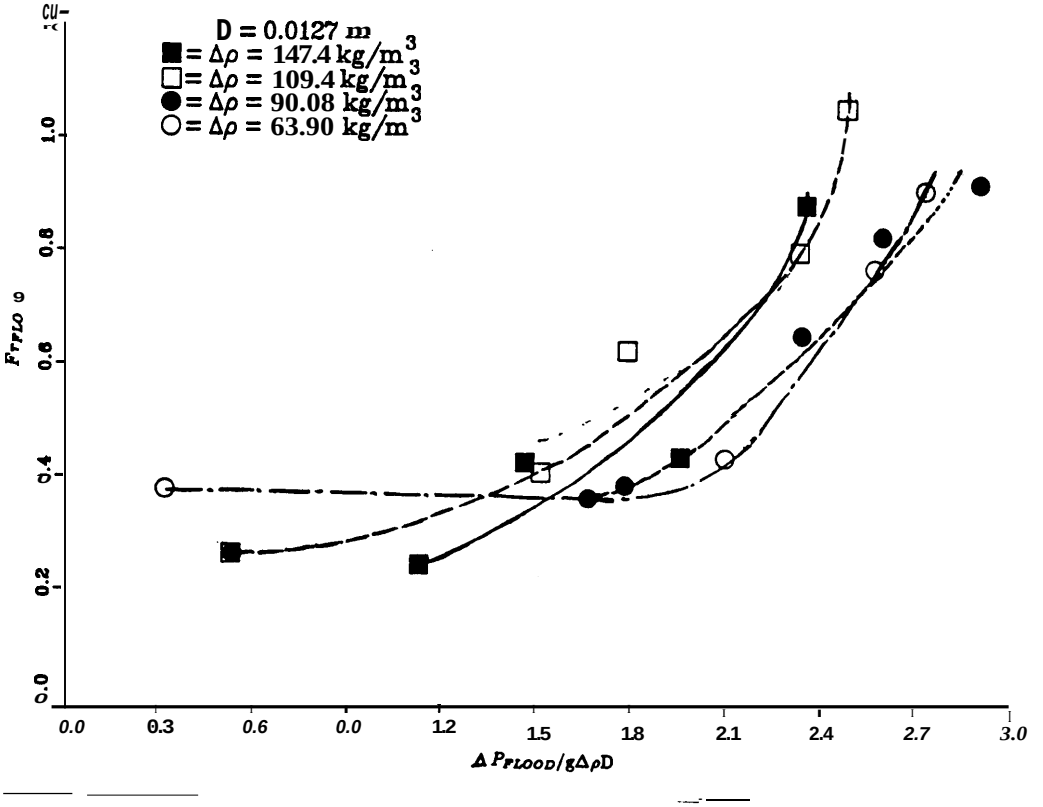

Figure 3.12: Purging flow experiment: The dependence of the purging flow rate on dimensionless parameter $AP/gA\rho D$.

ratio of the external force to the buoyancy force. Higher the $g\Delta\rho D$, the higher the ΔP needed to give rise to a given purging flow rate. Thus, this nondimensionalization eliminates the characteristics of different purging flows.

3.3 Combined Flows

The main intention of this portion of the study is to determine the effect of an imposed pressure difference on the mass flow rate across a vent opening in a horizontal partition. This flow exchange through a horizontal vent involves a combination of a buoyancy driven exchange flow and a forced flow. Buoyancy force due to the density difference across the vent opening gives rise to a bi-directional exchange flow through the vent. The imposed pressure difference gives rise to a forced upward flow through the vent. Thus, a mixed natural and forced convection flow arises due to the combination of these two forces. The apparatus used for the combined or mixed convection experiments is the same as the one for the purging flow experiments. Combined convection conditions were obtained simply by adjusting the value of ΔP, either raising or lowering the storage tank, to values below the corresponding purging pressure difference ΔP_{FLOOD}. The rate of dilution of the brine in the upper compartment was obtained by measuring the density and the volume flow rate of the overflow brine Q_O at the notch of the upper compartment. The buoyancy driven downflow of the brine solution Q_D and the forced upflow of the water Q_U can be shown to be given by (see appendix B):

$$Q_U = \frac{-V_H d\rho_H/dt}{\rho_H - \rho_L} \tag{3.8}$$

$$Q_D = \frac{-V_H d\rho_H/dt}{\rho_H - \rho_L} - Q_O \tag{3.9}$$

and

$$\rho_L = \rho_{L,0} - \frac{V_H}{V_L}(\rho_H - \rho_{H,0}) - \frac{Q_I \Delta t}{V_L}(\rho_H - \rho_{water}) \tag{3.10}$$

Where, V_H and V_L, ρ_H and ρ_L, $\rho_{H,0}$ and $\rho_{L,0}$ are the same as those defined for Eqn.(3.5), Q_I is the volume flow rate from the storage tank to the lower compartment, giving $Q_I = Q_O$, At is the time interval from the starting point to the current point, and

ρ_{water} is the density of the fresh water entering from the storage tank to the lower compartment. The density of the water in the storage tank is that of pure water at room temperature, that is about 1000.0 kg/m^3.

The shadowgraph photographs of combined natural and forced convection flow are shown in Figs.3.13 to 3.14. Some are with the down flow Q_D being smaller than upflow Q_U and some are with down flow Q_D being almost the same as the upflow Q_U, depending on the initial density difference and the pressure difference maintained. It was observed that the exchange phenomenon is similar to that with $\Delta P = 0$, except that amount of flow in the two directions need not to be equal now. For the experimental conditions chosen, most of the cases are with Q_U greater than Q_D. Thus, the effect of the imposed pressure is greater than that due to the buoyancy force.

The measured external pressure difference ΔP, the net volume overflow rate of brine at the notch of the upper compartment and the experimental variables are presented in Table 3.3. Also given in table 3.3 are the buoyancy driven component Q_D and the forced flow component Q_U of the flow rate determined from the experiments.

3.3.1 Density Variation Versus Time

Four typical plots of the brine density variation with time, as obtained from the hydrometer measurements, are shown in Figs.3.15(a) through (d). In each figure, two different experimental results, which were carried out for a given L/D ratio and essentially the same initial brine density $\rho_{H,0}$ but different pressure difference ΔP, are plotted to depict the effect of the externally imposed pressure on the combined convection transport. A linear best fit analysis was carried out for the linear segments of the density-time plots. It can be seen that an increasing ΔP value gives rise to an increasing absolute value of the slope $d\rho_H/dt$. This, in turn, indicates an increase in the forced upward flow component Q_U, from the lower compartment to the upper compartment, according to Eqn.(3.8). This is also confirmed by the calculations predicted in the following sections. The buoyancy driven downward flow component Q_D, from the upper compartment to

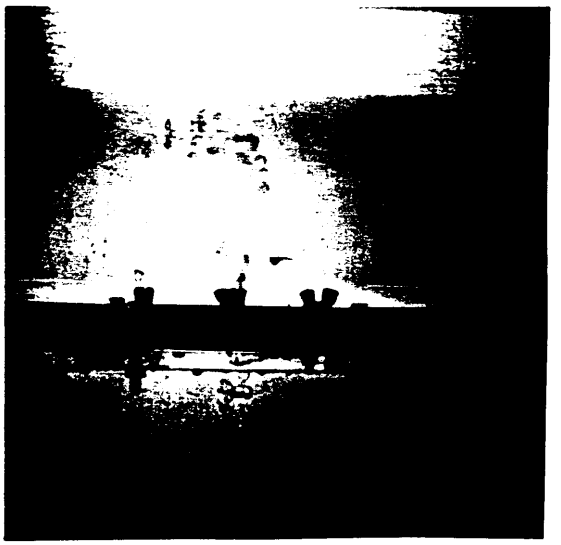

(a) D = 0.0127 (m), L/D = 2.75, $\rho_H = 1050.5(kg/m^3)$, $\rho_L = 1001.0(kg/m^3)$,

$\Delta P = 61.49\,(N/m^2)$

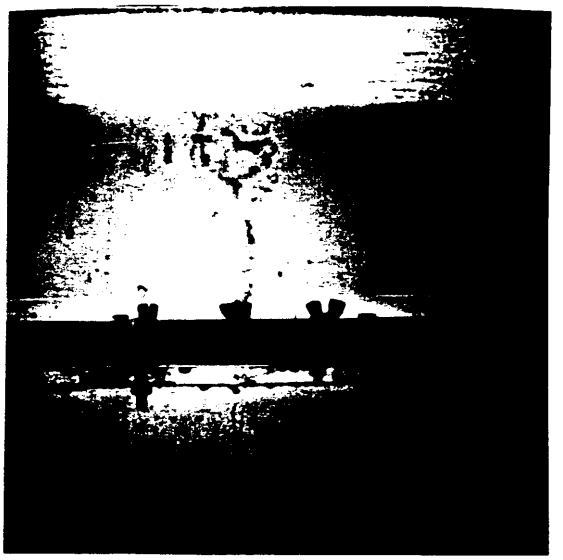

(b) D = 0.0127 (m), L/D = 2.75, $\rho_H = 1050.5(kg/m^3)$, $\rho_L = 1000.0(kg/m^3)$,

$\Delta P = 52.77\,(N/m^2)$

Figure 3.13: Combined flow under buoyancy and the imposed pressure: Shadowgraph photographs

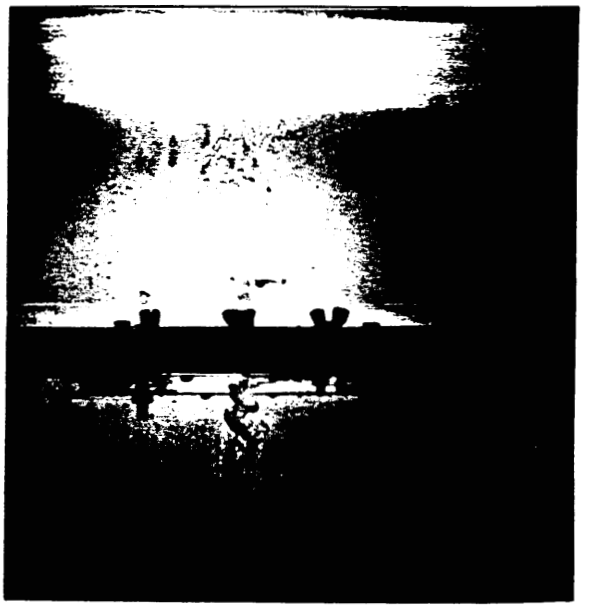

(a) D = **0.0127 (m)**, L/D = **2.75**, $\rho_H = 1090.6(kg/m^3)$, $\rho_L = 1000.0(kg/m^3)$,

AP = 36.51 (N/m^2)

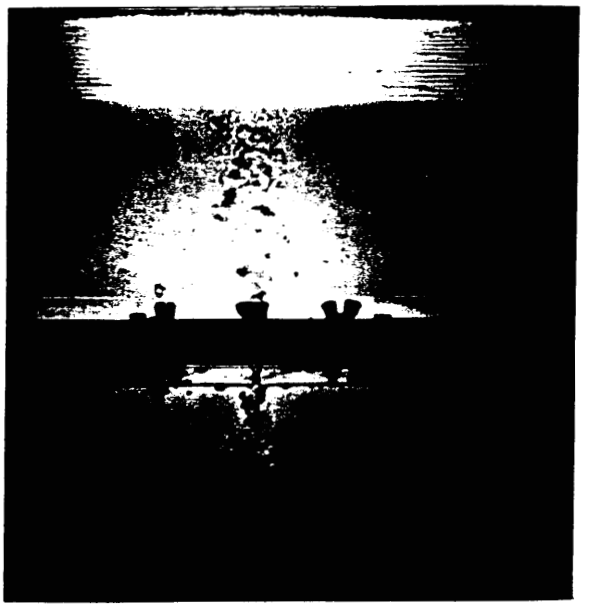

(b) D = **0.0127** (m), L/D = **2.75**, $\rho_H = 1089.0(kg/m^3)$, $\rho_L = 1000.5(kg/m^3)$,

AP = 39.95 (N/m^2)

Figure 3.14: Combined flow under buoyancy and the imposed pressure: Shadowgraph photographs

Table 3.3: Measured Combined Convective Flow Through a Vent Opening

D (m)	L (m)	ρ_H (kgm^{-3})	ρ_L (kgm^{-3})	AP (Nm^{-2})	$\times 10^{-}$ $m\ s^{-}$		
0.0127	0.0763	1090.5	1000.9	13.32	2.73	3.31	0.58
0.0127	0.0508	1151.5	1001.2	30.84	3.16	4.20	1.04
0.0127	0.0508	1151.0	1002.1	37.53	5.22	5.24	0.02
0.0127	0.0508	1110.0	1000.0	15.87	0.00	3.06	3.06
0.0127	0.0508	1110.0	1002.0	38.32	1.85	3.06	1.21
0.0127	0.0508	1111.0	1002.7	46.29	3.09	4.43	1.34
0.0127	0.0508	1112.0	1002.9	56.12	7.40	7.49	0.09
0.0127	0.0350	1050.5	1001.0	61.49	6.61	6.62	0.01
0.0127	0.0350	1050.5	1000.0	52.77	4.01	4.45	0.45
0.0127	0.0350	1052.0	1000.1	44.04	1.46	3.26	1.81
0.0127	0.0350	1147.5	1000.0	56.90	4.33	4.31	0.01
0.0127	0.0350	1147.0	1000.0	65.86	9.12	9.14	0.02
0.0127	0.0350	1146.5	1000.0	54.27	3.39	3.46	0.05
0.0127	0.0350	1090.6	1000.0	36.51	2.12	2.83	0.71
0.0127	0.0350	1089.0	1000.5	39.95	2.20	2.44	0.24
0.0127	0.0350	1099.5	1000.0	41.99	0.00	3.48	3.48
0.0127	0.0127	1102.0	1000.2	67.66	2.73	3.31	0.58
0.0127	0.0127	1099.5	1000.8	49.87	0.00	2.28	2.28
0.0127	0.0127	1097.0	1002.8	25.61	0.00	1.43	1.43
0.0127	0.0127	1092.1	1000.0	57.18	2.84	4.97	2.13
0.0127	0.0127	1088.7	1001.1	75.95	10.47	10.50	0.03
0.0159	0.0159	1107.0	1000.9	71.90	6.32	7.18	0.85
0.0159	0.0159	1101.5	1001.3	54.99	3.88	5.19	1.30
0.0254	0.0254	1090.9	1000.0	91.43	9.08	13.08	4.00
0.0254	0.0254	1091.5	1002.3	80.20	5.34	11.02	5.67
0.0254	0.0254	1095.5	1004.9	74.65	2.58	10.95	8.37
0.0254	0.0254	1091.5	1007.3	38.95	0.00	8.06	8.06
0.0254	0.0254	1049.1	1000.0	65.10	13.12	13.15	0.03
0.0254	0.0254	1045.5	1000.1	58.99	9.35	9.70	0.35
0.0127	3.18×10^{-3}	1049.6	1000.0	30.36	2.89	3.78	0.89
0.0127	3.18×10^{-3}	1049.5	1000.5	42.75	3.26	4.65	1.39
0.0127	3.18×10^{-3}	1049.5	1001.1	54.99	7.64	7.67	0.03
0.0127	3.18×10^{-3}	1099.0	1000.5	42.78	0.67	2.27	1.61
0.0127	3.18×10^{-3}	1100.0	1002.5	48.82	5.38	5.77	0.39
0.0127	3.18×10^{-3}	1100.0	1002.6	52.30	6.61	6.67	0.05
0.0127	3.18×10^{-3}	1146.0	1002.4	57.97	4.53	4.54	0.01
0.0127	3.18×10^{-3}	1146.0	1001.8	61.40	5.17	6.14	0.98
0.0127	3.18×10^{-3}	1146.0	1001.7	67.64	6.19	6.23	0.04

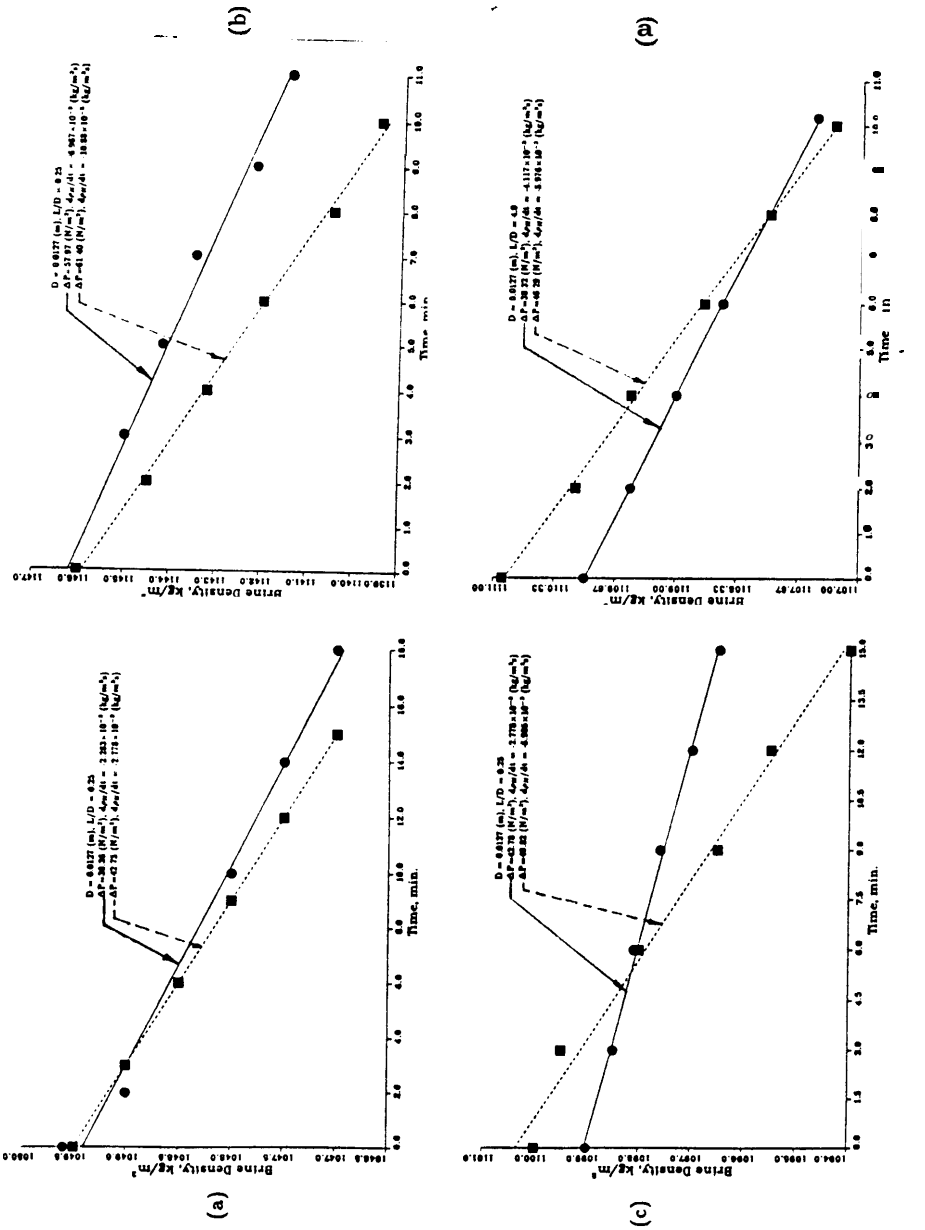

Figure 3.15: Combined natural and forced convection flow: Density variation versus time.

the lower compartment, is determined by both Q_U and Q_O and is difficult to predict in terms of the governing variables. However, the basics trends are discussed below.

3.3.2 Volume Flow Rate Results

Typical plots for the volume over flow rate Q_O which is equal to the net volume flow rate Q_N, versus **Ap,** at fixed d u e s of **AP,** opening diameter **D** and **L/D** ratio, are plotted in Figs.3.16 through 3.19. ***Also*** plotted in these figures are the buoyancy driven downward flow Q_D and the forced upward flow Q_U. The flow rates Q_O and Q_U were found to decrease with an increasing density difference **Ap,** while Q_D was found to increase.

The reason for this behavior **is** the same as that for the purging flow experiments. Higher the value of **Ap,** stronger is the downward buoyancy force, leading to a larger downward flow Q_D, and a weaker forced upward flow Q_U for a given pressure difference AP, since larger pressure is needed to overcome the buoyancy force. **This also** results in a smaller net overflow rate Q_O according to Eqn.(3.2). Therefore, the density difference $\Delta\rho$ across the vent opening has a negative effect **on** the volume overflow rate Q_O and forced upward flow Q_U, but a positive effect **on** the buoyancy driven downward flow Q_D.

Typical plots for the net volume flow rate Q_O or Q_N versus AP, at given values of Ap, opening diameter D and **L/D** ratio, are plotted in Figs.3.20 to Fig.3.23. *Also* plotted in Fig.3.22 and Fig.3.23 is the forced upward flow component Q_U. Q_O was observed earlier to increase with **an** increasing A P in the experiment. Q_U was found to increase with an increasing AP according to the calculation, while Q_D was found to fluctuate **as** A P **was** increased and did not give out any straightforward dependence on **AP.** Thus, Q_D is not shown in the figures. Consequently, the imposed pressure difference AP across the vent opening has **a** positive effect **on** the volume overflow rate Q_O and forced upflow rate Q_U. **This** is because the imposed positive pressure difference AP **was** designed to oppose the downward **buoyancy** force which is caused by the density difference $\Delta\rho$ across the vent opening. It is also noted that, for given opening diameter D and L/D ratio, AP needs to be maintained at higher values for experiments with

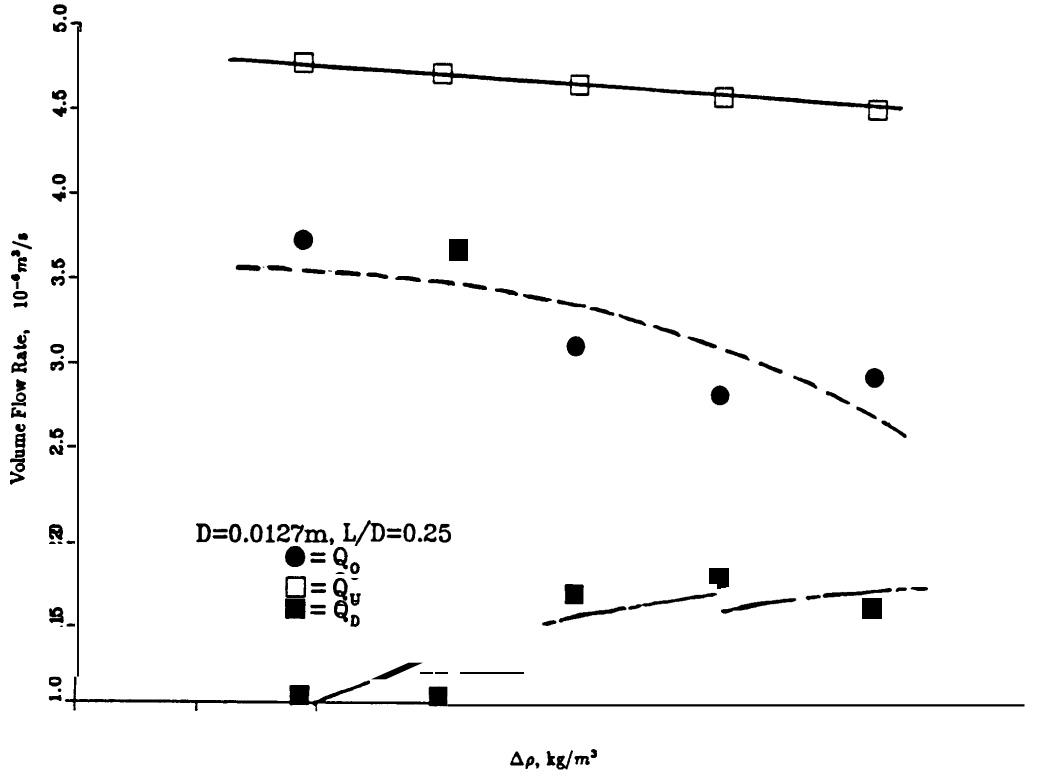

Figure **3.16:** Combined forced **and natural** convection flow: Volume flow rate Q_O versus **density** difference $\Delta\rho$ **at** $\boldsymbol{AP} = 42.75N/m^2$, **D** $=$ **0.0127** m, L/D $=$ **0.25.**

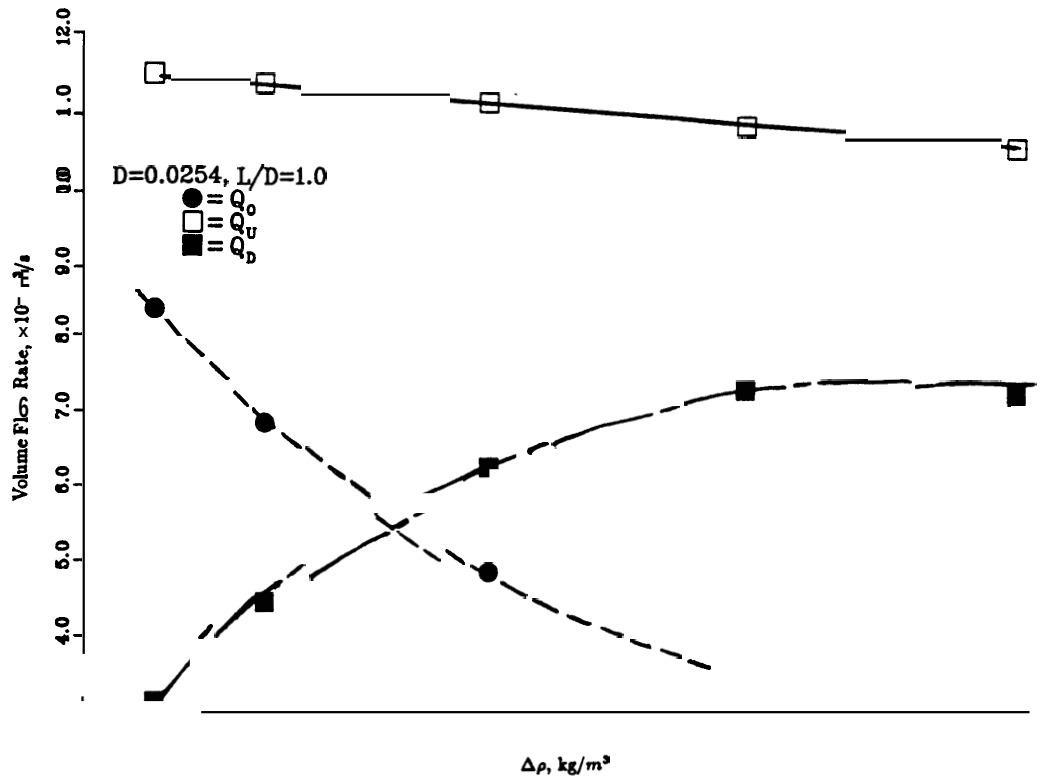

Figure **3.17:** Combined forced and natural convection **flow:** Volume **flow** rate Q_O **versus** density difference $\boldsymbol{\Delta p}$ at $\boldsymbol{\Delta P}$ = $80.20 N/m^2$, D = **0.0254** m, L/D = **1.0**

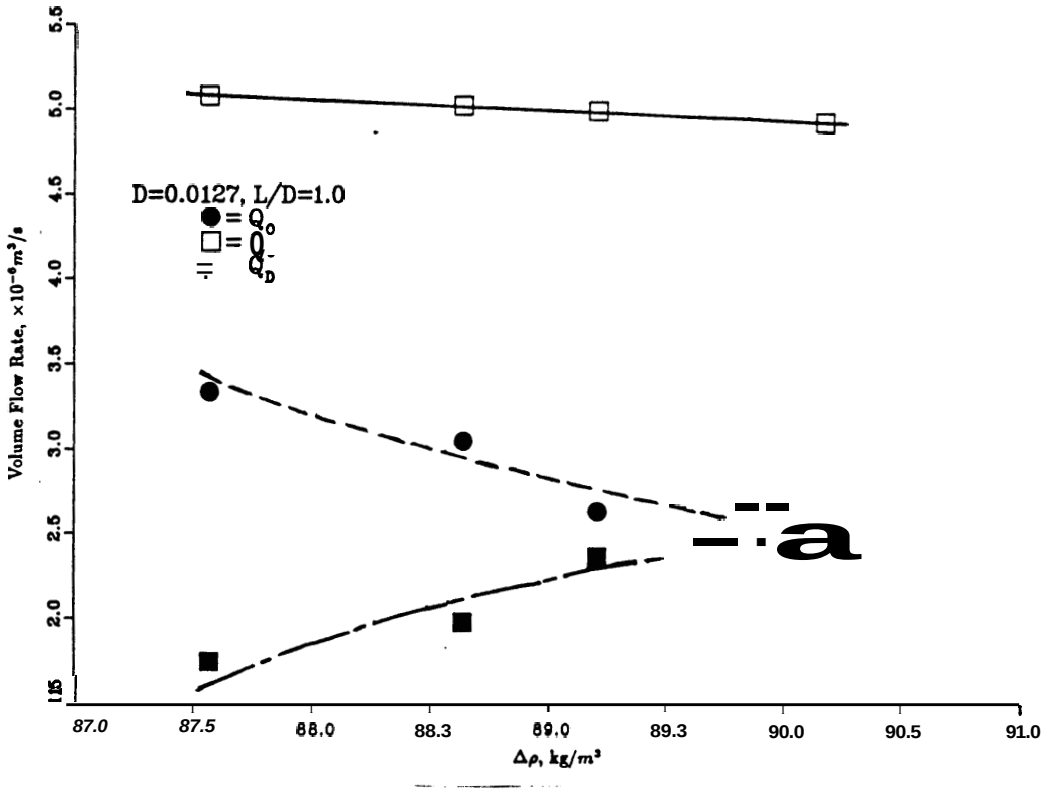

Figure 3.18: Combined forced and natural convection flow: Volume flow rate Q_O versus density difference $\Delta\rho$ at $\boldsymbol{AP} = 57.18 N/m^2$, D = 0.0127 m, L/D = 1.0

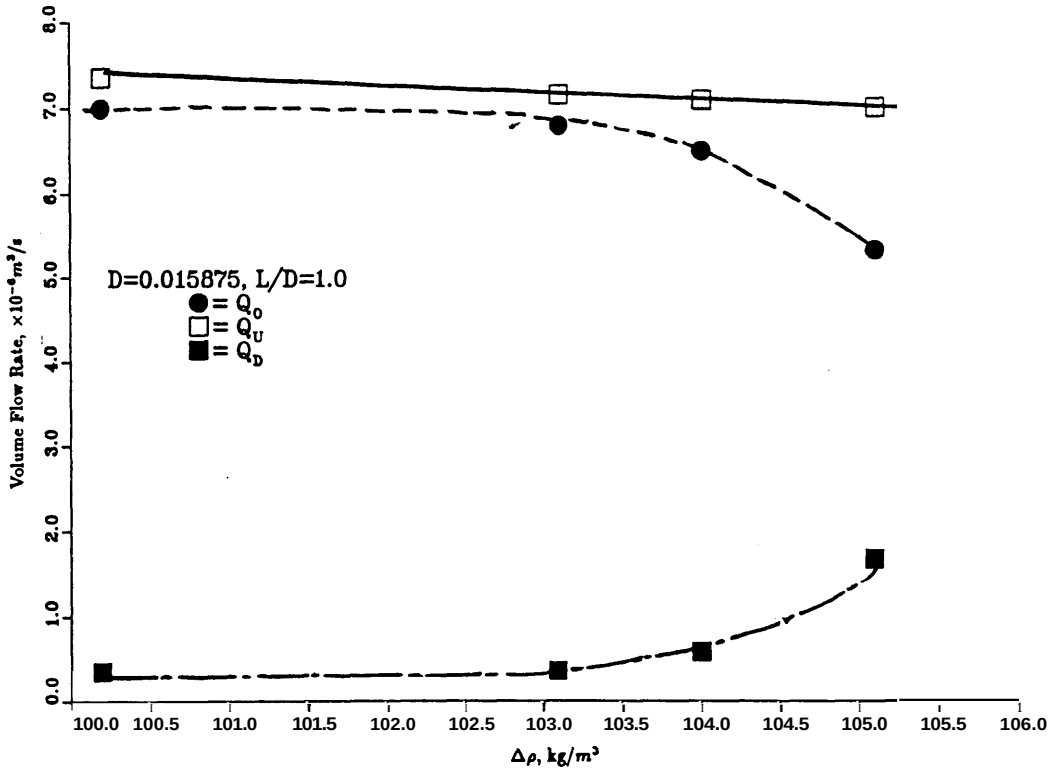

Figure 3.19: Combined forced and natural convection flow: Volume flow **rate** Q_O **versus density difference** $\Delta\rho$ **at** $\mathbf{AP} = 71.90 N/m^2$, $\mathbf{D} = 0.0159\ \mathbf{m}$, $\mathrm{L/D} = 1.0$

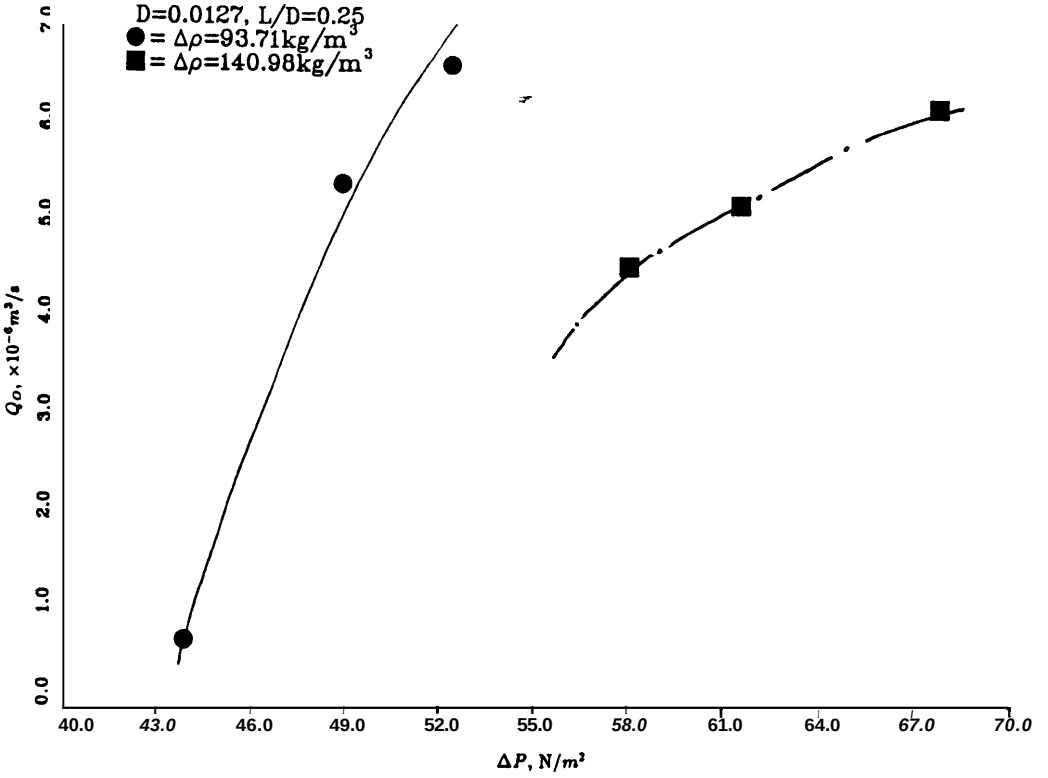

Figure **3.20:** Combined forced and natural convection **flow:** Volume **flow** rate Q_O **versus** pressure difference ***A P*** **at** fixed $\Delta\rho$, D = 0.0127, L/D = **0.25.**

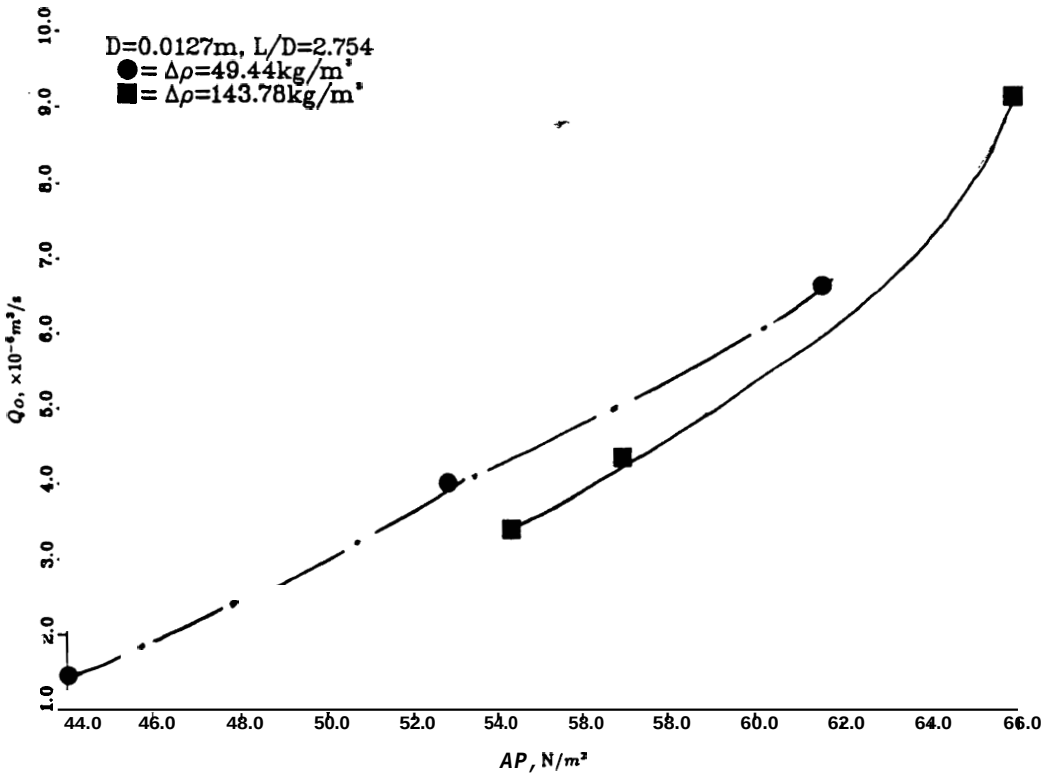

Figure 3.21: Combined forced and natural convection flow: Volume flow rate Q_O versus pressure difference ΔP at fixed Ap, D = 0.0127, L/D = 2.754.

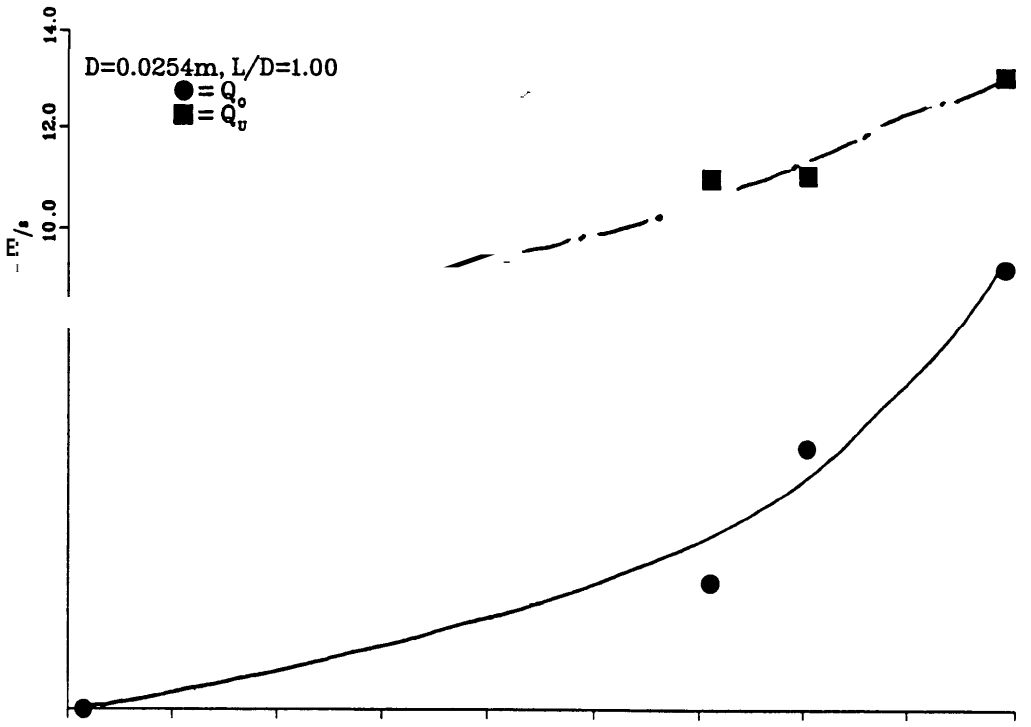

Figure 3.22: Combined forced and natural convection flow: Volume flow rates Q_O and Q_U versus pressure difference ΔP at $\Delta\rho$ = 84.42kg/m^3, D = 0.0254 and L/D = 1.00.

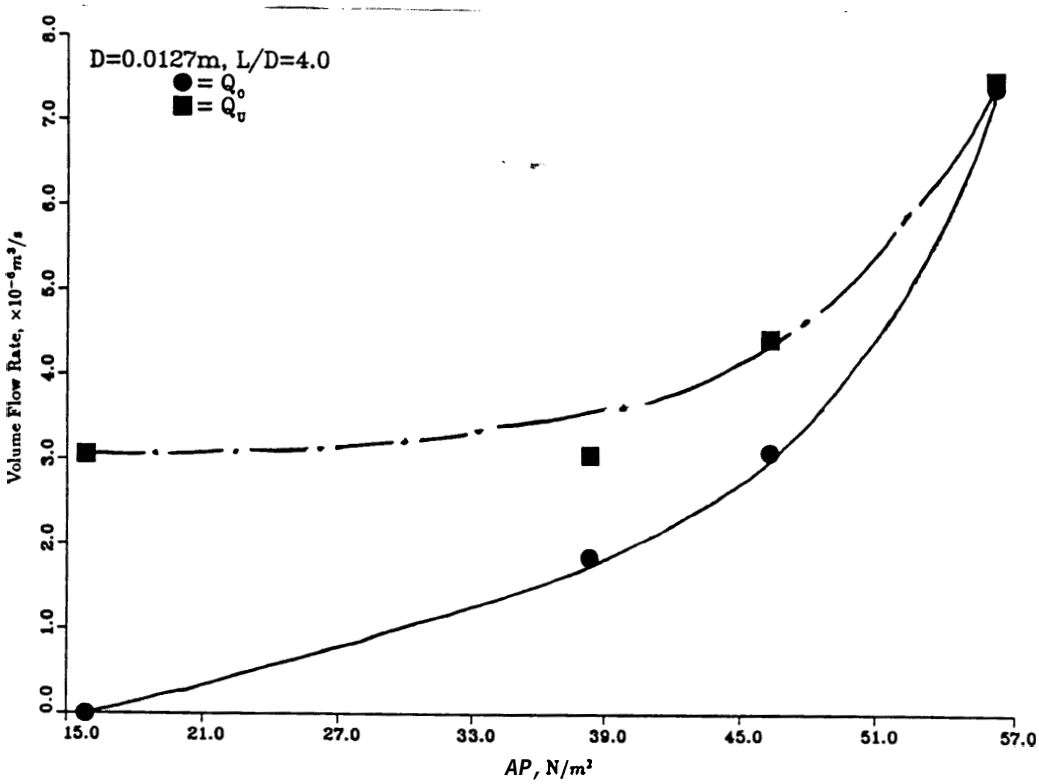

Figure 3.23: Combined forced and natural convection **flow:** Volume **flow** rates Q_O and Q_U **versus** pressure difference $\boldsymbol{\Delta P}$ at $\Delta\rho = 106.58 kg/m^3$, D = 0.0127 and L/D = 4.00.

higher ΔP, in order to obtain the same amount of net volume flow rate Q_N compared to the experiments with lower Ap(Fig.3.20 and Fig.3.21). This is obviously because a larger external pressure is needed to balance the downward buoyancy force for a higher density difference.

In Fig.3.24 and Fig.3.25, the volume flow rate Q_O is plotted in the form of the dimensionless Froude number, Fro, as a function of the dimensionless mixed convection parameter $\Delta P/g\Delta\rho D$. It is seen that Fr_O increases with an increase in $\Delta P/g\Delta\rho D$. This is again an expected behavior as discussed above.

3.4 Correlations for Combined Flow Through a Horizontal Opening

Correlation equations have also been derived for the combined flows, based on the experiments of uni-directional upward flows and bi-directional combined natural and force convection flows. These equations were developed to investigate the dependence of the net volume flow rate of Q_N , which is equal to volume overflow rate Q_O, on parameters such as the pressure difference ΔP across the vent opening, the density difference $\Delta\rho$ across the opening and the L/D ratio. The equation obtained from the data is shown below as:

$$Q_O = 6.7 \times 10^{-7}(\Delta P)^{0.83}(\Delta\rho)^{-0.29}(L/D)^{0.11} \tag{3.11}$$

The parameter ranges covered by this equation are:

$$0.25 < L/D < 6.08, \text{and} 0.043 < \Delta\rho/\bar{\rho} < 0.13 \tag{3.12}$$

The correlation coefficient for the equation obtained is 20 percent. The above correlating equation indicates that Q_O has a strong dependence on the imposed pressure difference ΔP, since it is proportional to ΔP to the power of 0.83, it shows that the pressure difference has a positive effect on Q_O which verifies the conclusion obtained in previous section. Q_O varies with the density difference $\Delta\rho$ across the opening as a power of -0.29, the effect of Δp on Q_O is little weaker comparing to the one of ΔP, and

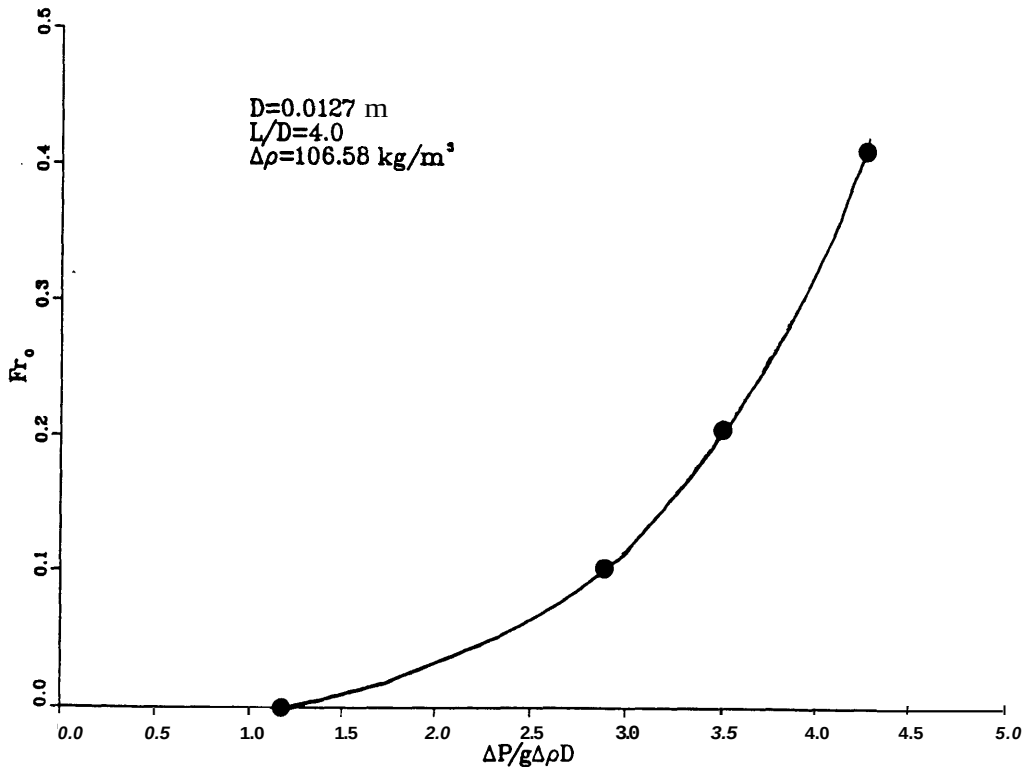

Figure 3.24: Combined forced and natural convection flow: Dimensionless volume flow rate Fr_O versus dimensionless mixed convection parameter $\Delta P/g\Delta\rho D$.

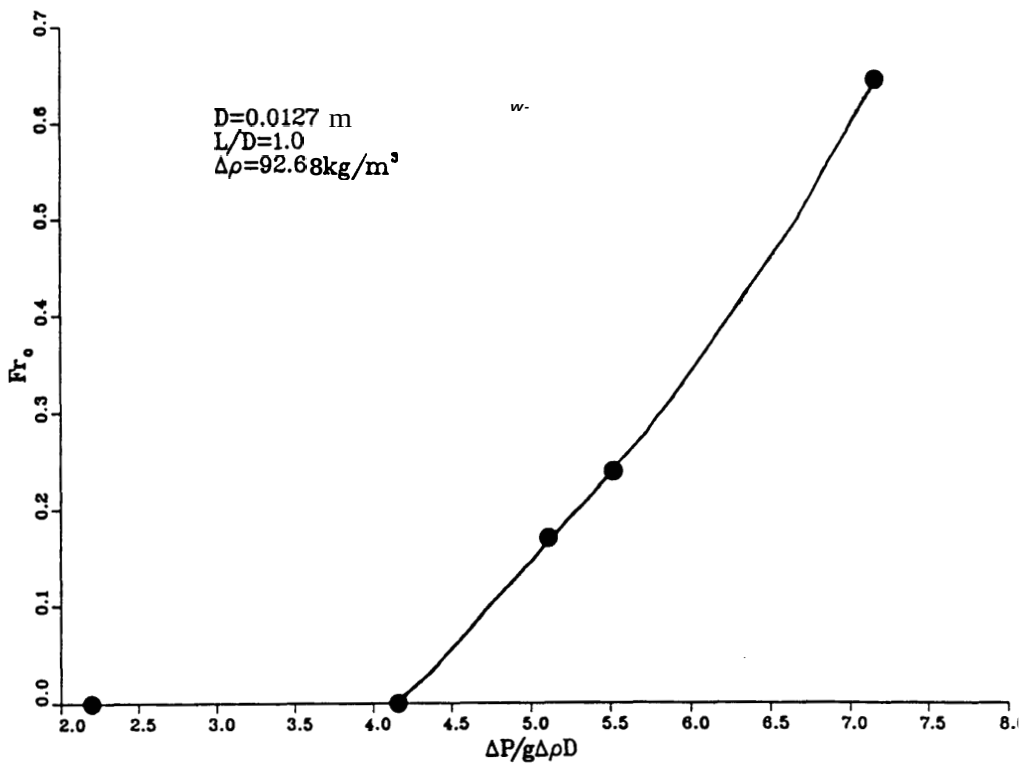

Figure **3.25:** Combined forced and natural convection **flow:** Dimensionless volume **flow rate** Fr_O versus dimensionless mixed convection parameter $\Delta P/g\Delta\rho D$.

Ap has an negative effect on Q_O since Ap is in the denominator, which also verifies the conclusion obtained by previous section. The variation of the opening ratio L/D has a small effect on the volume flow rate Q_N. The correlation shows that over the L/D range chosen, Q_N varies with L/D as a power of 0.11. Actually, at smaller L/D values, Q_O is proportional to L/D, but at larger L/D a negative exponent is obtained. Thus, "0.11" is the overall exponent for the whole L/D range.

A similar correlation equation had been obtained for the dependence of the unidirectional upward flow Q_U on the pressure difference AP, the density difference Ap and the opening ratio L/D. The equation is shown as:

$$Q_U = 5.01 \times 10^{-6}(\Delta P)^{0.75}(\Delta\rho)^{-0.66}(L/D)^{0.25} \tag{3.13}$$

where the parameter ranges covered are:

$$0.25 < L/D < 6.08, \text{and} 0.043 < \Delta\rho/\bar{\rho} < 0.13 \tag{3.14}$$

The correlation coefficient for the equation obtained is 18 percent. The equation shows that the effects of AP, Ap and L/D on Q_U are analogous to those on Q_O, except that the density difference Ap has stronger influence on Q_U and the pressure difference AP has weaker influence on Q_U, comparing to those on Q_O. For the effect of the density difference Ap, since Q_U is forced upflow, it is largely generated by imposed pressure difference which overcomes the downward buoyancy force due to the density difference Ap across the vent. In other word, more downward buoyancy force needs to be balanced in Q_U than in Q_O. For the effect of the pressure difference AP, since Q_O is the difference between the volume upward flow rate Q_U and the volume downward flow rate Q_D, which are both determined by the pressure difference AP. Thus, the pressure difference AP has stronger effect on Q_O than on Q_U.

Chapter 4

Conclusion and Future Work

4.1 Summary and Conclusions

A series of experiments has been carried out to investigate the combined natural convection and forced flow through a single horizontal vent opening in the ceiling of a room containing a fire. The buoyancy driven flow, without an imposed pressure, and the forced flow, without buoyancy effects, were also examined. A plexiglass tank with a vented partition in the middle was constructed to simulate the room with a fire and the ambient environment, by filling the upper and lower compartments with brine and pure water, respectively. Thus, the density difference is obtained due to the salt concentration. The lower compartment could also be raised to a pressure higher than the ambient by providing an inflow from an external tank of pure water that could be raised or lowered to vary the pressure.

The average net volume flow rate Q_O and forced volume upflow rate Q_U were experimentally obtained for a range of variation in the pressure difference A P across the opening, density difference $\Delta\rho$ across the opening and the opening aspect ratio L/D. For each geometrical configuration (fixed L/D ratio), the pressure difference across the opening was varied, while the density difference was maintained at a certain fixed value, and vise versa. Flow visualization using the shadowgraph technique was employed to study the flow pattern in the vicinity of the vent opening. Data on the mean volume flow rates Q_U, Q_O and Q_D were obtained by measuring the brine density in the upper compartment resulting from the flow exchange across the opening.

The experiments demonstrated that for combined natural and forced convection flow

and for the range of opening ratio L/D, density difference $\Delta\rho$ and pressure difference A P considered, the pressure difference has the strongest effect on the volume flow rates Q_O and Q_U. Both of these were found to increase with an increase in the pressure difference. The density difference $\Delta\rho$ across the opening, however, has a negative effect on the volume flow rates Q_O and Q_U, the effects being weaker compared to the effect of the pressure difference, over the ranges considered. The opening ratio L/D was found to have only a small effect on the volume flow rates. In the smaller L/D range, an increase in the L/D ratio gives rise to an increase in the volume flow rates. In the larger L/D range, an increase in the L/D ratio gives rise to a decrease in the volume flow rates. It was found that, for the range of parameters considered, the average volume flow rates could be correlated fairly accuratly using two separate correlations. For the different volume flow rates considered, the effect of the same parameter was found to be quite different. For example, the effect of the pressure difference on Q_O is stronger than the one on Q_U with the exponent of the pressure difference A P in Eqn.3.13, the correlating equation, being higher than the one in Eqn.3.12. Similarly, the effect of the density difference on Q_O is weaker than the one on Q_U, with the exponent of the density difference in Eqn.3.11 being lower than that in Eqn.3.14.

Purging flow experiments were carried out to determine when the downward flow due to buoyancy force is completely stopped by the imposed pressure difference. It was found that the density difference across the opening and the opening size determine the flooding pressure ΔP_{FLOOD} required to generate a uni-directional upflow. That is, higher the density difference or larger the opening diameter, higher is the ΔP_{FLOOD} needed to prevent any buoyancy driven down flow from entering the lower compartment. It was found that the density difference also affects the dimensionless flooding flow rate. The deviation in Fr_{FLOOD} was more than 20 percent as $\Delta\rho/\bar{\rho}$ varied from 0.03 to 0.17. This indicates that the dimensionless flow rate used in earlier studies dose not correlate the data satisfactory over the entire parameter range. But the trend of the variation in the averaged dimensionless flooding rate with the opening L/D ratio agreed very well with the previous work.

Experimental results on pure natural convection, with no externally imposed pressure, were compared with a earlier study, indicated that, within the same opening diameter range, the results were in very good agreement. For much smaller opening diameters, higher dimensionless Froude numbers were obtained at the same opening L/D ratio, compared with the previous study. Again, this suggests the need for a different nondimensionalization. Experiments with forced uni-directional upflow and without buoyancy effects indicate that an increase in the externally imposed pressure gives the rise to an increase in the upflow, which is also the net flow across the opening. The velocity calculated from the measured pressure difference A P across the vent, using Bernoulli's equation, agrees very well with the velocity obtained from the overflow measurement, if a flow coefficient is taken into consideration. This leads support to the pressure measurement procedure employed in the current study.

Flow visualization experiments revealed a fairly symmetric one way or two way flow pattern in the vicinity of the vent opening. For a zero pressure difference, a bi-directional symmetric flow across the vent was observed, with the amount of the flow in upward and downward directions being equal. As the external pressure was increased from zero, the amount of the buoyancy-driven down flow was observed to decrease. As the external pressure difference reached a certain value, for the parametric experimental conditions chosen, the buoyancy-driven down flow was observed to drop to zero, i.e., the flow was prevented from entering the lower compartment. Thus, only a uni-directional upflow was generated, this being the purging flow.

4.2 Future Work

A Dantec brand hot film probe(Model 55A76) and a constant temperature hot wire anenometer (Model 55M01) had been procured for velocity measurements near the vent opening. A plexiglass positioner was fabricated to move the hot film to the desired location. It can be moved over the X-Y plane and the height of the hot film can also be

adjusted. Thus, the hot film can be either placed at the top center of the vent opening during the experimental run or at the comer of the plexiglass tank during the mixing process. Due to time limitations, experiments for the velocity measurements could not be carried out. Experiments on the velocity distribution at the top of the vent opening (upper compartment side) will provide inputs to an analysis of the transient flow across the vent and the pressure distribution in the vicinity of the vent opening.

Further improvements in the pressure measurements, with a salt-water compatible transducer, will eliminate the inaccuracy caused by the air column used in the current study. The inconvenience caused by the calibration needed before each experiment can also be eliminated.

Experiments can also be carried out with square horizontal vent openings, with different aspect ratio S, defined as the ratio of the opening height to the side of the square opening, that is, L/S. The results can be compared with the results with circular openings by making the characteristic identification $D = 1.1S$. It is expected that these two results would be similar. Also, inclined vents are of interest in many pratical circumstances and need further investigation. The effect of multiple openings on the flow and transport processes is another area of considerable importance.

Appendix A

Exchange Volume Flow Rate Through Vent Opening with Zero External Pressure Difference

Equation **(3.5)** was derived on the basis of mass conservation. The mass balances on the brine and water compartments give

$$V_H \frac{d\rho_H}{dt} = -Q\rho_H + Q\rho_L \tag{A.1}$$

$$V_L \frac{d\rho_L}{dt} = -Q\rho_L + Q\rho_H \tag{A.2}$$

Solving equation **(A.l) for** Q yields

$$Q = \frac{-V_H d\rho_H/dt}{\rho_H - \rho_L} \tag{A.3}$$

Adding equation **(A.l) and (A.2)** and integrating the result from the initial time, with densities $\rho_{H,0}$ and $\rho_{L,0}$ we obtain

$$V_H(\rho_H - \rho H, 0) + V_L(\rho_L - \rho_{L,0}) = 0 \tag{A.4}$$

Equation **(3.5)** is then derived by solving the above expression for ρ_L and substituting the result into the equation (A.3) as:

$$Q = \frac{-V_H(d\rho_H/dt)}{(\rho_H - \rho_{L,0}) - \frac{V_H}{V_L}(\rho_{H,0} - \rho_H)} \tag{A.5}$$

Appendix B

Volume Flow Rate Through Vent Opening with Non-Zero External Pressure Difference

Equations (3.8) through (3.10) were obtained in a similar way to that as follows: The discussion in Appendix A Mass balances on the brine and water compartments give

$$V_H \frac{d\rho_H}{dt} = -Q_D \rho_H + Q_U \rho_L - Q_O \rho_H \tag{B.1}$$

$$V_L \frac{d\rho_L}{dt} = -Q_U \rho_L + Q_D \rho_H + Q_I \rho_{water} \tag{B.2}$$

Also,

$$Q_I = Q_O = Q_U - Q_D \tag{B.3}$$

Adding Equation (B1) and (B2) and integrating the result from the initial time, with densities $\rho_{H,0}$ and $\rho_{L,0}$, we obtain

$$V_L(\rho_L - \rho_{L,0}) = -V_H(\rho_H - \rho_{H,0}) - (\rho_H - \rho_{water})Q_I \Delta t \tag{B.4}$$

Equation (3.10) is then derived by solving the above expression for ρ_L:

$$\rho_L = \rho_{L,0} - \frac{V_H}{V_L}(\rho_H - \rho_{H,0}) - \frac{Q_I \Delta t}{V_L}(\rho_H - \rho_{water}) \tag{B.5}$$

Substituting Equation (B3) into the Equation (B1), Equation (3.8) and (3.10) were thus obtained:

$$Q_U = \frac{-V_H d\rho_H/dt}{\rho_H - \rho_L} \tag{B.6}$$

$$Q_D = \frac{-V_H d\rho_H/dt}{\rho_H - \rho_L} - Q_O \tag{B.7}$$

References

[1] Jaluria, Y., "Natural Convection Heat and Mass Transfer", Pergamon Press, Oxford, U.K., 1980.

[2] Gebhart, B., Jaluria, Y., Mahajan, R.L. and Sammakia, B., "Buoyancy Induced Flows and Transport", Hemisphere Pub. Corp., N.Y., 1988.

[3] Brown, W. G., and Solvason, K.R., "Natural Convection Through Rectangular Openings in Partitions-Vertical Partitions', Int. J. Heat Mass Transfer, Vol. 5, 859-867, 1962.

[4] Shaw, B. H., Heat and Mass Transfer by Natural Convection and Combined Natural Convection and Froced Air Flow Through Large Rectangular Openings in a Vertical Partition", Symposium on Heat and Mass Transfer by Combined Forced and Natural Convection, IMechE, Paper No. C117/71, 1971.

[5] Leach, S. J., and Thompson, H., "An Investigation of Some Further Aspects of Flow Into Gas Cooled Nuclear Reactors Following an Accidental Depressurization,' J. Br. Nucl. Energy Soc., Vol. 14, 243-250, 1975.

[6] Bejan, A., and Rossie, A. N., "Natural Convection in Horizontal Duct Connecting Two Fluid Reservoirs," J. of Heat Transfer, Vol. 103, 108-113, 1981.

[7] Prahl, J., and Emmons, H. W., "Fire Induced Flow Through an Opening", Combustion and Flame, Vol. 25, 369-385, 1975.

[8] Steckler, K.D., Quintiere, J. G., and Rinkinen, W.J., "Flow Induced by Fire in a Compartment", 19th Symposium (Int.) on coombustion, The Combustion Institute, 913-920, 1982.

[9] Steckler, K.D., Baum, H.R. and Quintiere, J. G., "Fire Induced Flows Through Room Openings - Flow Coefficients", 20th Symposium (Int.) on Combustion, The Combustion Institute, Pg. 1591 - 1600, 1984.

[10] Emmons, H., " SFPE Handbook of Fire Protection Engg., Soc. Fire Protection Engg., Boston, Sec. 1, Ch. 8, 1988.

[11] Chan, Y. L., and Tien, C. L., "Numerical Study of Two-Dimensional Laminar Natural Convection in Shallow Open Cavities", Int. J. Heat Mass Transfer, 28, 603-611, 1985.

[12] Abib, A. H., and Jaluria, Y., "Numerical Simulation of the Buoyancy -Induced Flow in a Partially Open Enclosure", Num. Heat Transfer, 14, 1988.

[13] Brown, W. G., "Natural Convection Through Rectangular Openings in Partitions-2. Horizontal Partitions", Int. J. Heat Mass Transfer, Vol. 5, 869-878, 1962.

[14] Mercer, A., and Thompson, H., "An Experimental Investigation of Some Further Aspects of the Buoyancy-Driven Exchange Flow Between Carbon Dioxide and Air Following a Depressurization Accident in a Magnox Reactor, Part I: The Exchange Flow in Inclined Ducts", J. Br. Nucl. Energy Soc., No. 4, 327-334, 1975.

[15] Thomas, P. H., Hinkly, P. L., Theobald, C. R. and Simms, D. L., "Investigations into the Flow of Hot Gases in Roof Venting," Fire Research Tech. Paper No. 7, Fire Res. Stn., Boreham Wood, Herts, U.K., 1963.

[16] Hinkley, P. L., "The Effect of Vents on the Opening of First Sprinklers ," Fire Safety J., 11, 211-225, 1986.

[17] Myrum, T. A., "Natural Convection from a Heat Source in Top-Vented Enclosure," J. Heat Transfer, Vol 112, 632-639, 1990.

[18] Cooper, L. Y., "Estimating the Environment and the Response of Sprinkler Links in Compartment Fires with Draft Curtains and Fusible Link-Actuated Ceiling Vents-Part I: Theory," Tech. Rep. NBSIR-88-3734, Nat. Bur. Stds., Gaithersburg, Maryland, 1988.

[19] Epstein, M., "Buoyancy-Driven Exchange Flow Through Small Openings in Horizontal Partitions," J. Heat Transfer, Vol 110, 885-893,1988.

[20] Mercer, A. and Thompson, H., "An Experimental Investigation of some Further Aspects of the Buoyancy-Driven Exchange Flow Between Carbon Dioxide and Air Following a Depressurization Accident in a Magnox Reactor, Part II: The Purging Flow Requirements in Inclined ducts", J. British Nuclear Energy Society, 14, 335-340, 1975.

[21] Cooper, L. Y., "An Algorithm for Flow Through Horizontal Ceiling/Floor Vents." Proc. Eastern Sect. Combustion Inst. Meeting, Albany, NY, Paper No. 55, 1989.

[22] Epstein, M. and Kenton, M. A., "Combined Natrual Convection and Forced Flow Through Small Openings in a Horizontal Partition, with Special Reference to Flows in Multicompartment Enclosures," J. Heat Transfer, Vol. 111, 980-987, 1989.

[23] Taylor, G. I., "The Instability of Liquid Surfaces When Accelerated in a Direction Perpendicular to their Planes. I," Proc. Roy. Soc., A201, 192-196, 1950.

[24] Jaluria, Y., and Tan, Q., "Flow Through Horizontal Vents in Compartment Fires," Proc. Eastern Sect. Combustion Inst. Meeting, Orlando, FL, Paper No.61, 1990.

[25] Merzkirch, W., "Flow Visualization," Academic Press, N.Y., U.S.A., 1974.

NIST-114A
(REV. 3-90)

U.S. DEPARTMENT OF COMMERCE
NATIONAL INSTITUTE OF STANDARDS AND TECHNOLOGY

BIBLIOGRAPHIC DATA SHEET

1. PUBLICATION OR REPORT NUMBER
NIST-GCR-92-607

2. PERFORMING ORGANIZATION REPORT NUMBER

3. PUBLICATION DATE
June 1992

. TITLE AND SUBTITLE

Flow Through Horizontal Vents as Related to Compartment Fire Environments

. AUTHOR(S)

Qing Tan and Yogesh Jaluria

. PERFORMING ORGANIZATION (IF JOINT OR OTHER THAN NIST, SEE INSTRUCTIONS)

Rutgers University
Mechanical & **Aerospace Engineering Dept.**
Rutgers University

7. CONTRACT/GRANT NUMBER
NIST **Grant No. 60NANB7D0743**

a. TYPE OF REPORT AND PERIOD COVERED

U.S. Department of Commerce
National Institute of Standards & Technology
Gaithersburg, MD 20899

0. SUPPLEMENTARY NOTES

1. ABSTRACT (A **200-WORD OR LESS** FACTUAL SUMMARY OF MOST SIGNIFICANT INFORMATION. IF DOCUMENT INCLUDES A SIGNIFICANT **BIBLIOGRAPHY OR** LITERATURE SURVEY, MENTION IT HERE.)

A detailed investigation **has** been carried out on the flow exchange through a horizontal vent in a compartment containing a fire. **A** plexiglass tank with a vented horizontal partition in the middle was constructed to simulate the warmer interior environment due to a fire and the cooler ambient environment by filling the upper and lower compartment with brine and pure water, respectively. Experiments have been carried out on the combined natural and forced convection flow by imposing a pressure difference across the vent. The flow rates through the vent were determined over wide ranges of the governing variables, such as the pressure difference **AP** across the opening, density difference $\Delta\rho$ across the opening and the opening length to diameter ratio L/D. the basic characteristics of the flow, particularly whether it is unidirectional or bidirectional, was also studied. Volume flow rates were obtained as functions of the governing parameters in terms of correlating equations, from which quantitative information of the effect of **AP,** $\Delta\rho$, and L/D on the flow exchange through the vent can be determined. These results can thus be applied to the modeling of fire growth in vented rooms.

12. **KEY** WORDS **(6** TO 12 ENTRIES; ALPHABETICAL ORDER; CAPITALIZE ONLY PROPER NAMES; AND SEPARATE **KEY** WORDS BY SEMICOLONS)

compartment fires; convective flow; fire growth; flow rate; room fires; vents

X	UNLIMITED
	FOR OFFICIAL DISTRIBUTION. DO NOT RELEASE TO NATIONAL TECHNICAL INFORMATION SERVICE (NTIS).
	ORDER FROM SUPERINTENDENT OF DOCUMENTS, **U.S.** GOVERNMENT PRINTING OFFICE, WASHINGTON, DC 20402.
X	ORDER **FROM** NATIONAL TECHNICAL INFORMATION SERVICE (NTIS), SPRINGFIELD, VA 22161.

14. NUMBER OF PRINTED PAGES
105

15. PRICE
A06

ELECTRONIC FORM